NOTE TO USERS

Université d'Ottawa · University of Ottawa

Université d'Ottawa · University of Ottawa

FACULTÉ DES ÉTUDES SUPÉRIEURES ET POSTDOCTORALES

FACULTY OF GRADUATE AND POSTDOCTORAL STUDIES

Patrick GERMAIN

AUTEUR DE LA THÈSE - AUTHOR OF THESIS

M. Sc. (Chemistry)

GRADE - DEGREE

Department of Chemistry

FACULTÉ, ÉCOLE, DÉPARTEMENT - FACULTY, SCHOOL, DEPARTMENT

TITRE DE LA THÈSE - TITLE OF THE THESIS

The Stability of Anodic Oxide Films on Gold and the Difference Between their Interfacial Capacitance and that at the Au-metal Surface

B.E. Conway

DIRECTEUR DE LA THÈSE - THESIS SUPERVISOR

CO-DIRECTEUR DE LA THÈSE - THESIS CO-SUPERVISOR

EXAMINATEURS DE LA THÈSE - THESIS EXAMINERS

M.H. Back

J. Giorgi

J.-M. De Koninck, Ph.D.

LE DOYEN DE LA FACULTÉ DES ÉTUDES SUPÉRIEURES ET POSTDOCTORALES

DEAN OF THE FACULTY OF GRADUATE AND POSTDOCTORAL STUDIES

The Stability of Anodic Oxide Films on Gold and the Difference Between Their Interfacial Capacitance and That at the Au-metal Surface

Patrick Germain

A Thesis Submitted to the School of Graduate Studies and Research in Partial Fulfillment of the Requirements for the Degree of Master of Science

Ottawa-Carleton Chemistry Institute
Department of Chemistry
University of Ottawa
Ottawa, Canada

Candidate

Patrick Germain

Supervisor

Dr. B. E. Conway

University of Ottawa
May 2004

Your file Votre référence
ISBN: 0-494-01479-2
Our file Notre référence
ISBN: 0-494-01479-2

Acknowledgments

The author would like to thank Professor Brian E. Conway for his direction of this work throughout these two years under his supervision. Professor Conway was always willing and able to give assistance at any moment, no matter how busy he was. It was a real privilege for the author to work with a well-known scientist such as Dr. Conway. He gave me a strong support during these two years in the lab, or for the preparation of poster / seminars and also during his course or tutorials. Thank you very much. I also have to thank my "second" supervisor, Dr. Wendy G. Pell who helped me so much during this work. She is the one who introduced me to all the equipment in the lab, how to run it and I should also say how to debug it. Both, Dr. Conway and Dr. Pell, have been nice enough to read and discuss the two papers I have written, often in more than one version, and their comments have always been very positive and helpful. In addition to their careful reading, they provided me with much additional information and also good discussion.

Finally I would like to thank my colleagues, Dr. Tian and Dr. Niu for their support in the lab and for all the good conversations we have had. I wish them very good results in their research and the best success in all their future projects.

Table of Contents

List of Figures

Figure 9. Nyquist (a) and Bode (b) diagrams for the impedance behaviour of the oxidized gold electrode. Oxide films were formed potentiostatically at 2.20 V for 30 seconds in 0.5 M $HClO_4$ at 1.75 V (▲), 1.55 V (●) and 1.35 V(■). Fitted data at 1.75 V (--), 1.55 V (·····) and 1.35 V (—) are also shown on the figure.

Figure 10. Nyquist (a) and Bode (b) diagrams for the impedance behaviour of the oxidized gold electrode in the presence of 10^{-3} M Cl^- for films were formed at during 30 seconds potentiostatic polarization at 1.90 V in 0.5 M $HClO_4$. Measurements were made at 1.75 V (▼), 1.65 V (▲) and 1.55 V (●). Insets in shows the Nysquist diagrams recorded at 1.45 V (■). Symbols show the experimental data, lines show how the experimental results are closely fitted to the parameters of the appropriate equivalent circuit (6b and 6c).

Figure 11. Nyquist (a) and Bode (b) diagrams for the impedance behaviour of the oxidized gold electrode in the presence of 10^{-3} M Cl^-. Oxide films were formed at 2.20 V during 30 seconds in 0.5 M $HClO_4$. Measurements were made at 1.75 V (▼), 1.65 V (▲) and 1.55 V (●). Insets in (a) shows the Nyquist diagrams recorded at 1.35 V (■), experimental data symbols; fitted data lines, as for Fig. 10.

Figure 12. Nyquist (a) and Bode (b) diagrams for the impedance behaviour of the oxidized gold electrode in the presence of 10^{-4} M Cl^-. Oxide films were formed at 2.20 V during 30 seconds in 0.5 M $HClO_4$. Measurements were made at 1.75 V (▼), 1.65 V (▲), 1.55 V (●) and 1.35 V (■); experimental data symbols; fitted data lines, as for Figs. 10 and 11.

Figure 12. Nyquist (a) and Bode (b) diagrams for the impedance behaviour of the oxidized gold electrode in the presence of 10^{-4} M Cl^-. Oxide films were formed at 2.20 V during 30 seconds in 0.5 M $HClO_4$. Measurements were made at 1.75 V (▼), 1.65 V (▲), 1.55 V (●) and 1.35 V (■); experimental data symbols; fitted data lines, as for Figs. 10 and 11.

Figure 13. Capacitance values derived from EIS experiments at stable oxide films formed by anodic polarization at 1.80 V(■), 1.90 V(●), 2.00 V(▲) 2.10 V(▼), 2.20 V(◆) for 1 minute in 0.5 M $HClO_4$ corresponding, respectively to 1.48, 1.86, 2.19, 5.8 and 44.5 equivalent O monolayers.

Figure 14. (a) Capacitance values derived for various potentials with (●) and without (▼) Cl^- anions present at 10^{-3} M concentration for an oxide film formed at a potential of 1.90 V for 1 minute in 0.5 M $HClO_4$ electrolytes (1.86 equivalent O monolayers); (b) capacitance values derived for various potentials with (●) and without (▼) Cl^- anions (10^{-3} M) for an oxide film formed at a potential of 2.20 V for 1 minute in 0.5 M $HClO_4$ electrolytes (44.5 equivalent O monolayers).

Figure 15. Combined diagram of the double-layer capacitance results as a function of electrode potential at Au metal and oxidized Au surfaces, with (—) or without (·····) Cl^- ions in a 0.5 M $HClO_4$ solution.

Figure 16. Reduction profiles of a Au electrode at 50 mVs^{-1} in 0.5 M $HClO_4$ after oxide growth at a) 1.80 V, b) 1.90 V, c) 2.0 V, d) 2.1 V, e) 2.2 V and f) 2.3 V. Oxide films were grown during (—) 30 sec, (– –) 1 minute, (·····) 2 minutes and (–·–) 5 minutes. Insets show charges for the reduction peaks.

Figure 17. Reduction profiles (·····) of a Au electrode at 50 mVs^{-1} in 0.5 M $HClO_4$ + Cl^- 10^{-3} M after oxide growth at a) 1.80, b) 1.90, c) 2.0, d) 2.1 V (RHE). Oxide films were grown during 1 minute. CV's recorded before each experiments, without halide in solution, are also shown (—).

Figure 18. Reduction profiles (·····) of a Au electrode at 50 mVs^{-1} in 0.5 M $HClO_4$ + Br^- 10^{-3} M after oxide growth at a) 1.80 V, b) 1.90 V, c) 2.0 V, d) 2.1 V. Oxide films were grown during 1 minute. CV's recorded before each experiments, without halide in solution, are also shown (—).

Figure 19. UV-Vis spectra of the electrolyte sampled in the electrochemical cell during impedance measurements for an oxide film formed at a) 2.20 V and b) 1.90 V. Halide ion, 10^{-3} M of Cl^-, was added to the cell after the oxide formation.

Figure 20. Cyclic voltammogram (·····) and EQCN profile (—) of a Au electrode in 0.5 M $HClO_4$ at 50 mV s^{-1}.

Figure 21. (a) EQCN response of an Au electrode having a thin oxide film (ca. 1 ML) in 0.5 M $HClO_4$ during potential polarization at 1.45 V (—), 1.60 V (- - -) and 1.75 V (·····) for 15 minutes immediately following oxide formation at 1.80 V (RHE); (b) cyclic voltammograms recorded at 50 mV s^{-1} subsequent to the potentiostatic polarization experiments.

Figure 22. Schematic representation of a gold oxide film before (a) and after (b) the reconstruction of the surface. In (c) is shown a schematic representation of a reconstructed oxide film in presence of Cl^- (○) presumably forming a gold chloride complex (■).

Figure 23. EQCN profile of a Au electrode in 0.5 M $HClO_4$ showing a decrease in Δf of 13.5 Hz due to the reduction of the oxide film, after a period of holding at 1.60 V.

Figure 24. EQCN profiles (a) of oxides films in contact with Cl^- 10^{-3} M at 1.45 V (·····) and at 1.75 V (—) during 10 and 15 min, respectively. In (b), Cyclic voltammograms of oxide films in contact with Cl^- 10^{-3} M after an holding period of 10 min at 1.45 V (·····) and 15 min at 1.75 V (—).

Figure 25. (a) EQCN response of an Au electrode during potentiostatic polarization at 1.00 V (RHE) for a period of 10 minutes in absence (1) of Cl^- and in presence (2) of Cl^-; (b) current profile of the electrode in the absence (—) of Cl^- and in the presence (·····) of Cl^- during the holding period.

Figure 26. Current (—) and potential (·····) profiles for a Au electrode; Cl^- (10^{-3} M) is added at A.

Figure 27. Sensitive scale voltammograms of a Au electrode in 0.5 M $HClO_4$, 10^{-3} M Cl^- with stirred (—) between 0.60 V and 1.35 V (RHE) and without stirring (·····) between 0.05 V and 1.35 V (RHE).

Figure 28. UV-Vis spectra of a standard 8.0 E^{-5} M $AuCl_4^-$ solution in 0.5 M $HClO_4$ (a); of 0.5 M $HClO_4$, 10^{-3} M Cl^- electrolyte following 1500 CV cycles of a metallic Au electrode between the potential limits 0.80 and 1.50 V (RHE) (b); and of 0.5 M $HClO_4$, 10^{-3} M Cl^- electrolyte in contact with an oxidized Au electrode (c).

Figure 29. EQCN profiles (a) of oxides films in contact with Br^- 10^{-3} M at 1.45 V (·····) and at 1.75 V (—) during 10 and 15 min, respectively. In (b), current profile of the electrode in the presence of Br^- during the holding period at 1.45 V (·····) and at 1.75 V (—).

List of Tables

Preface

Patrick Germain completed his bachelor degree with honors in chemistry at the Université de Sherbrooke in December 2001. He was registered in the materials science coop program of the University, which allowed him to acquire various areas of professional experience through the B.Sc. Hons. program. His first work experience in the field of chemistry was in the aluminum industry. He was the junior chemist in charge of an aluminum can plant located in Montréal. The main task consisted in the monitoring and control of concentrations of acids in various acid baths used to clean the cans after their production, before the application of a varnish, inside the can to avoid the corrosive dissolution of the aluminum can itself by most soft drinks, e.g. Coca-Cola or Pepsi. In the absence of such varnish the cans would therefore dissolve within a period of 3 weeks, i.e. the period usually needed to distribute the product. After his first experience in industry, he decided to consider a work term in applied research. He finally got two work terms successively at the Institut National de Recherche Scientifique (INRS) under the supervision of Dr. Daniel Guay. The first project consisted in the preparation of Ruthenium oxide, RuO_2, electrode material principally for use in wastewater purification. Antimony oxide was used as a doping material in the RuO_2 matrix and electrodes were prepared with this material. The ability of such electrodes to oxidize phenol, present in waste-water, was studied for electrodes with various concentrations of Sb and also after various heat treatments of the electrodes.

The second project consisted in the preparation of another type of electrode used in the chlorate industry. They were prepared with ruthenium oxide, iron and titanium oxide. In the industrial process chromium salts are usually added in the electrolyte to avoid the reduction of the hypochlorite (intermediate of reaction) or chlorate (product). Chromium salts are known to be very toxic and therefore the disposal of the electrolyte is complicated by their presence.

The main idea was to add directly various types of chromium salts in the Ru, Fe and Ti material. The ideal situation would be the direct use of these types of electrodes containing chromium instead of the addition of chromium directly into the electrolyte. These two projects were actually his first introduction to techniques of electrochemistry such as cyclic voltammetry and galvanostatic experiments. For his final work term he finally had the chance to fly to Victoria in British Columbia at the University of Victoria where he worked on a project under the supervision of Dr. Alexandre Brolo. The project consisted in the setting up of a Second Harmonic Generation, SHG, system used for in situ spectro-electrochemical experiments. After the realization of the setup and many adjustments of the optics, the adsorption of L-Cysteine on polycrystalline silver electrodes was studied with the SHG system. Interesting results were obtained about the orientation of the adsorbed molecule on the Ag surface which led to his first paper, published in the Journal of Physical Chemistry B. The title of the article was "*Investigation of the adsorption of L-Cysteine on a Polycrystalline Silver Electrode by Surface-Enhanced Raman Scattering (SERS) and Surface-Enhanced Second Harmonic Generation (SESHG)*", J. Phys. Chem. B 106, (2002) 5982 . Back in Sherbrooke, he did his honour's project under the supervision of Dr. Yue Zhao in the polymer/liquid-crystal field. In order to be useful, liquid crystals have to be aligned at a substrate. The technique used in that lab involved the addition of an azo-monomer in a liquid-crystal phase, followed by a photo-polymerization with linearly polarized light. One characteristic of the azo-monomer is to align itself in the direction of polarization. Once it is polymerized, the network of aligned polymer molecule induces an alignment of the liquid-crystal that can therefore be used in further applications.

After completion of his first degree, Germain joined Dr. Brian Conway's research group at the University of Ottawa. His project consisted in the determination of the capacitance of the electrical double-layer on anodically oxidized gold electrode surfaces in

aqueous acidic solutions, with or without the presence of halide anions such as Cl^- and Br^-. In previous works, usually the capacitance of the double-layer over the oxide region had been extrapolated from the capacitance measurements over the potential range where unoxidized Au surfaces exist, < 1.32 V, RHE. Electrochemical Impedance Spectroscopy, EIS, revealed that the capacitance on the oxide film was much lower than on the metallic surface and therefore the extrapolation of the capacitance from data for the metallic surface is inappropriate. These results led to the publication of a paper in Electrochimica Acta submitted in 2003 and accepted in 2004, titled "*Evaluation and Origins of the Difference between double-layer capacitance behaviour at Au-metal and oxidized Au Surfaces*", Electrochim. Acta 49, (2004) 1775.

Through these experiments where the formation of oxide films were involved, the depletion of oxide extents of oxide species in these films in the presence of Cl^- or Br^- anions was observed. The Electrochemical Quartz Crystal Nano-balance, EQCN, was then used to monitor the nano-scale mass changes associated with the formation and depletion of the oxide film on the oxidized Au electrode when halide anions were added to the electrolyte at low concentration. UV-Vis spectroscopy was also used as a complementary technique to detect the presence of any dissolved gold (as complex anion) in the electrolyte resulting from the above surface processes. More recently, a paper based on this study has been submitted to the Journal of Thin Solid Films at the end of February 2004.

Abstract

In studies of processes at oxidized compared with unoxidized electrode surfaces by transient methods, corrections for double-layer charging are usually required and have often been made by extrapolation of double-layer capacitance (C_{dl}) data for the metallic surface, e.g. at Au or Pt, into the potential region of oxide-film formation. Voltammetry and impedance spectroscopy provide direct information on C_{dl} values determined at *unoxidized*, i.e. metallic, Au surfaces compared with those of anodic oxide films generated potentiostatically to various extents that are stable in time, and characterized by reductive linear-sweep voltammetry. Using Electrochemical Impedance Spectroscopy, C_{dl} is derived from constant-phase element (CPE) values and the CPE parameter, φ, which is found to be near unity for most conditions.

At *oxidized* Au surfaces, C_{dl} depends on potential for various extents of oxide formation; it increases from 15 (±1) μF cm^{-2} at 1.75 V (RHE) to 25 (±1) μF cm^{-2} at 1.45 V (RHE) and is independent of added Cl^- or Br^- for concentrations 0 to 10^{-3} M of both anions, while, at *unoxidized* Au electrodes in the absence of halide anions, C_{dl} has a maximum value of 60 (±2) μF cm^{-2} at 0.80 V (RHE) and is now dependent on concentration of added Cl^- or Br^- ion due to chemisorption of these anions on the Au-metal surface. These major differences of C_{dl} for the oxidized and unoxidized Au surfaces indicate that double-layer charging corrections cannot be made simply by extrapolation of C_{dl} data for unoxidized Au metal surfaces into the potential region for oxide formation.

In the second part of this thesis, the stability of the compact, so-called α-oxide film on gold electrodes in contact with halide solutions was investigated by means of voltammetry coupled with nanogravimetry, using an EQCN. The latter technique provides a new dimension for such studies, complementary to simultaneously employed voltammetry.

Oxide films of the α-type were formed potentiostatically in 0.5 M $HClO_4$ at 1.80 V (RHE) for a period of 30s. From the EQCN measurements, the mass-to-charge ratio in the Au oxide formation region is found to be ca. 8 g per mole of electrons, which is consistent with the formation of Au/O_{ads} at the electrode surface. Immediately after formation of the oxide film, a negative-going sweep was applied and then arrested at values in the potential range of virtually zero Faradaic currents (1.75 to 1.45 V, RHE) and held at such values for 15 minutes. Chloride anions (as KCl) or bromide anions (as NaBr) were added to the electrolyte at those potentials and mass changes were recorded during the holding period and also during subsequent reduction of the oxide film in a continuing potential sweep. Of special interest is that the EQCN frequency change of the oxidized electrode in contact with Cl^- or Br^- can be related both to mass changes due to Au dissolution and oxide reduction and also, under such conditions, to displacement of adsorbed anions and surface roughness or restructuring.

By means of UV spectrophotometry, Au dissolved as $AuCl_4^-$ or $AuBr_4^-$ was directly identified in experiments on Au dissolution in Cl^- or Br^--containing solutions, respectively.

Introduction

For interpretation of results from transient type experiments on the surface electrochemistry of noble metals, e.g. cyclic voltammetry, it is necessary to make "double-layer charging" corrections to the response currents. At oxidized noble metal surfaces, it has been common to make such corrections simply by extending the double-layer charging response recorded over the potential range of the profile for the unoxidized metal surface, e.g. of Pt or Au, into and through the potential range where surface oxidation is occurring. This seems intrinsically unreliable since the surface condition of anodic oxide films is completely different from that of the corresponding unoxidized electrode surface.

The significance of the above requirements arises as follow. Electrode processes are of two principal and distinguishable kinds: a) non-Faradaic, in which charges (electronic and ionic) are transferred to, and accumulated at, a metal or semiconductor interface with an electrolytic solution forming a double-layer, but *are not* transferred across such an interface; and b) in which electrons *are* transferred *across* the interface, i.e. across the double-layer, resulting in chemical change in the solution or at the electrode surface. This process (b) is the basis of Faraday's Laws of electrochemical change.

Process (a), at some electrode metals, e.g. Hg or Au over certain ranges of potential, can take place without participation of an electrolytic process (b). Such electrode interfaces are termed "ideally polarizable" and exhibit pure double-layer capacitance.

Importantly for the material reported in the first section of this thesis, processes (b) of the Faradaic kind are usually coupled with non-Faradaic charging of the double-layer as electrode potential is changed, e.g. as in a polarizing experiment, or chronoamperometry. In such transient processes, conducted over a significant range of change of voltage, the non-Faradaic component of passage of charge can be up to ca. 10% of the simultaneous change of

Faradaic current. Corrections for this non-Faradaic component are thus usually necessary and can be made for certain electrode interfaces for which independent information exists on the double-layer capacitance as a function of potential.

In the case of 2 dimensional electrode processes such as underpotential deposition of H or metal adatom monolayers, or electrosorption or electrodesorption of monolayer oxide films at e.g. Pt or Au, corrections for the double-layer charging currents have commonly been made, empirically, e.g. in cyclic voltammetry simply by extrapolating the double-layer charging current measured over, say, the oxide-free potential range (Pt, Au) into and through the oxide coverage and formation potential range, normally substantially more positive than that for the oxide-free, metal-double layer charging region. As noted above there are good intuitive reasons why the above procedure is fundamentally unsound.

By direct cyclic voltammetric and especially by means of AC impedance spectroscopy, the double-layer capacitance of Au electrode/solution interfaces has been directly compared at the non-oxidized Au surface with that at Au surfaces at which oxide films have been generated anodically to various thicknesses from ca. 1 ML to ca. 200 MLs.

In a recent paper [1], from this laboratory, it was shown experimentally how very different double-layer capacitance behaviour (derived from impedance spectroscopy), in fact, arises at oxidized Pt electrodes beyond ca. 0.90 V (RHE) from that observable below that threshold potential, characterizing the oxide-free Pt surface. This work showed directly that "double-layer charging corrections" to results of transient or voltammetry experiments at oxide-free Pt-electrode surfaces cannot be extended to, or over, the oxide formation potential range at Pt, and probably at other noble metals (cf. ref. 2 for Au), without introduction of substantial or major errors [1].

The present work extends the above comparison of double-layer capacitance behaviour at oxide-covered and oxide-free surfaces at Pt [1] to the case of polycrystalline Au electrodes

studied by means of linear-sweep voltammetry, complemented by impedance spectroscopy for direct evaluation of the interfacial capacitance behaviour and by nanogravimetry to follow surface mass changes. This work is motivated by the large volume of publications on the cyclic voltammetry of poly-, and single-crystal electrode surfaces of Au and other noble metals [3, 4, 5], as reviewed in detail in ref. [6]. Also, in recent years, major interest has arisen in the anodic surface electrochemistry of Au in comparison with that at Pt. Although Pt and Au are congeners in the Periodic Table (electronic configurations Pt: Xe, $4d^9\ 5s^1$; Au: Xe, $4d^{10}\ 5s^1$), the surface chemical properties of these two metals are very different, especially the absence of catalytic properties of Au surfaces and of chemisorption of H (although, interestingly, molecular H_2 can become oxidized at the potential for onset of "preoxidation" [7] in surface oxide formation at Au [8], mediated by anion chemisorption [9]). In most respects, however, the properties of Au surfaces are more similar to those of Hg (the next congener, Xe, $4d^{10}\ 5s^2$) than to Pt, though strong anion adsorption behaviour, e.g. of HSO_4^-, is common between Pt and Au, but the latter anion is not strongly adsorbed at Hg as indicated by the only very small shift of potential of zero charge of Hg caused by that anion at moderate concentrations [10]. These observations illustrate the major dependence of surface electrochemical properties of Pt, Au and Hg on small but significant differences of 4d, 5s electron-shell configuration at the end of the 4d transition-element series. Of course, the vacant 4d orbital (and resulting d-band character) of Pt determines its specific difference of catalytic and chemisorptive properties from those of Au or Hg.

The states of noble-metal surfaces prior to, during and following surface oxide formation are thus very different from one another [5, 6, 11], chemically and physically. Comparative measurements of double-layer capacitance of noble metal surfaces in these two states, referred to above, can provide a sensitive probe for this difference of properties, and for characterization of electrode processes that can proceed quite differently on the oxide-free

surfaces of noble metals in comparison with oxide-film covered surfaces of the same or other metals [12, 13]. Information on the difference of states of oxidized and non-oxidized Au electrodes, as also at Pt [1], is hence desirable for interpretation of electrode processes at Au, e.g. reduction and evolution of O_2 [13], adsorption and reactivity of organics [14, 15, 16], etc. over various ranges of potentials.

Of special interest is the transitional region between capacitance behaviour of the unoxidized metal surface and that of the developing oxide film, eventually up to nominal monolayer coverage or greater [17]. It is in this transitional region [7] at low coverage of electrosorbed OH or O species (cf. refs. 18 and 19) that appreciable adsorption pseudocapacitance [20] can arise, associated with almost reversible deposition and desorption of O species [17, 18].

Anodic polarization of noble metals provides the opportunity of following the transition between an unoxidized surface and one on which an oxide film becomes progressively formed [6, 17] through an initial sub-monolayer of O species [5] or, in the very initial stages, through an "incipient" oxide film formation process [7]. Depending on conditions, e.g. the presence of Cl^- or Br^- ions [21], onset of surface oxide film formation may be preceded or accompanied by [21, 22] dissolution of the noble metal as complexed ions, as with Pt, Pd and especially Au. As explained in a previous review [6], the early stages of oxide film formation on noble metals can be regarded as a "surface electrochemical process".

Polarization positive to the reversible H_2 electrode potential at the catalytic noble metals such as Pt, Rh, Ir, Ru and Pd initially involves oxidation of molecular H_2, coupled with desorption of sorbed H (Pd, Ru) and / or of underpotentially deposited (UPD) H. Prior to initiation of deposition of oxygen species, chemisorption of anions of the electrolyte usually takes place, e.g. in aqueous H_2SO_4 (HSO_4^- ions [4, 9, 17,]), ClO_4^- in aqueous $HClO_4$ or in such solutions containing added Cl^-, Br^- or I^- anions (cf. ref. 3). Such adsorption of anions is

usually competitive with the initial stages of oxide film formation as shown in the voltammetric studies of Novak and Conway [3], the radio-tracer ion studies of Wieckowski et al. [4, 9] and of Horanyi [23], as well as in reflectivity studies of Paik and Bockris [24], Cahan and Yeager [25] and Xia and Birss [5] in the case of Au (voltammetry, nanogravimetry with the EQCN and ellipsometry).

Interest in competitive adsorption of Cl^- or Br^- vis a vis anodic development of oxide films on noble metals arises in relation to a) the state of oxidized Pt or Ru surfaces for anodic Cl_2 or Br_2 generation [26] and b) the promotion of corrosion of Au in the presence of Cl^- or Br^- anions [21], and is hence of relevance to the present work. General aspects of factors determining adsorption of halide ions, including Cl^- and I^- at various metals, e.g. Au, have been treated by Trasatti [27, 28] covering specificity of interfacial properties of single-crystal faces of Au, such as the possibility of prediction of inner-layer capacitance [28].

The competitive effects of chemisorbed Cl^- and Br^-, which arise vis à vis the early stages of oxide film formation at Pt [3] and at Au [29, 30], have been quantitatively studied in a variety of previously published papers by means of cyclic voltammetry (CV) and also using the EQCN [30]. Additionally, in the present work, CV, complemented by electrochemical impedance spectroscopy (EIS), has been employed to determine the influence of adsorption of the above two halide ions on the double-layer capacitance behaviour of the unoxidized Au electrode surfaces in relation to that of Au bearing an oxide film that had been formed under conditions of controlled potential and time, ensuring its stability, e.g. during the course of EIS measurements. Thus, dynamics and mechanisms of oxide film growth itself are not the subject of the work described in the present thesis; they have been extensively treated elsewhere [3, 5, 29, 30].

At noble metals, the anodic formation of oxide films can be followed under control of anodization potentials from low, sub-monolayer coverages of O species [5, 6, 31, 30] through

to multilayer thick films [6]. As noted above, the initial stages of surface oxidation of these metals are to be regarded as "surface-electrochemical" processes [6] and are hence usefully examined by methods of electrochemical surface science. Experiments on such processes, e.g. at Pt, Rh and Au, provide the opportunity for study of the transition between electrosorption of O species at low coverages and development first of monolayer [5, 6], then on to thicker oxide films that are multilayer hydrous oxide layers [32]. In the case of Au and Pt [33], an initially formed, compact, thin-layer oxide film (α-state) can be distinguished [5] from a thicker, hydrous oxide, type of film (β-state), formed at high anodic potentials for extended periods of polarization. In the case of Pt, over controlled ranges of potential, the compact α-state can be formed below the β-state and reduced independently of the latter, as shown in ref. [33].

The oxide films anodically formed at Au or Pt and their electrochemical behaviour provide model systems for understanding corrosion and passivity of metals, and breakdown of passive films, e.g. in halide solutions. This is the subject of one section (Part II) of the present work which examines the formation and reduction of the compact, α-oxide film at Au, and its stability in Cl^- and Br^- containing acid solution. Interest in adsorption of Cl^- or Br^- at Pt or Au arises from the strong competitive adsorption between these ions and the processes of electrosorption of O species, leading to oxide film formation at these metals, as studied previously in refs.[3] and [29].

Purposes of the work

The purposes of the work were to determine if and how the capacitance of the electrical double-layer at an oxidized electrode differs from that at a non-oxidized electrode. The effects of variation of the thickness of the oxide films were studied and also the effects of several anions, Cl^- and Br^- on the values of the capacitance. In order to achieve our objective, oxide films of various thicknesses were grown on gold electrodes and impedance measurements were run in the presence of a gold oxide film in a state stable in time. Before each experiment, it must be ensured that the oxide growth has reached a stable state, i.e. the film is not growing or being reduced. Therefore, the potential has to be held at a value somewhat less positive than that for continuing oxide growth and also more positive than the reduction peak potential. A zero current where neither oxide formation or reduction is taking place has to be found in order to run the impedance measurements reliably. Cyclic voltammetry and electrochemical impedance spectroscopy (EIS) are the two techniques that have been used in these experiments. A part of this work (Part II) was also concerned with the stability of the various types of oxide films, α and β, in the presence of halide anions at various concentrations. In order, complementarily, to follow changes of the mass of the oxide film with time, the electrochemical quartz crystal nano-balance was employed to record such mass changes on the nanogram scale.

Chapter 1 Theory

1.1 The Electrical Double-Layer

1.1.1 Historical aspects of the concept of the double-layer

The main concept of the double-layer of charges existing at the frontier of one phase with another that contains ions in solution originated in the nineteenth century. In 1852, Eilhard Ernst Gustav Wiedemann (1853-1928) made the first quantitative measurement of electroosmosis. He showed that the hydrostatic pressure developed upon opposition to the tendency for electroosmotic flow was directly proportional to the electric potential applied between two electrodes. Later, Arne Wilhelm Tiselius (1902-1971) designed a special type of U-shaped apparatus and made the first quantitative measurements of electrophoresis. He observed that when a suspension of charged particles in an electrolyte solution is subjected to an electrical field between two electrodes, then the particles moved in response to the applied field in a direction which depends of the net sign of their charge. These two effects arise at interfaces when separation of positive and negative charges arises in layers or regions, at or near an interface, the resulting configuration being referred to as the electrical "double-layer".

1.1.2 Origins of concepts of the charge in the double-layer

There are various types of process that create a charge separation at interfaces or in other words, the formation of the double-layer. One way is when there is differential adsorption of cations and anions at an interface, as at colloids. The anions are usually preferentially adsorbed because the have a greater polarizability, a better electron-donor

character and a weaker hydration than cations of comparable size. Chemical ionization is also a type of process where separation of charge may occur. An example of such a process is the protonation or deprotonation of a base or acid functional group bonded to a surface, or to a colloidal particle or polymer:

$$|\text{----COOH} + H_2O \rightarrow |\text{----}COO^- + H_3O^+ \quad (1)$$

Another way in which charge separation in double-layers may arise is by a Faradaic electrochemical equilibrium process at an electrode surface. An electrical surface charge density can arise thermodynamically by a spontaneous corrosion process or at a metal surface that is in a solution of its own ions as is the case for a reversible electrode. The silver electrode is an example of the latter case:

$$Ag \leftrightarrow Ag^+ + e^- \quad (2)$$

In this situation, Ag^+ is the silver ion in solution and in the double-layer, and the electron charge, e^-, resides on the metal surface at a charge density proportional to the metal/solution potential that arises on account of the electrochemical equilibrium. Therefore, it will create a negatively charged surface that faces the layer of positive ions in the solution, i.e. a double-layer of charges is generated. This charge density may also arise from creation of an excess electron density in the case where a negative polarization is applied or from electron deficiency when a positive polarization is applied. Thus, an electrical double-layer can arise by polarization of a metal or semi-conductor by an external source of voltage such as a potentiostat, especially in the case of a so-called ideal polarizable electrode [34]. For this type of electrode, no charge transfer can occur across the metal/solution interface regardless of the potential imposed and during the polarization, there is accumulation of electrons (or electron-deficiency) on the metal and complementary ionic charges in solution.

The mercury electrode can approach ideal polarizability over a specific potential range close to 2 V depending on the decomposition potential of the solution. Within this range, the surface charge density can be varied with the potential, E, in such a way that no process passing Faradaic currents arise. The only Faradaic currents that could flow in this region would be due to charge-transfer reactions of trace impurities. If the potential is driven sufficiently positive or negative, Faradaic currents may eventually arise and pass across the electrical double-layer, leading to electrolysis of the electrolyte.

1.1.3 Models of the double-layer

Herman Ludwig Ferdinand von Helmholtz (1821-1894) was the first scientist to propose a model of the electrical double-layer. In his model, the double-layer of charges was represented in terms of two parallel plates of a capacitor (Fig. 1a). The main aspect of this concept was that the counter charge in solution resides next to the surface with its complementary charge on or "in" the surface. Thus, there would be two sheets of charge, having opposite polarity, separated by a distance of molecular order: one sheet of charge being on the surface, the other adjacent, in the solution. Such a structure is equivalent to a parallel-plate capacitor which has the following relation between the stored specific charge density, σ, i.e. per cm^2, and the potential drop, V, between the two plates:

$$\sigma = \frac{\varepsilon\varepsilon_0}{d} V \tag{3}$$

where ε is the dielectric constant of the medium, ε_0 is the permittivity of free space and d is the distance between the plates. The capacitance of such device per unit area, cm^2, is then represented by the following equation:

$$C_d = \frac{\partial \sigma}{\partial V} = \frac{\varepsilon \varepsilon_0}{d} \tag{4}$$

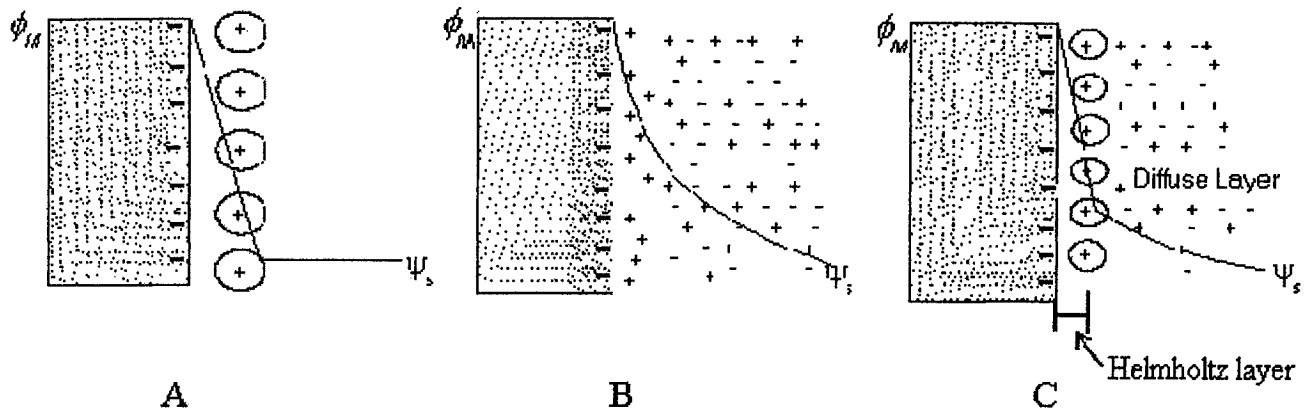

Figure 1. Helmholtz model of the double-layer (A), Gouy-Chapman diffuse-layer model of the double layer (B) and Stern model of the double-layer (C)

The weakness of this model is due to the fact that the capacitance of the double-layer would be only proportional to the dielectric constant of the medium and to the separation between these sheets of charge. Even if the charge on the electrode is confined to the surface, the same is not necessarily true of the solution. Louis Georges Gouy (1854-1926) and David Leonard Chapman (1869-1958) independently proposed a second model named the Gouy-Chapman diffuse-layer model (see Fig 1b). In his model, Gouy proposed the idea of a diffuse-layer and offered a statistical-mechanical approach to describe it. It was based on ion distribution, like in the Debye-Hückel electrolyte ionic atmosphere model, developed for ionic solution some ten years later. The population of ions far from the electrode is at the bulk concentration, n_i^0. Therefore, the population closer to the electrode can be treated by a Boltzmann relation:

$$n_i = n_i^0 \exp\left(\frac{-z_i e \phi}{kT}\right) \tag{5}$$

where ϕ is the potential (measured with respect to the bulk solution), e is the charge of an electron, k the Boltzmann constant, T the absolute temperature and z_i the charge on the ion i. Now the total charge per unit of volume, ρ, is given by:

$$\rho(x) = \sum_i n_i z_i e \tag{6}$$

$$= \sum_i n_i^0 z_i e \exp\left(\frac{-z_i e\phi}{kT}\right)$$

where the summation is over all the ionic species of types, i. From classical electrostatics, we know that ρ(x) is related to the potential at distance x by the Poisson equation:

$$\rho(x) = -\varepsilon\varepsilon_0 \frac{d^2\phi}{dx^2} \tag{7}$$

Finally, equations 6 and 7 can be combined to give the famous Poisson-Boltzmann equation that describes here the field-gradient of the ionic atmosphere conjugate to the electrode surface charge density:

$$\frac{d^2\phi}{dx^2} = -\frac{e}{\varepsilon\varepsilon_0} \sum_i n_i^0 z_i \exp\left(\frac{-z_i e\phi}{kT}\right) \tag{8}$$

This equation was then applied in one dimension, normal to the electrode surface, to solve the problem of charge distribution in and capacitance of the diffuse part of the double-layer. The predicted capacitance curves were similar to those observed but only at potentials close to the potential of zero charge, pzc and in dilute solutions. Further from the pzc, the predicted capacitance by this model was much higher than the actual values. Therefore, this suggests that only some aspects of the model were correct but the treatment was oversimplified and inapplicable.

Later, Otto Stern (1888-1969) identified the major problem in the Gouy-Chapman model. The high values of predicted capacitance arose because the ions in the latter model are not restricted with respect to distances of approach to the surface because they were considered as point charges that can hence approach to the surface very closely. This model had thus not taken into account the finite size of ions and their solvation shells in solutions. Thus, such ions cannot approach the surface closer than their own hydrated ionic radius. Stern proposed the idea of the double-layer as incorporating a Gouy diffuse-layer charge distribution coupled with a compact layer (Helmhotz model) at the surface (see Fig. 1c).

At higher polarization or concentration, the charge distribution in solution near the surface becomes more compressed against a boundary located at a certain distance of closest approach to the surface. The system then begins to tend toward the Helmholtz model. The plane located at this distance is called the outer Helmholtz plane. The inner region of the inner Helmholtz plane is named the compact inner region of the double-layer. The inner Helmholtz plane is located where the anion adsorption occurs. The diffuse region of the double-layer is located a little further, i.e. further from the outer Helmholtz plane that is located where the cations, having a bigger hydration shell, are usually found.

Therefore, the overall capacitance of a metal surface arises from two components that can be separated in the reciprocally added way for two capacitors in series. One component C_H, represents the capacitance of the Helmholtz (compact) region and the other, C_D, represents the capacitance of the diffuse region. The overall, measurable differential capacitance, C_d, is then expressed by:

$$\frac{1}{C_d} = \frac{1}{C_H} + \frac{1}{C_D} \tag{9}$$

The value of the capacitance in the Helmholtz region, C_H, is independent of the potential applied but the value of the capacitance in the diffuse region, C_D, is dependent on potential and also on electrolyte concentration. The differential capacitance, C_d, is then governed by the reciprocal relation (Eq. 9) between C_H and C_D and will therefore be controlled by the *smaller* of the two components. At larger concentrations of the electrolyte or at high polarization in a lower concentration medium, we can expect C_D to be very large. Therefore, if the value of C_D becomes sufficiently large, it will contribute less and less (Eq. 9) to the overall differential capacitance. C_d would then be governed principally by the capacitance of the Helmholtz region.

This model gives good prediction of the behaviour in many systems but still has some failure. C_H is not truly independent of potential and it also ignores the presence of dipolar solvent molecules. This aspect must be taken into account in relation to the structure of the dielectric in the compact layer because the orientation of the solvent dipoles is field dependent and therefore can play a major role in the evaluation of the capacitance. Workers such as Watts-Tobin, Mott and Bockris [35] proposed a model to take into account the field-dependent orientation of the solvent dipoles (see Figure 2). As represented on this figure, the electric permittivity, ε, of the water depends on the field at the electrode interface. For example, the primary water layer would have a value of electric permittivity of ca. 6 compared to that of the second water layer, which has a value of ca. 32. Finally, once the bulk solution region is reached, the regular electric permittivity (at 298K) of 78.5 applies. The capacitance is thus related to the electric permittivity of the medium as shown in Eq. 4. Therefore, a complete model of the electrical double-layer could not ignore the field dependence of the orientation of solvent dipoles.

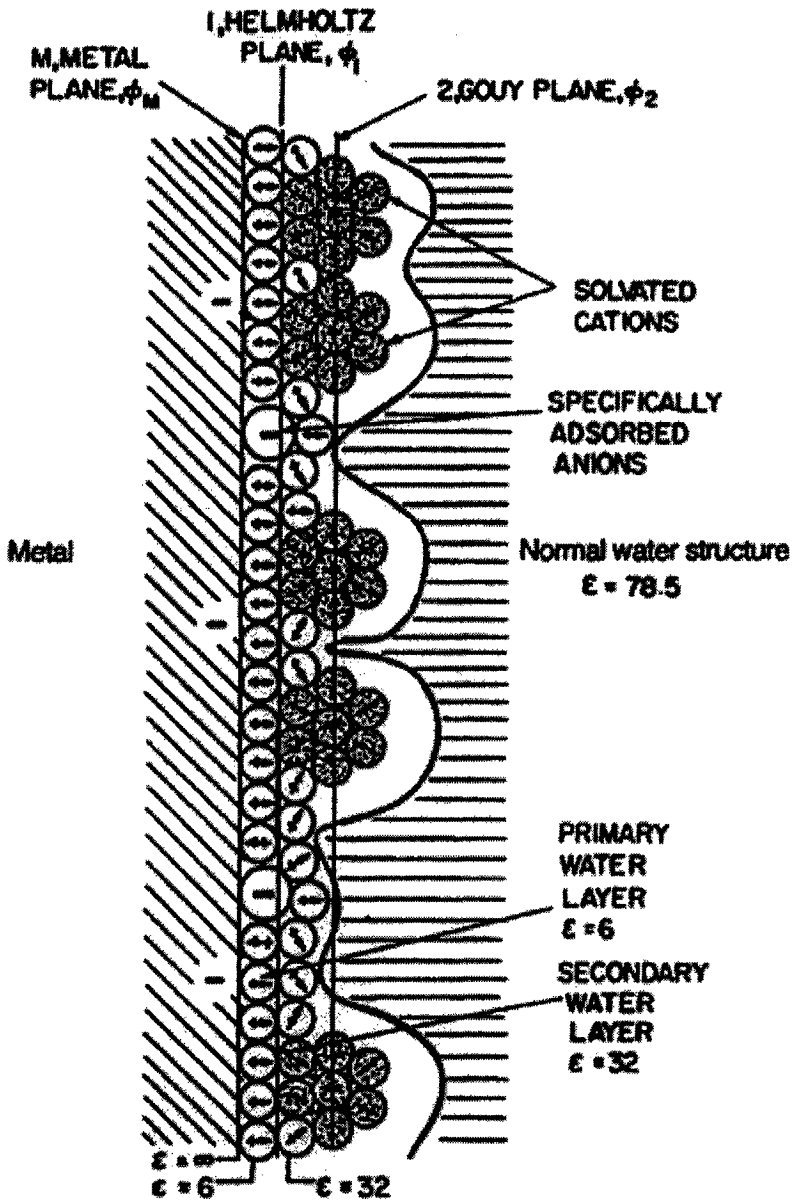

Figure 2. Model of the double-layer illustrating role of solvent dipole orientation

1.1.4 Other factors related to properties of the double-layer

In order to have a good understanding of the theory of the double-layer several further factors have to be introduced. Many papers in the field of electrochemistry present electrocapillary curves, which are very important for studies on the capacitance of the double-layer, e.g. at Hg. These curves result from a plot of the surface tension of the electrode, when

it is a liquid, e.g. Hg as a function of its potential. They usually have a bell shape where the negative of the slope of the curve at any potential E, represents the excess charge on the electrode given by the following equation:

$$\sigma^M = -\left(\frac{\partial \gamma}{\partial E}\right)_E \tag{10}$$

The apex of this curve represents the so-called *electrocapillary maximum* and, because at that point the slope is zero, it is also named the *point of zero charge, PZC.* See Figure 3. At this potential, the excess of charge on the electrode is zero and at more negative polarizations the electrode will carry a negative excess of charge and correspondingly, at more positive potentials, a positive excess of charge. It should be noted that at the *PZC*, no electrostatic adsorption of ions occurs on the surface but chemisorption, e.g. of Cl^-, Br^-, S^{2-} etc can arise.

The capacitance description arises from the Helmholtz model in that the double-layer is like an electrical capacitor. We could define the capacitance of an interface as its ability to store charge in response to a perturbation in potential. The capacitance is actually the first derivative of the excess of charge, σ^M, against potential.

This is commonly named the differential capacitance, C_d, expressed by:

$$C_d = \left(\frac{\partial \sigma^M}{\partial E}\right) \tag{11}$$

In order to determine the excess of charge, cyclic voltammetry can be used and therefore the value of capacitance of an interface can be calculated. The concepts involved in this technique will be discussed in the following section.

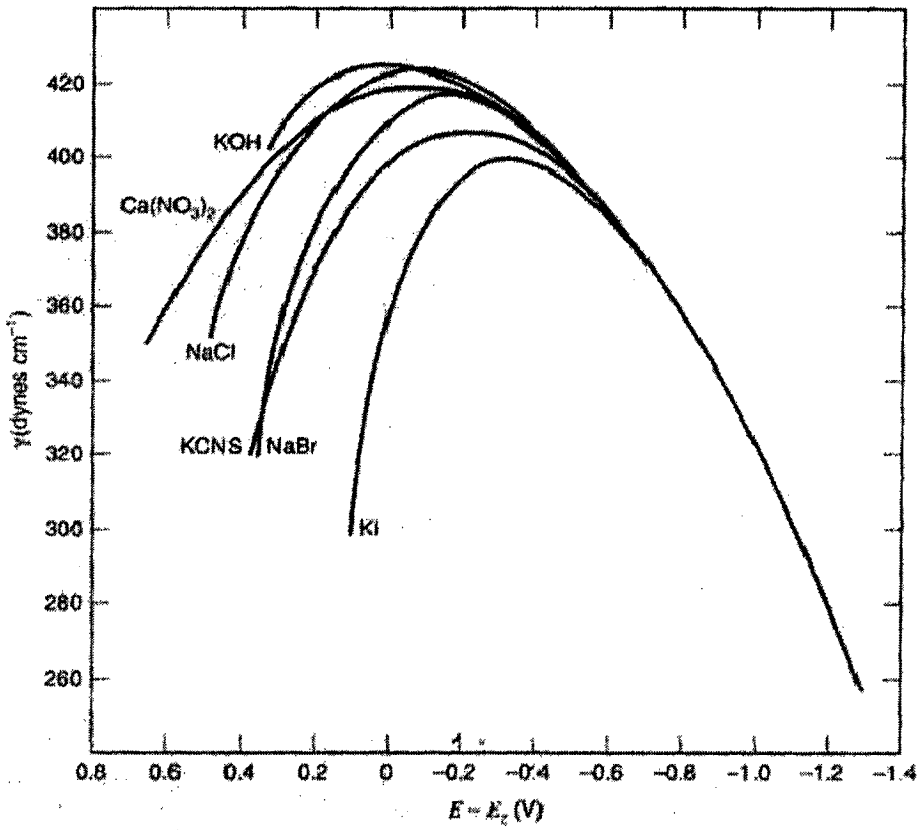

Figure 3. Electrocapillary curves at a mercury electrode

The present work is addressed to electrochemical characterization of the interface, with aqueous solutions, of Au electrodes that are either in the "free" metallic state or bear anodically formed, thin oxide films. The nature of the work therefore requires information on a) the interfacial capacitance of both the "free" metal surfaces and those bearing controllably formed, thin oxide films; and b) on the state of such oxide films in relation to extents of oxide formation and double-layer capacitance, and their possible reactivity with Cl^- or Br^- ions, leading to corrosion.

None of the above electrochemical processes is continuous in nature or in time, as with a Faradaic reaction such as O_2 or H_2 evolution taking place on the metal or oxide interface.

Thus, although surface-oxide formation and reduction are Faradaic processes in the sense that charge transfer takes place across the double-layer with resulting chemical changes, they differ from continuous Faradaic reactions such as anodic O_2 evolution since such surface processes cannot be maintained continuously because they are limited either by consumption of the oxide, on reduction, or by limitation of its extent of anodic formation, per cm^2, to one or two monolayers on the given electrode-metal surface. The same principle applies to use of CV to studies of double-layer charging/discharging.

Hence, study of the interfacial processes (double-layer charging and oxide film behaviour) requires the use of so-called *transient methods* such as Cyclic Voltammetry (CV) and Electrochemical Impedance Spectroscopy (EIS) as used in the present work, and complemented by use of the Electrochemical Quartz Crystal Nano-balance (EQCN) that is capable of recording transient mass changes in sub-monolayer oxide film formation and reduction process, associated with the electrochemical reactions involved.

1.2 Cyclic voltammetry for oxide-film growth and capacitance measurements

1.2.1 Diffusion-control in cyclic voltammetry

Electrode reactions can be studied through both large and small perturbations of the system. By imposing a sweep of potential, linear in time, the electrode is typically progressively driven to a condition far from equilibrium and therefore a response is observed which is usually manifested by a transient current-signal in time. One of the most useful techniques used currently in electrochemistry is probably cyclic voltammetry. This technique is derived from a procedure first developed by Jaroslav Heyrovsky (1890-1967) and has been widely used throughout this work. If a reaction at an electrode does not involve adsorption,

such a process can be regarded as involving three steps. First, the reactants must diffuse to the electrode surface before electron transfer can occur. The second step is the electron transfer itself, the rate of which depends on the potential, E, applied to the electrode (relative to that of some reference), as described by the Nernst equation, $\Delta G = -nF\Delta E$. Then thirdly, when products are formed, their diffusion takes place back into the bulk solution.

In semiclassical electron-transfer theory, three parameters govern the reaction rates: *i*) the electronic coupling between the donor and the acceptor, κ_E, *ii*) the free energy change for the reaction, ΔG^0, and *iii*) a parameter λ related to the extent of inner coordination-shell and solvent nuclear reorganisation accompanying the electron transfer reaction. These parameters describe the rate of electron transfer between a donor and acceptor held at a fixed distance and orientation as shown by the following equation;

$$k_{ET} = \upsilon_N \kappa_E \exp\left[-\frac{(\Delta G^0 + \lambda)^2}{4\lambda RT}\right] \tag{12}$$

where ν_N is the frequency factor (taken as 10^{12} s^{-1} at 298 K), R the gas constant and T the absolute temperature.

Fundamental to the theoretical descriptions is the Franck-Condon principle which states that because the time required for electron transfer is much less than that for nuclear motion the nuclear configuration and momentum cannot change during the electron transfer. For a molecule in a polar solvent, the orientation of the surrounding solvent molecules, as well as the bond lengths and bond angle in the molecule, depend upon its charge. Then, the equilibrium configuration of a molecule and of the surrounding solvent is, in general, different before and after electron transfer. For reaction with no net free-energy change, the difference

between the free energy of the reactants in their equilibrium configurations (initial state) and their energy immediately after the electron has been transferred (at the products' equilibrium nuclear configuration) is an important quantity signified by the parameter λ introduced previously. Two contributions to this energy difference are recognized; one (λ_{out}) from the change in solvent polarization from an equilibrium to a nonequilibrium one and the second (λ_{in}), from the changes in the reacting species themselves. The total energy difference is the sum of these two contributions ($\lambda = \lambda_{out} + \lambda_{in}$).

Marcus developed a model for calculating the solvent contribution to the free-energy barrier. It assumes that the energy barrier to electron-transfer is due to the solvational reorganization energy of the reactant species, caused by the change of the charge of the molecule or ion. This is the energy for the internal reorganization of a molecule or solvated ion associated with the electron transfer, coupled with the reorganization of the solvation sphere of the molecule in response to a change of charge number. In this model, the two redox sites are assumed to be centrally located in two noninterpenetrating spheres. The expression derived by Marcus is:

$$\lambda_{OUT} = (\Delta e)^2 \left(\frac{1}{2a_i} + \frac{1}{2a_j} - \frac{1}{r_{ij}} \right) \left(\frac{1}{D_{op}} - \frac{1}{D_s} \right) \tag{13}$$

where Δe is the charge transferred, a_i and a_j are the radii of the two reactants, r_{ij} the distance between their centres, D_{op} is the optical dielectric constant (usually taken as the square of the refractive index), and D_s is the static dielectric constant of the medium. In a polar solvent, the second part of the equation becomes important but in a non-polar solvent, that part contributes only a little. λ_{inner} is defined by Marcus by the following relation:

$$\lambda_{in} = \frac{1}{2} \sum_i f_i \left(r_R^{eq} - r_P^{eq} \right)^2 \tag{14}$$

where f_i is the bond length changes from equilibrium, r_R^{eq} the bond length of the reactants at equilibrium and r_P^{eq} the bond length of the products at equilibrium. The λ(inner) is also usually small except when there is a large difference in bond length between products and reactants.

Usually, in most electrochemical reactions, but depending on potential, the electron-transfer rates tend to be faster than that of diffusion of the reactant molecule. Therefore, rate of diffusion can be the limiting factor determining the rate of the electron transfer.

A well known example, where cyclic voltammetry can be used, is the study of the ferri/ferrocyanide reversible reaction:

$$Fe(CN)_6^{3-} + e^- \Leftrightarrow Fe(CN)_6^{4-} \qquad (15)$$

If the scan is started at a potential well positive of the reduction potential, E^0, only non-Faradaic currents arising from charging of the capacitance, C, of the double-layer at the electrode will flow; for a constant sweep-rate of v Vs^{-1}, this current is $CdV/dt \cong Cv$. When the electrode potential approaches E^0, reduction of the $Fe(CN)_6^{3-}$ begins and a cathodic current flows. As the potential becomes more negative, the surface concentration of $Fe(CN)_6^{3-}$ is depleted, which creates a concentration gradient causing diffusion of the reactant from the bulk solution to the electrode surface. Therefore, the flux at the surface and the corresponding current increases to reach a maximum at the potential of E^0. As the potential goes further negative to E^0, the surface concentration of oxidized species drops towards zero and the mass transfer (flux) increases as the depletion takes place. At this point, the concentration of $Fe(CN)_6^{4-}$ species becomes relatively high compared to that of the $Fe(CN)_6^{3-}$ species which are then almost absent so that a limiting, diffusion-controlled current is approached. Now if the

potential is reversed in a positive direction, as the potential approaches E^0, the reduced species, $Fe(CN)_6^{4-}$ here, will become re-oxidized so that an anodic current then flows. This reverse current-potential profile has a shape very similar to that for the forward sweep peak, see Figure 4b, but displaced from it.

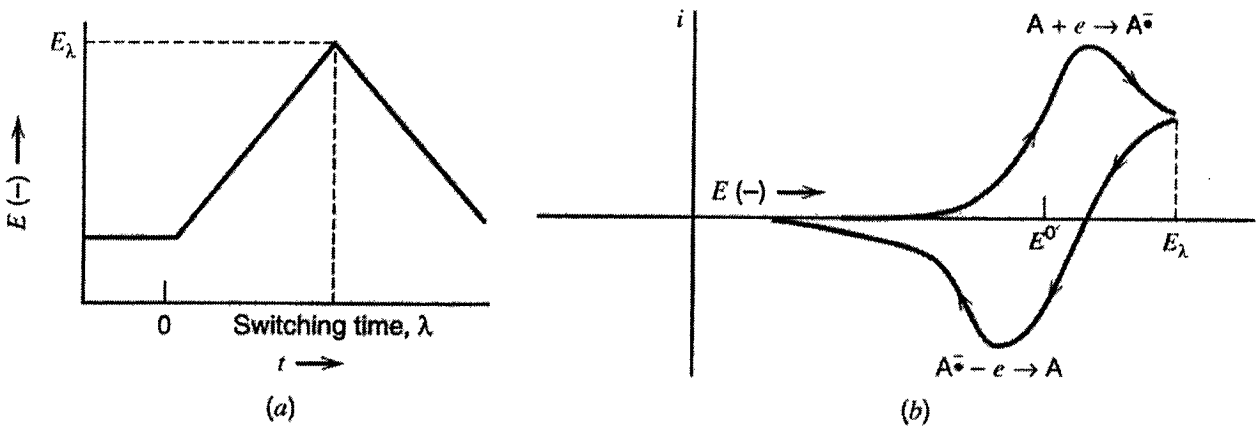

Figure 4 (a) Cyclic potential sweep, (b) Cyclic voltammogram

The kinetic behaviour of the Nernstian system, as exemplified by process (15), under diffusion-control, can be treated for conditions where semi-infinite linear diffusion obtains, giving a current defined by:

$$i = nFAC_0(\pi D_0)^{\frac{1}{2}}\chi(\sigma t) \tag{16}$$

where n is the number of electrons transferred in the redox process, F is the Faraday number (96 485 C mole^{-1}), A the surface area (cm^2), c_0 the concentration of the solution (mole cm^{-3}), D_0 the diffusion coefficient (cm^2 s^{-1}), σ is (nF/RT)v and v is the sweep-rate (V s^{-1}). At any given point, $\chi(\sigma t)$ and hence the current, gives the functional relationship between the current at any point on the curve and the variables. Actually, i is proportional to c_0 and to $v^{1/2}$. The solution of this equation has been provided numerically by Nicholson and Shain [36]. The

general results of solving this equation is a set of values of $\chi(\sigma t)$ as a function of $n(E-E_{1/2})$. The half-wave potential, $E_{1/2}$, is defined as the potential at the point, on the rising part of a voltammetric wave, where the difference between the total current and the residual current is equal to one half of the limiting current. From these calculations, the function $\chi(\sigma t)$ reaches a maximum where $\pi^{1/2}\,\chi(\sigma t) = 0.4463$.

Then the current i reaches a peak value, i_p given by:

$$i_p = 0.4463nFAC_0D_0^{1/2}\sigma^{1/2} \tag{17a}$$

or

$$i_p = 0.4463nFAC_0D_o^{1/2}\left(\frac{nF}{RT}\right)^{1/2}\nu^{1/2} \tag{17b}$$

or

$$i_p = 2.68\times10^5\left(n^{3/2}AD_0^{1/2}C_0\nu^{1/2}\right) \tag{17c}$$

The corresponding peak potential, E_p, can also be found according to the following equation where:

$$E_p = E_{1/2} - 1.109\frac{RT}{nF} \tag{18}$$

1.2.2 Cyclic voltammetry at the Au electrode

Throughout this study, cyclic voltammetry and potentiostatic techniques have been combined to control anodic oxide film growth at Au in 0.5 M $HClO_4$ and in 0.5 M in H_2SO_4, and its reduction. During the process of the electrode preparation, prior to electrochemical measurements, the Au electrodes were first cycled during 2 hours between 0.05 and 1.70 V(RHE) to relieve any stress from the surface region. After this treatment, the surface state of the Au electrodes was found to be stable, i.e. it did not show any further changes in time as could be observed from the oxide formation/reduction CV profiles, which maintained their

characteristic constant forms. The shapes of the CV profiles also indicated that both the solution and the electrodes were free of impurities (cf. ref. [18]).

The capacitance of the electrical double-layer at an unoxidized Au electrode can be calculated from the voltammogram recorded over the appropriate potential range where no surface oxidation or reduction takes place and no Faradaic solution decomposition arises. Oxide film formation on Au usually begins around a potential of 1.35 V (RHE). Below this potential, the CV shows a region for only charging of the double-layer. By integration of the CV, the charge accumulated at the interface of the electrode over the studied range of potential can be accurately found. Therefore, the capacitance can be calculated with the aid of Eq. 11. For potentials above 1.35 V (RHE), oxide film growth becomes significant and Faradaic oxygen evolution can also practically occur above 1.80 V (RHE) (theoretically above E = 1.23 V at standard pH). The charge given by the integration of the voltammogram corresponds therefore to two processes in parallel: oxide-film formation and double-layer charging at the oxide film. The capacitance cannot then be calculated as for the unoxidized region.

As noted earlier in the introduction, extrapolation of the current response at the unoxidized surface region into the oxide region has usually been made in earlier work in the literature but is clearly unsatisfactory and values of capacitance of the same order or magnitude were calculated. The aim of the present work has been to *independently* measure the values of capacitance over the oxide potential region using a different and direct technique, *electrochemical impedance spectroscopy*, and hence establish if the extrapolation assumption is valid or not.

1.2.3 Cyclic voltammograms for Faradaic surface processes

A different class of interfacial surfaces processes arises when very thin, initially monolayer, films of e.g. oxide or H are Faradaically deposited (or, in reverse, desorbed) over a range of anodic or cathodic currents and corresponding potentials. Usually these are *not* diffusion controlled, so their study by cyclic voltammetry or DC charging curves is simpler than for the situation treated in Section 1.2.1 above.

A one-electron Faradaic deposition process leading to e.g. a monolayer of electrosorbed H (e.g. UPD H at Pt) or of OH species (e.g. at Pt or Au) requires a specific charge of 210 $\mu C\ cm^{-2}$ (real) [30]; for a monolayer of O species, as involved in the present work at Au, the charge requirement is 420 $\mu C\ cm^{-2}$ (real). These figures are estimated for polycrystalline but annealed surfaces of Pt or Au. They give an idea of the great sensitivity of electrochemical DC charging or CV experiments in which 10% of a monolayer can be measured with a ca. 2% accuracy and various changes of coverage, e.g. by H or O ad-species, can be followed with similar accuracy.

Application of CV to study of oxide-film formation and reduction at noble metals such as Pt, Rh, Ru, Pd, Au has provided a large body of precise information on the electrochemical surface science of the initial stages of anodic oxide film formation or reduction at such metals [7].

Cyclic voltammetry has provided the most sensitive procedure for studying such surface electrochemical processes as it leads to a "differential" response function to the modulation signal applied at a rate dV/dt, having the form of a pseudocapacitance $C_\phi = dq/dV$, for the potential dependance of the quantity (as charge, q) of Faradaically electrosorbed (or desorbed) species such as H, or OH or O species in the cases of anodic 2-d oxide-formation at noble metals.

Then, for cyclic voltammetry, the response function, *i*, is

$$i = C_{\phi} \frac{dV}{dt} \tag{19}$$

$$= \left(\frac{dq}{dV} \right) \frac{dV}{dt} = \frac{dq}{dV} v \tag{20}$$

where v is again the voltage sweep-rate in Vs^{-1}. The overall charge passed between two potential limits, V_2 and V_1 can then be accurately determined by integration of the CV response-function between the experimentally selected limits. The CV, in effect, provides a direct differential plot of the charging curve function q(V), the slope of which is formally a capacitance quantity, dq(V)/dV.

In an important part of this work, the CV procedure, thus analyzed, has been applied complementary to: a) EQCN measurements (section 1.4) and b) EIS measurements (section 1.3). It provides the high sensitivity required to characterize the charge, mass and pseudo-capacitance behaviour of the 2-dimensional, sub-monolayer processes involved in the initial stages of formation of anodic oxide films at noble metals (here Au), and their reduction. Note that unlike charging and discharging of the double-layer, which is largely reversible, formation or reduction of monolayers of oxide species are not reversible on the potential scale but are with respect to anodic/cathodic charge balance except when oxide films or metal dissolution occurs.

1.3 Electrochemical Impedance Spectroscopy (EIS) for capacitance measurements

A complementary way to study the electrical interfacial behaviour of a system is to perturb the latter with a sinusoidal alternating signal of quite small magnitude (ca. ± 5 mV) and observe how the system responds to this perturbation at an otherwise steady-state. In the

present work, the steady-states of the system were achieved both before and after the formation of the oxide films. Many advantages arise from this technique. High precision measurements can be achieved from a relatively sensitive experimentation procedure, conducted over a wide range of frequencies, i.e. 10^{-2} to 10^{5} Hz. In deriving the theory of impedance spectroscopy, analogies are commonly made between the interfacial processes involved in electrochemical cells and networks of resistors and capacitors that can represent the electrical behaviour at electrodes of the cell. Electrochemical Impedance Spectroscopy is the name of an impedance technique where a three-electrode cell is used in the usual manner, and a DC-potential program is imposed on the working electrode, in our case, an holding potential, E_H, on which is superimposed a sinusoidal component, E_{ac}, of approximately 5 mV peak-to-peak amplitude. The measured responses are the magnitude of the thus generated AC component of the current and also its phase-angle with respect to phase of the applied AV modulation signal. The major role of the DC potential is to set at some stable fixed value the mean surface concentration of oxidized, O, or reduced, R, species, or, in the present case, the state of the unoxidized Au surface or of the anodically formed oxide film.

If we consider the time-dependence of a purely sinusoidal voltage E, as

$$E = \dot{E} \sin \omega t \tag{21}$$

where ω is the angular frequency, which is 2π times the conventional frequency in Hz (s^{-1}). It is convenient to represent this voltage as a rotating vector (phasor). The amplitude of this phasor is represented by $\dot{E}$ and its frequency of oscillation is ω. A useful relationship to consider is that between the two sinusoidal signals, the potential E and the current I. Each of them are also represented by a phasor, $\dot{E}$ and $\dot{I}$, respectively, which rotate at the same frequency but are not in phase. The phasors will be separated by an angle termed the *phase*

angle, ϕ, measured relative to the potential phasor, $\dot{E}$. Therefore, the current can be represented by the following relation:

$$I = \dot{I}\sin(\omega t + \phi) \tag{22}$$

where ω again represents the frequency and ϕ the phase angle. Figure 5 represents the relation between the current and the potential phasors as described above.

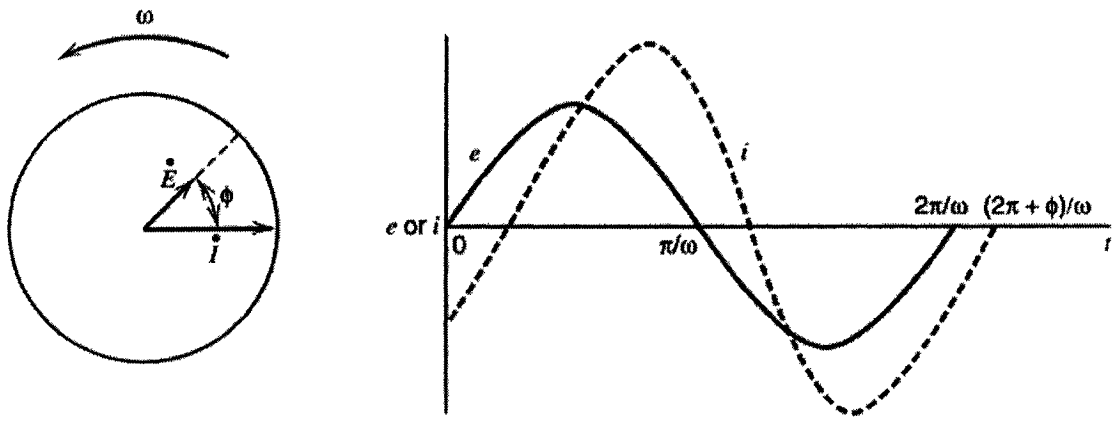

Figure 5. Phasor diagrams showing the relation between E and I

These concepts can be applied to analyze a simple circuit composed first, of a single resistance, R. If a sinusoidal voltage of ca. 5 mV peak to peak, is applied across the resistance, R, the potential should be defined by Eq. 21. The alternating currents that cross R obey Ohm's law are hence E/R or at any time in the cycle:

$$\dot{E} = \dot{I}R \tag{24}$$

In this situation where only a pure resistance is present, the value of the phase angle is zero. On the other hand, in a circuit comprising a single capacitor, the current response measurements will differ from those arising with a pure resistor circuit. The capacitance, C, of a pure capacitor is defined by the relation q = CE from which the charging current can be expressed giving:

$$I = C\left(\frac{dE}{dT}\right) \tag{25}$$

i.e from Eq. 21: $$I = C\omega E\cos\omega t \tag{26}$$

or $$I = \frac{E}{X_C}\sin\left(\omega t + \frac{\pi}{2}\right) \tag{27}$$

where X_c is the capacitive reactance and represents $1/C\omega$. In this situation, the phase angle between the current and potential phasors is $-\pi/2$ or -90°. Because the vector diagram is expanded in a plane, it is useful to represent phasors in complex notation. All components along the ordinate axis are said to be imaginary and thus multiplied by j, = $\sqrt{-1}$, and the components along the axis of abscissae are real. Both types of components are "real" and thus can be measured but to handle mathematically such values, complex numbers are needed and used. Therefore, in a circuit containing a pure capacitor, the voltage phasor can be expressed as $\dot{E} = -jX_c\dot{I}$. We now consider a simple circuit composed of a resistor in series with a capacitor where a potential E is applied across the whole circuit. The summation of potentials across the capacitor, E_c and the resistance, E_R must equal the overall circuit potential, i.e. :

$$E = E_R + E_C \tag{28}$$

or $$E = \dot{I}(R - jX_C) \tag{29}$$

which can be written as $$E = \dot{I}Z \tag{30}$$

where Z is called the impedance. In Eq. 30, it is seen that the current is linked to the potential by a vector Z. The latter vector has two impedance components said to be the real part, Z_{Re} that is equal to R and the imaginary part, Z_{Im} that equals $-jX_C$, from Eq. 31. The magnitude of the impedance Z, usually found in impedance works, is represented by $|Z|$. It is given by the following equation where:

$$|Z|^2 = (Z_{Re})^2 + (Z_{Im})^2 \quad (31)$$

or, in convenient abbreviated form:

$$|Z|^2 = (Z')^2 + (Z'')^2 \quad (31a)$$

1.4 Electrochemical Quartz Crystal Nano-balance for surface mass changes

The so-called Electrochemical Quartz Crystal Nano-balance (EQCN) technique has been first used in electrochemical surface science for studies of thin metal, e.g. Pt, Au, films at electrodes evaporated on a quartz single-crystal resonator. In this section will be described the use of this technique to measure mass changes in situ at an electrode surface in contact with an electrolyte solution that arise during an electrochemical process and to study the associated interfacial phenomena. The EQCN technique was created after the discovery that quartz crystals can be made to controllably oscillate when they are immersed in a liquid phase and not only in the gas phase. The so-called Quartz Crystal Microbalance was first used by Sauerbrey [37] in 1959 for the study of the rate of deposition of thin films in an ultra-high vacuum system. Several years later, a group of scientists leaded by Nomura [38] demonstrated the use of the quartz-crystal microbalance for mass measurements in a liquid during an electrochemical experiment. When the latter technique is used *in situ* with an electrochemical procedure, simultaneous monitoring of the electrochemical parameters by voltammetry and the mass of the electrode is possible. Under such conditions, nano-scale (N) changes of mass can be recorded, thus leading to the term "EQCN" for the instrument. This combined technique provides ultra-high sensitivity of electrochemical surface-science measurements including charge/mass ratios for sub-monolayer processes.

Jacques and Pierre Curie discovered the piezoelectric effect in 1880. They found that when a mechanical stress was applied to a quartz surface, a corresponding electrical potential is generated across the crystal and was proportional to the initial stress applied. A little later, they found that this effect was reversible. Actually they observed that if a voltage is applied across the quartz crystal, a mechanical stress arose, giving rise to physical deformation along the direction of the applied field. They named this effect the converse piezoelectric effect. This effect is the basis of the EQCN technique in which a potential is applied across an oscillating quartz crystal. A quartz crystal can be sliced at various angles across the crystallographic axes in order to obtain different properties. The most common type of quartz cut used in the surface science field is the so-called AT- cut which is achieved by slicing through a quartz crystal at an angle of 35°15' with respect to the x-axis. The AT-cut is usable at high frequencies and provides high-temperature frequency stability and is available at a reasonable cost. All these factors explain why this cut is the most popular. This quartz cut oscillates in a shear mode and the fundamental frequency of vibration of the AT-cut is inversely proportional to the crystal thickness. With a thickness of 0.132 mm, a frequency of 10 MHz can be attained but if higher frequencies are needed, thinner crystals are required but would be too thin to be handled without risk of damage.

The relationship between the frequency and the mass changes was developed by Sauerbrey:

$$\Delta f = -2 f_0^2 \left(\mu_q \rho_q\right)^{\frac{1}{2}} \frac{\Delta m}{A} \tag{32}$$

where Δf is the frequency shift, f_0 is the frequency of the crystal before a mass change and Δm is the mass change, A is the piezoelectric active surface area of the quartz crystal, μ_q is the shear modulus (2.947×10^{11} g cm^{-1} s^{-2}) and ρ_q is the quartz density (2.648 g cm^{-3}). If mass is

deposited or removed from the electrode, this linear relationship very accurately describes the frequency change. In addition to mass effects, the measured frequency shift, Δf, of the EQCN can be a result of several other identifiable factors. For example, interaction of an electrode with a medium of different viscosity can affect the Δf. This factor is usually neglected if the viscosity of solution is constant during the electrochemical experiment. Surface roughness, pressure and temperature can also have significant effects on Δf. These factors will be discussed in detail in chapter 3 for the interpretation of results obtained through the present study.

Chapter 2 Experimental

2.1 Conditions for formation and stability of thin anodic Au oxide films on Au

One of the two principal sections of the present work (see Part I) is addressed to determination of the difference of double-layer capacitance at oxide-film covered Au electrodes compared with that at oxide-free Au metal surfaces over a lower range of potentials in aqueous H_2SO_4 and $HClO_4$ electrolytes. Double-layer capacity measurements on oxide films formed anodically at Au are meaningful only a) if the state of formation or reduction of the film is stable in time, i.e. during the required duration of capacitance measurements involved in impedance spectroscopy measurements, and b) if the potential range for pseudocapacitative responses that can arise at low oxide coverage is avoided, or otherwise evaluated.

In the present work, oxide films were formed anodically at polycrystalline Au electrodes under the following well-defined conditions. Oxide films, stable in time, were generated at high-purity (99.99%) Au electrodes in aqueous H_2SO_4 or $HClO_4$ by application of a linear, positive-going potential sweep at 50 mV s^{-1} up to a series of constant, potentiostatically-controlled potential limits, E_f (the "formation potentials"), between 1.80 and 2.20 V vs. RHE for various recorded times. Purified N_2 was bubbled during this procedure to displace any anodically evolved O_2, which necessarily accompanies oxide film formation that detectably commences beyond ca. 1.34 V vs RHE. The anodically formed film was characterized by the reduction-current response to application of a negative-going potential sweep at 50 mV s^{-1}. The charges required to reduce these oxide films to Au metal varied from that corresponding to 1 to several hundreds of O-monolayers in thickness, as determined by a

comparison with the charge for reduction of a single monolayer of oxide formed (calculated in terms of O species using the procedure of Burshtein et al. [39]) by cycling at 50 mV s^{-1} between 0.05 and 1.70 V, RHE. The same conditions were also used to form stable oxide films in aqueous $HClO_4$.

2.1.1 Instrumentation employed in the work

A Solartron S1287 electrochemical interface and 1255 HF frequency-response analyzer were used in conjunction with CorrWare for Windows and Zplot for Windows software programmes (Scribner and Associates, Charlottesville, VA) to conduct both CV and EIS experiments. The latter were primarily for evaluation of the double-layer capacitance or its equivalent in the constant-phase elements required to represent the results.

The real surface area was determined by taking the charge for monolayer O deposition as 400 $\mu C\ cm^{-2}$ according to the method of Burshtein et al. [39]. Impedance spectra, based on the standard ± 5 mV potential modulation, were recorded over a frequency range of 100 kHz to 10 Hz. All potentials were measured with respect to a Pt RHE immersed in the same electrolyte but in a separate compartment provided with a Luggin capillary.

2.1.2 Choice and purity of electrolyte solutions

All experiments were conducted at 298 K in 0.5 M H_2SO_4 and 0.5 M $HClO_4$. Solutions were prepared from SEASTAR double-distilled H_2SO_4 and SEASTAR double-distilled $HClO_4$ in nanopure water (18.4 MΩ cm), respectively. Electrolyte solutions of KCl, to provide added Cl^- anion in some experiments, were prepared from the research grade, 99.999% salt (Aldrich Chem. Co.). "Stock" solutions of KCl were prepared in 0.5 M H_2SO_4 and 0.5 M $HClO_4$.

Electrolyte solutions of NaBr (99.99% salt, Aldrich Chem. Co.) were also prepared under the same conditions for experiments with added Br^- ion.

All experiments were conducted in a Pyrex, three-compartment electrochemical cell, which was pre-cleaned according to well-established procedures [40]. During the experiments, pre-cleaned H_2 gas was bubbled through the compartment containing a Pt/Pt-black reference electrode. High-purity N_2 was passed through the working electrode compartment. The Pt counter-electrode was contained in a separate compartment through which N_2 was also bubbled.

2.1.3 Impedance measurements at the oxide-free Au metal surface

A first series of cyclic voltammetry (CV) and electrochemical impedance spectra (EIS) measurements was conducted on a *non-oxidized* Au surface in each of aq. 0.5 M H_2SO_4 and 0.5 M $HClO_4$ solutions containing Br^- or Cl^- at 0 and 10^{-3} M concentrations over the potential range 0.05 to 1.30 V. In this series of experiments, the Au electrode was cycled at 50 mV s^{-1} between the potential limits 0.05 and 1.30 V, *i.e.* up to the potential where oxide is just beginning to form. [6, 19] The potential was then stepped to 0.10 V, held for 2 minutes, after which an EIS experiment was performed; the potential was then stepped to 0.20 V, held for 2 minutes following which a further EIS experiment was conducted. This procedure was repeated with EI spectra being collected every 100 mV up to 1.30 V, i.e. over a range of potentials for which the Au surface remains oxide-free.

2.1.4 Impedance measurements at the oxide-covered Au surface

From the well known hysteretic behaviour between formation and reduction of oxide films at Au and Pt, once a film has been formed at a given potential, diminution of potential to a lower value, but above that for onset of oxide reduction, results in a film that undergoes no detectable continuing formation in time. This is the condition required for EIS measurements on a stable oxide-film at controlled potentials requiring a duration of ca. 5 minutes.

The sequence of applied potential changes in experiments conducted to determine the double-layer capacitance at oxidized Au surfaces in the absence of added Cl^- or Br^- was as follows. The oxide was formed in 0.5 M H_2SO_4 or 0.5 M $HClO_4$ by application of a linear, positive-going, potential sweep at 50 mV s^{-1} to a selected, constant controlled potential limit, E_f, between 1.80 and 2.20 V. The potential was then held at those E_f values for selected periods of time (30 sec, 1 min, 2 min and 5 min) and then stepped down to 1.75 V, held for 10 min, after which an EIS experiment was performed; the potential was then stepped to 1.70, held for 2 minutes after which a second EIS experiment was conducted.

The arrests of potential at 1.75 V, following oxide-film formation up to 2.20 V, correspond to zero anodic or cathodic continuing passage of current and were introduced to enable any O_2, generated at the higher oxide formation potential, to be removed by bubbling of N_2, also avoiding any continuing change of extent of oxide film formation. The above procedure was repeated every 50 mV down to 1.45 V and provided very reproducible results. After completion of the EIS experiment at 1.45 V, CVs at 50 mV s^{-1}, were recorded between the potential limits of 1.45 to 0.05, and 1.70 to 0.05 V, i.e. into and through the region where the Au electrode becomes free from any oxide film. This series of experiments are termed "halide-free".

In a second series of experiments, Au oxide was again formed, as in the halide-free

experiment above. The potential was then stepped down to 1.75, held for 10 minutes during which time a required aliquot of "stock" Cl^- or Br^- solution was added to the cell, by means of a micrometer syringe, to give the desired concentration of Cl^- or Br^- anion, followed by an EIS experiment. The subsequent procedure was identical to that conducted in the "halide free" series of experiments described above. EI spectra were collected every 50 mV between 1.75 and 1.45 V. After completion of the experiment at 1.45 V, CVs were again recorded at 50 mV s^{-1}, between the potential limits of 1.45 and 0.05 V, and then up to 1.70 V and again down to 0.05 V

2.1.5 Circuit modeling for impedance analysis

Evaluations of data from the recorded impedance behaviour were made by means of fitting of equivalent-circuit models involving constant-phase elements (*CPE*: see below), and solution and faradaic resistances (R_s and R_f, respectively), as shown in Fig. 6, to the experimental results using Zview for Windows software (Scribner and associates, Charlottesville, VA). The *CPE* element shown in Figs. 6a, b and c is a simple distributed element [41] which produces a frequency-dependent impedance having a constant phase angle of $\phi = \varphi(\pi/2)$, where φ is the usual *CPE* parameter [41]. The impedance of this element is defined [1] as:

$$Z(CPE) = \frac{1}{T(j\omega)^{\varphi}} \tag{33}$$

A *CPE* impedance element, rather than a pure capacitance, was required, as at Pt [1], in this analysis as the $-Z''$ vs Z' response, represented in the complex plane, gave rise to almost straight lines but significantly oriented to the $-Z''$ axis with $|\phi| < \pi/2$ [42]. The *CPE* element describes a "leaking" capacitor of non-zero real and imaginary parts [43] resulting

from (*i*) microscopic roughness of the surface [42] and/or (*ii*) capacitance dispersion of interfacial origin [44].

Values of the components of the equivalent circuit model shown in Fig. 6a were fitted to the ω-dependence of the impedance data obtained between 1.75 and 1.45 V (RHE) for the oxide region in the absence of Cl^- and Br^- as well as for the oxide-free surface (0.05 to 1.30 V), both in the presence and absence of Cl^- or Br^-. The double-layer capacitance for the equivalent circuit model shown in Fig. 6a has been represented by Brug et al. [42] and a recent paper from this laboratory on Pt [1] in terms of the T and φ values in Eq. (33) above as:

$$C_{dl} = \sqrt[\varphi]{\frac{T}{R_s^{(\varphi-1)}}} \tag{34}$$

In the limiting case where φ approaches 1, T becomes a good approximation of C_{dl}. It is this derived double-layer capacitance which is plotted and analyzed throughout the present paper, as was also done in ref. 1 for the case of Pt.

Components of the model 2 (Fig. 6b) were fitted to the frequency-dependence of the interfacial Au-oxide impedance data obtained comparatively over the oxide region in the presence of Cl^- and Br^- in H_2SO_4 and $HClO_4$ solutions at potentials higher than 1.60 V.

a)

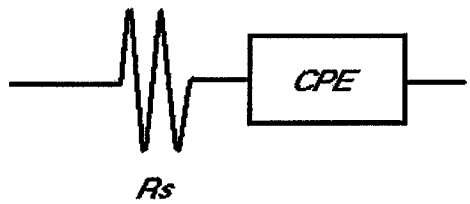

b)

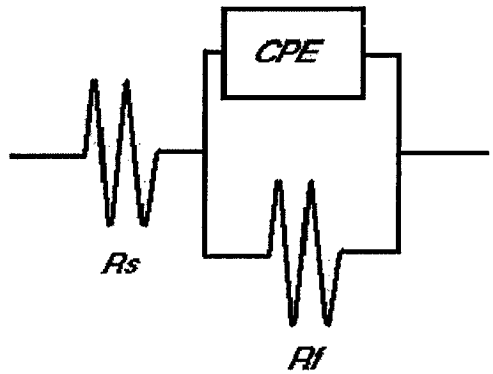

c)

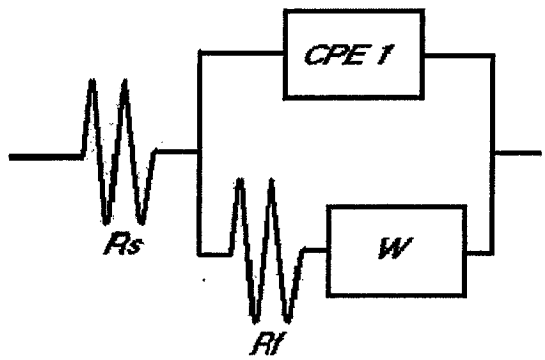

Figure 6. The equivalent circuits used; R_s = solution resistance; *CPE* = constant phase element; W = Warburg element; R_f = parallel faradaic resistance for: a) unoxidized and oxidized films in the absence of halide anions, b) oxide films in the presence of Cl^- or Br^-, for potentials between 1.60 and 1.75 V and c) for an oxide film in the presence of Cl^- and Br^- between 1.40 and 1.60 V (diffusion-controlled process involved).

The double-layer capacitance for the equivalent circuit shown in Fig. 6b may be derived from [42] as:

$$C_{dl} = \sqrt[\varphi]{\frac{T}{\left(\frac{1}{R_s}+\frac{1}{R_f}\right)^{(1-\varphi)}}} \tag{35}$$

which reduces to Eq. (34) for $R_s << R_f$.

Below this potential, down to 1.45 V, components of model 3 (Fig. 6c) were fitted to the impedance data. The latter model includes an additional distributed element of the Warburg, diffusional type (W). A significant change in the impedance behaviour was observed between 1.45 and 1.60 V in the presence of Cl^-/Br^- ions, resulting from the onset of a diffusion-controlled Faradaic process to be discussed in the later sections of this thesis.

2.2 Electrochemical and nanogravimetry measurements at Au electrodes

The potential of the Au electrode was repetitively cycled between +0.40 V and +1.70 V (RHE) at 50 mV s^{-1} during two hours in order to provide a first electrochemical cleaning of the surface and to ensure that good and reproducible cyclic voltammetry and nanogravimetry responses were obtained. Surface roughness of the electrodes was estimated by the method of Burshtein et al. [45], based on voltammetric evaluation of accommodation of electrosorbed O species up to supposed monolayer coverage attained at a critical minimum in the anodic response-current profile [45]. This procedure is the analogue, for Au, of that available at Pt by evaluation of accommodation of UPD H. The determined roughness factor for the EQCN electrode was 1.62 ± 0.02, which is sufficiently small that solution entrainment effects [46] could be neglected.

Thin oxide films in the so-called compact α-state [5] were generated at the Au electrode in 0.5 M $HClO_4$ by application of a linear, positive-going potential sweep at 50 mV s^{-1} to 1.80 V, RHE, the potential being then held at that value for 30s. The subsequent negative-going sweeps were arrested at a series of potentials at, and between, 1.75 V and 1.45 V vs RHE. The choice of these potentials is based on the fact that, following oxide film formation at 1.80 V for the controlled period of 30s, diminution of the potential down to values in that range leads to virtually zero Faradaic currents either for continuing oxidation or for onset of oxide film reduction which does not commence until ca. 1.25 V (RHE) when continuation of a negative-going sweep is initiated. These conditions are important for the present work and arise because the process of oxide-film reduction is highly irreversible with respect to oxide formation, a well known phenomenon in surface oxidation studies of noble metals [6]. This situation enables studies to be made of the stability of the α-oxide film on Au in Cl^- or Br^- solutions within the potential range 1.75 to 1.45 V (RHE) where no significant net Faradaic anodic or cathodic currents would otherwise be passing.

For study of the effects of presence of Cl^- or Br^- ions, these were added as KCl or NaBr, respectively, during a second holding period of 15 min in the above potential range. Current (i) and EQCN frequency changes (Δf) vs. potential (E) profiles were recorded digitally on two Nicolet 310 oscilloscopes during this holding time, and during the subsequent reduction of the oxide by a cathodic sweep at 50 mVs^{-1} in the presence of Cl^- or Br^- (10^{-3} M). The charge-density for oxide reduction was determined at the end of each experiment by integration of the i vs E profiles.

2.2.1 Instrumentation (EQCN) for nanogravimetry measurements

EQCN measurements were performed using a Seiko/EG&G Quartz Crystal Analyser (model QCM 917) connected to a Hokuto Denko HA501 potentiostat and Hokuto Denko HB 105 programmable function generator. The quartz crystals employed (diameter 2.5 mm) were of the AT-cut type, coated on both sides with vacuum-sputtered gold. The fundamental frequency of the crystal was f_0 = 8.9 MHz, the latter being measured with an accuracy of 0.1 Hz, a figure that can be converted to a weight-change (Δm) sensitivity of 0.56 ng cm^{-2}, based on Sauerbrey's equation [37]. The calibration constant value was experimentally obtained and critically discussed [47] in a recent paper, originating, in part, from a paper from this laboratory.

2.2.2 The electrochemical cell

In order to provide "reference data", each CV and corresponding EQCN profile was recorded 10 seconds before the addition of Cl^- or Br^- ion, at selected potentials. Experiments were conducted in a Pyrex, two-compartment, EQCN-type electrochemical cell [48] provided with a Pt/Pt-black hydrogen reference electrode in a separate compartment.

2.3 UV-Vis Spectroscopy

Absorption spectra required for optical characterization of dissolved Au III complex-ion species, arising in some experiements were determined by sampling the investigated solution of the electrochemical cell. The UV-Vis experiments were carried out using a Varian CARY 1E UV-Visible spectrophotometer. A scan rate of 300 nm min^{-1} was used during all the experiments.

Part I. Double-layer Capacitance at Au-metal and oxidized Au Surfaces

Chapter 3

3.1 Double-layer capacitance of the unoxidized Au interface

Figure 7 shows typical CVs initiated cathodically at 1.45 V (RHE) (point B in Fig. 7) obtained at polycrystalline Au electrodes on completion of impedance experiments detailed above, in 0.5 M $HClO_4$ and in the additional presence of 10^{-4} M Cl^- and 10^{-3} M Cl^-. Cl^- was added, as KCl, after the formation of the oxide (see section 2.1.4). These voltammograms are, as expected, substantially similar to those reported in the literature [3,4,5,8].

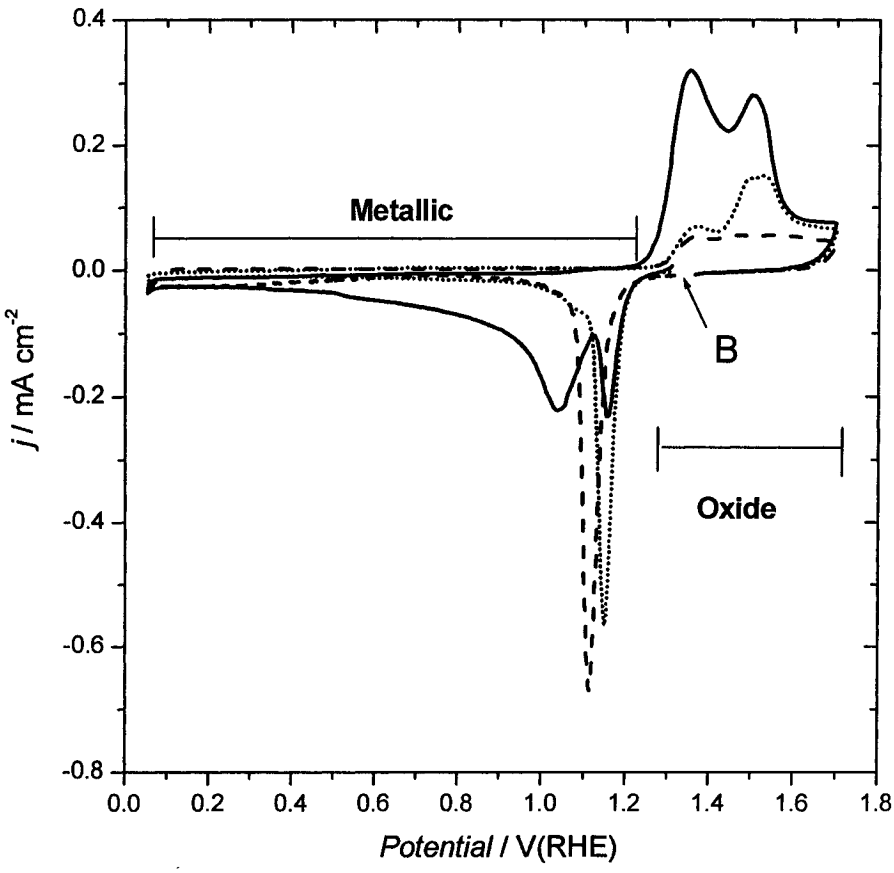

Figure 7. Cyclic voltammograms for polycrystalline Au electrodes in 0.5 M $HClO_4$ (– – –) and in 0.5 M $HClO_4$ in the presence of 10^{-3} M (·····) and 10^{-4} M Cl^- (——).

Figure 8a and Fig. 8b show, respectively, the double-layer capacitance derived from *EIS* experiments (employing Eqs. (34) and (35) as required and the circuit shown in Fig. 6a) and the usual CPE parameter, φ (defined in Eq. (33)) for the Au electrode in the non-oxidized state over the potential range 0.10 V to 1.30 V (RHE) in 0.5 M $HClO_4$.

Figure 8b shows that φ is, within experimental error, independent of potential over a range of 1.3 V. Qualitatively similar results were obtained in H_2SO_4 solutions.

Pajkossy et al. [49] have proposed the use of a more complicated circuit including adsorption resistance, Warburg (to describe diffusion-controlled adsorption) and adsorption capacitance components, in parallel with the double-layer capacitance component, to model the behaviour of metallic surfaces of Au electrodes in the presence of specifically adsorbed anions. Such a circuit was used to successfully model the impedance behaviour at Au (100) and (111) surfaces in the presence of Cl^-, Br^-, I^- and SO_4^{2-} anions for which the capacitance spectra in the Nyquist plane are mostly arc-shaped [49, 50]. They found, however, that under certain potential conditions the impedance, even at Au(111), cannot be characterized by such a model owing to the onset of capacitance dispersion attributed to the start of a new process or due to so-called "transition kinetics"[50].

The triangle symbols (Fig. 8a) represent the derived capacitance for the Au electrode in the absence of halide anions. Two humps are observed in the capacitance profile for both electrolytes. In $HClO_4$, the first hump is located ca. 0.10 V with a capacitance value of 60 (±2) $\mu F\ cm^{-2}$ and the second, located at 0.80 V, has a capacitance close to 66 (±2) $\mu F\ cm^{-2}$. The circle symbols (Fig. 8a) represent the capacitance of an Au electrode in the presence of 10^{-4} M Cl^- over the same range of potential, i.e. 0.10 to 1.30 V. An appreciable increase in the capacitance was observed. In $HClO_4$ solutions, containing 10^{-4} M Cl^- (Fig. 8a), the capacitance values at 0.10 V and 0.80 V were 130 and 175 (±5) $\mu F\ cm^{-2}$, respectively, corresponding to an

increase in the double-layer capacitance at polycrystalline Au at 0.80 V, by a factor of 1.90 due to the presence of Cl^- anions. In H_2SO_4, little change was observed at 0.10 V but again, an increase of capacitance by a factor of 1.87 (maximum of 86 μF cm^{-2}) was found in the presence of 10^{-4} M Cl^- at ca. 0.80 V RHE.

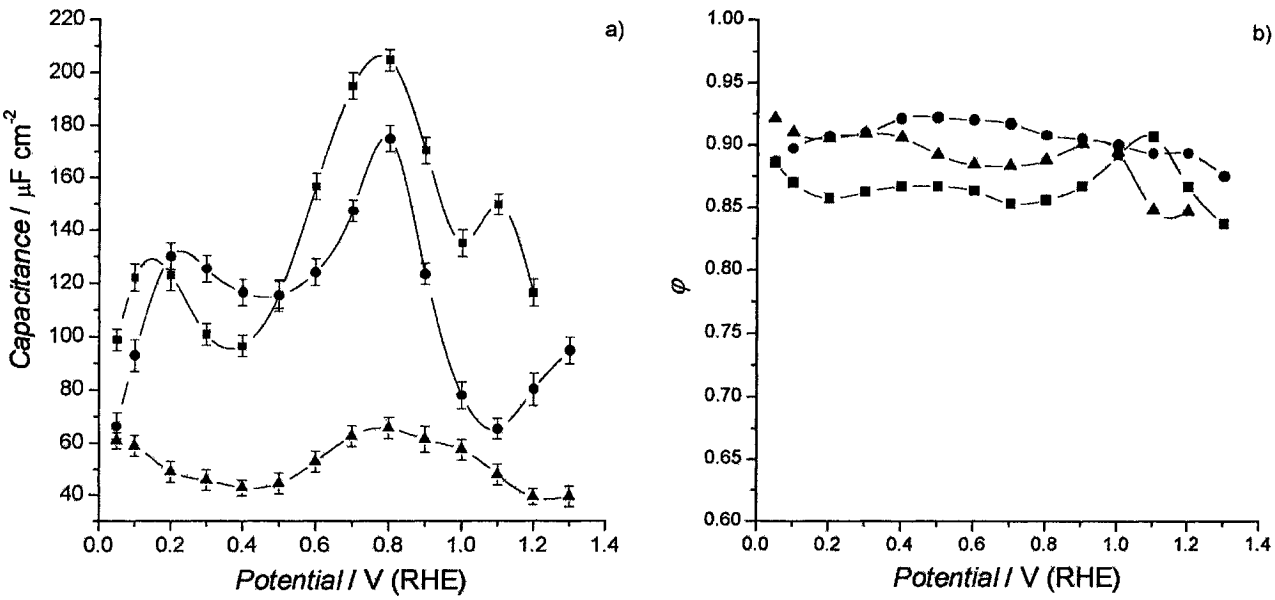

Figure 8. (a) Capacitance values measured for a series of potentials in the oxide-free, double-layer region (▲) without halide anions in 0.5 M $HClO_4$ and in the presence of 10^{-3} M (■) and 10^{-4} M Cl^- (●); (b) corresponding CPE φ parameter.

The square symbols in Fig. 8a represent the capacitance data for the electrode in the presence of 10^{-3} M Cl^-; values for both $HClO_4$ and H_2SO_4 electrolytes were higher than in 10^{-4} M Cl^- but each of the capacitance maxima remained, respectively, at ca 0.10 and 0.80 V (RHE). Values of 125 (±5) μF cm^{-2} for the first hump and 205 (±5) μF cm^{-2} for the second at 0.80 V in Fig. 8a were derived from the impedance measurements in 0.5 M $HClO_4$, corresponding to an increase by a factor of 2.1 and 3.1 over the respective values in the absence of halide anions. In 0.5 M H_2SO_4, 10^{-3} M Cl^- solution, relatively large increases of

capacitance were observed, as for $HClO_4$, values at 0.10 and 0.80 V being 150 (±5) μF cm^{-2} and 205 (±5) μF cm^{-2}, respectively, while values at 1.30 V were higher in the presence of Cl^- or Br^- anions for both concentrations, *viz* 10^{-4} and 10^{-3} M. These large capacitances may include a potential-dependent adsorption pseudocapacitance component, of the type discussed by Delahay [51] and in our own paper on Pt [1], that is unavoidably measured and coupled together with the double-layer capacitance. In the presence of such anions in solution, the potential of the "pre-oxidation" region [7, 52] of the Au electrode is shifted positively to 1.55 V, probably due to competitive Cl^- chemisorption with charge transfer [52]. Lack of detection of a "pre-oxidation" region film at 1.30 V in the presence of Cl^- is due to competitive adsorption by the latter (cf. refs.3 and 17).

3.2 Impedance results for the Au oxide interface

3.2.1 Comparative Behaviour in 0.5 M H_2SO_4 and 0.5 M $HClO_4$

Capacitance values were derived from impedance results, determined in 0.5 M H_2SO_4 and $HClO_4$, plotted as Nyquist diagrams with the components of the circuit models shown previously (Fig. 6) being fitted to the experimental data. The purpose of performing experiments in $HClO_4$ and H_2SO_4 (0.5 M) is to check if there is any specific anion adsorption effect of HSO_4^- compared with that of the isoionic ClO_4^- anion, as there is at the Pt (metal) interface. Fig. 9 shows the Nyquist and Bode representations of the EIS results obtained in 0.5 M $HClO_4$ in the absence of Cl^- or Br^- anions, for an oxide layer having a thickness of ca. 200 equivalent monolayers, formed at 2.20 V for 30 s but evaluated by EIS in the potential range 1.75 to 1.35 V (RHE) within which, importantly, no continuing oxide film growth or O_2 evolution takes place.

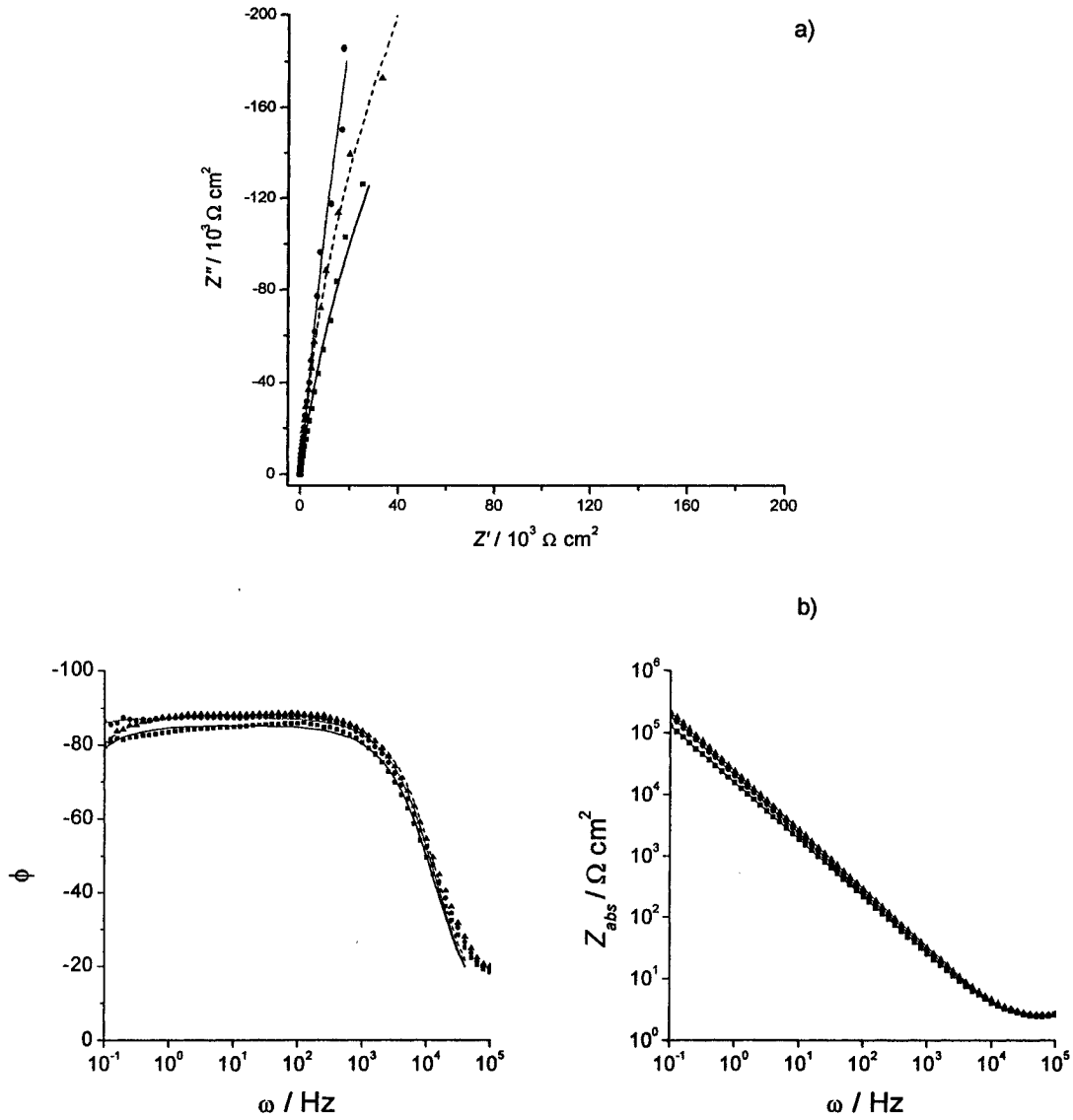

Figure 9. Nyquist (a) and Bode (b) diagrams for the impedance behaviour of the oxidized gold electrode. Oxide films were formed potentiostatically at 2.20 V for 30 seconds in 0.5 M $HClO_4$ at 1.75 V (▲), 1.55 V (●) and 1.35 V(■). Fitted data at 1.75 V (--), 1.55 V (·····) and 1.35 V (—) are also shown on the figure.

Qualitatively similar results were obtained for thinner oxide layers (1.5 equivalent monolayers, formed at 1.8 V for 30s) in both 0.5 M $HClO_4$ and 0.5 M H_2SO_4, and for oxide layers formed at 2.20 V (30 s) 0.5 M H_2SO_4. The near vertical Nyquist plots, and the low-

frequency phase-angle approaching -90 ° indicated an approach to pure capacitative behaviour of the oxide film in the absence of Cl^- and Br^- ions.

3.3 Behaviour in 0.5 M H_2SO_4 and 0.5 M $HClO_4$ in the presence of halide anions

Figure 10 shows Nyquist and Bode plots for the impedance behaviour of oxide films that had been formed at 1.90 V for 30 s in 0.5 M $HClO_4$ and then exposed to Cl^- ions at a concentration of 10^{-3} M. EI spectra were again collected at a series of successively decreasing potentials, beginning at 1.75 V (RHE) at which, in the absence of halides, no continuing oxide formation is taking place. Impedance data collected over the potential range 1.75 to 1.55 V (RHE) were best modeled by the equivalent circuit shown in Fig. 6b in which a Faradaic resistance is in parallel with a constant-phase element. The impedance results recorded between 1.75 V and 1.55 V show an increase of R_f (Fig. 6b) from 28 kΩ at 1.75 V up to 55 kΩ at 1.65 V and to ca. 100 kΩ at 1.55 V (RHE). Qualitatively similar values for R_f of 42 kΩ, 80 kΩ and 200 kΩ were found in 0.5 M H_2SO_4 for the same respective potentials.

The inset in Fig. 10a is the Nyquist plot recorded at 1.45 V (RHE). This EI spectrum is evidently dominated by a fundamentally different process from that occurring at more positive potentials. The Nyquist response tends to become semi-circular over the high-frequency region followed by a straight line, sloping at ca. -45°, at lower frequencies. The former is characteristic of a kinetically-controlled Faradaic reaction compared to the low-frequency region that is related to mass-transport control in a Faradaic reaction coupled with diffusion [43].

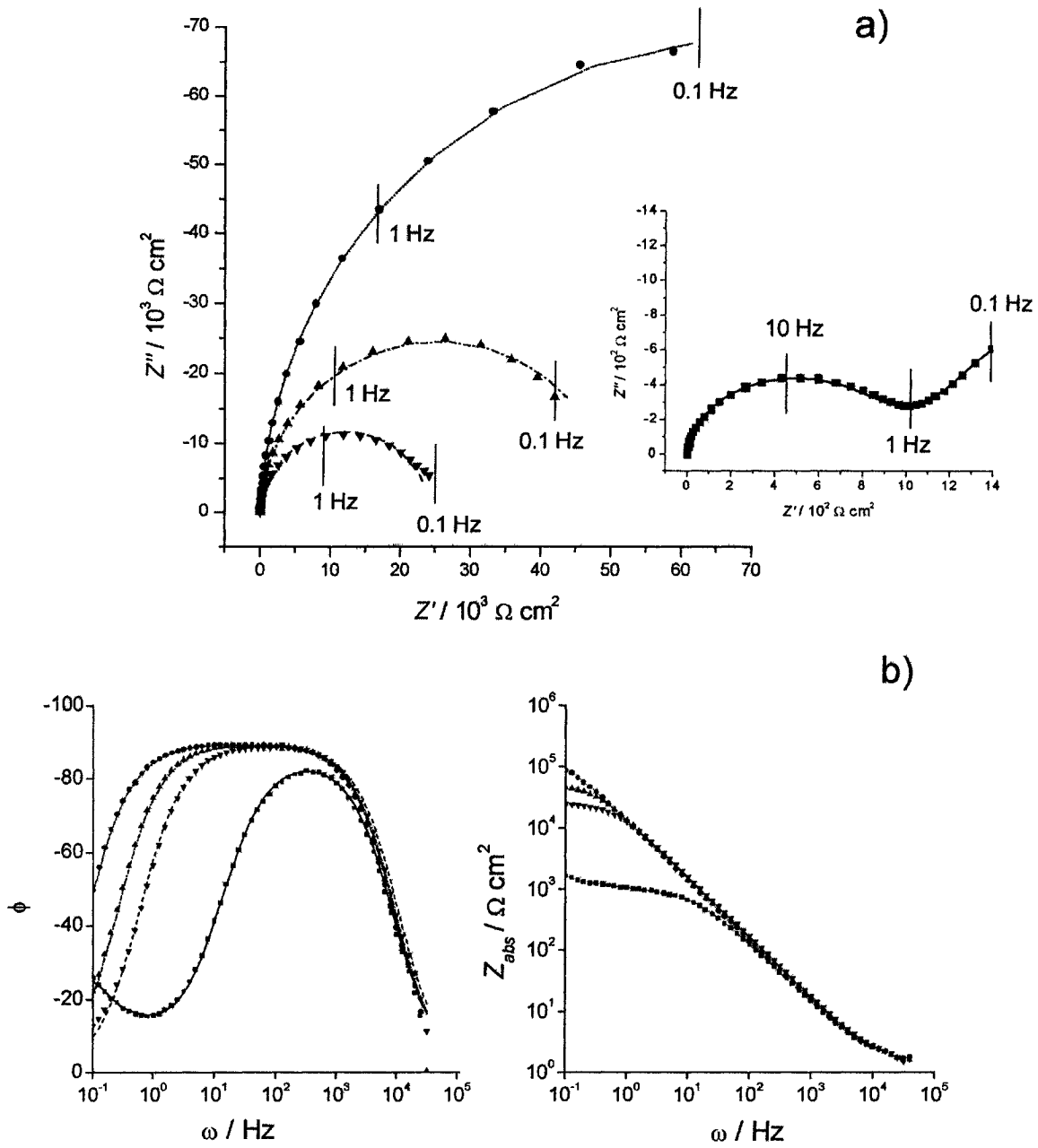

Figure 10. Nyquist (a) and Bode (b) diagrams for the impedance behaviour of the oxidized gold electrode in the presence of 10^{-3} M Cl^- for films were formed at during 30 seconds potentiostatic polarization at 1.90 V in 0.5 M $HClO_4$. Measurements were made at 1.75 V (▼), 1.65 V (▲) and 1.55 V (●). Insets in shows the Nysquist diagrams recorded at 1.45 V (■). Symbols show the experimental data, lines show how the experimental results are closely fitted to the parameters of the appropriate equivalent circuit (6b and 6c).

Previous studies made in our laboratory [21] and elsewhere [22], with Br^-, showed that dissolution of a gold electrode arises Faradaically in the presence of halide anions to a maximum extent at 1.45 V (RHE) which would explain the form of the impedance plots, exhibiting a -45° phase-angle at low frequencies.

Figure 11 shows Nyquist and Bode plots for a thick (ca. 200 nominal O monolayers) oxide film in the presence of 10^{-3} M Cl^-. The EIS responses at 1.75 V for oxides formed at 2.2 and 1.90 V are significantly different (cf. Figs. 10 and 11). The film formed at 1.90 V is primarily of the α-oxide type and that formed at 2.20 V, is the so-called β (hydrous)-oxide [53]. At 1.75 V, values of R_f of 90 k Ω for the $HClO_4$ solution, up to 240 kΩ for the H_2SO_4 solution arise (cf. 28 kΩ in Fig. 10, 42 kΩ in H_2SO_4).

For potentials of 1.65 and 1.55 V, values of R_f are, however, quite similar to those determined for thin films. Some dissolution (see below) of the β-oxide film that can occur in the halide solutions (see below) may account for the difference in EIS results at 1.75 V and lower potentials.

After formation of the thick film at 2.20 V, the potential was swept negatively to 1.75 V. Chloride ion (as KCl) was then added and the potential held for 15 minutes (at 1.75 V) to allow degassing of the solution from any O_2 evolved at the 2.20 V oxide-formation potential. Recent studies [21] in our laboratory have shown that dissolution of such oxide films takes place under these conditions during a period of 20 minutes or more.

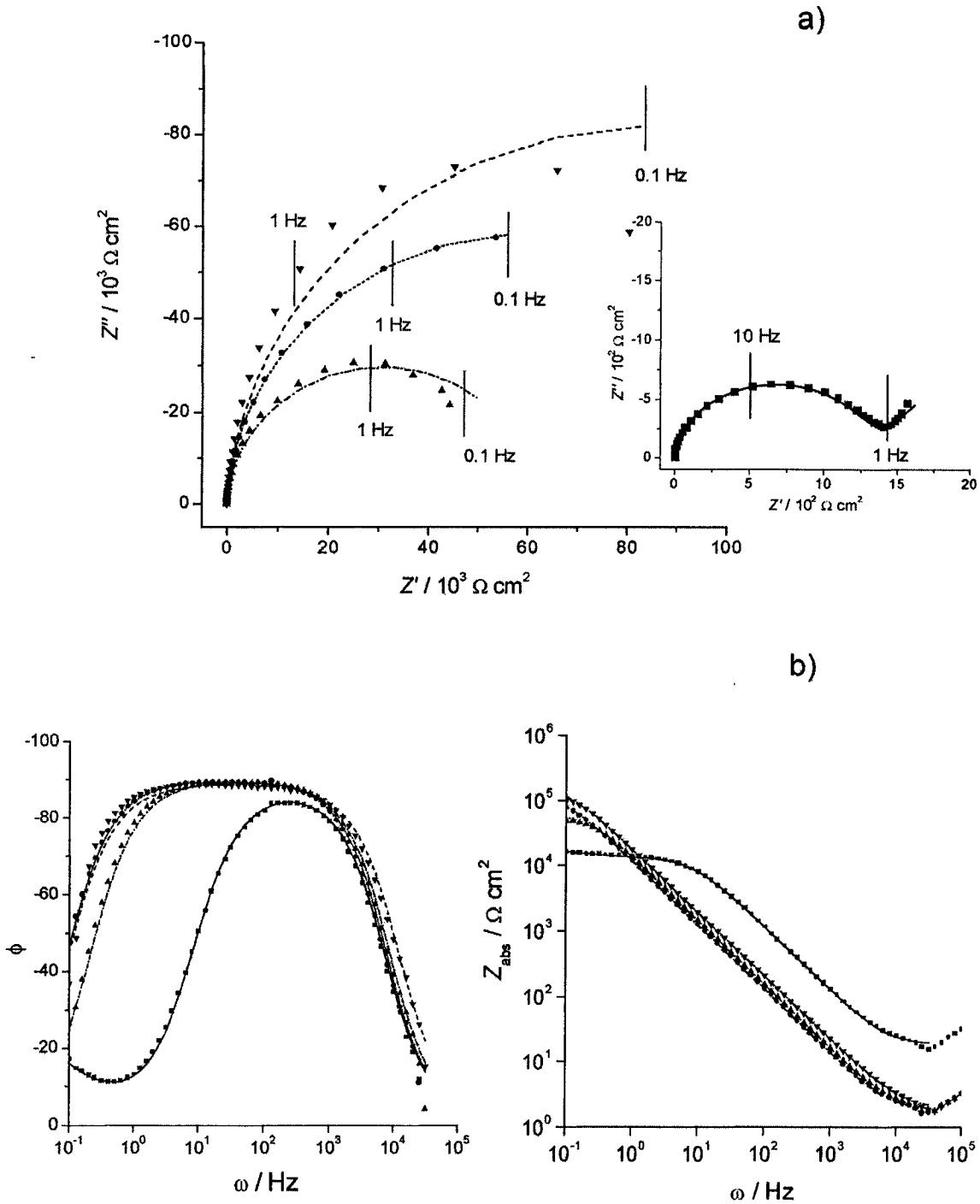

Figure 11. Nyquist (a) and Bode (b) diagrams for the impedance behaviour of the oxidized gold electrode in the presence of 10^{-3} M Cl^-. Oxide films were formed at 2.20 V during 30 seconds in 0.5 M $HClO_4$. Measurements were made at 1.75 V (▼), 1.65 V (▲) and 1.55 V (●). Insets in (a) shows the Nyquist diagrams recorded at 1.35 V (■), experimental data symbols; fitted data lines, as for Fig. 10.

The dissolution of the thick oxide is, however, not complete when the first EIS-impedance measurement is made (at 1.75 V), thus accounting for the results shown in Fig. 11. The duration of one frequency scan is 5 minutes. After the first impedance experiment, the potential was stepped down to 1.65 V and held for a further 5 minutes before a second EI spectrum was recorded. Approximately 25 minutes had elapsed since the addition of Cl^- before the second EIS experiment was begun. Over this time, ca. 90% of the hydrous (β) Au oxide film [5, 7, 53] that had been formed at 2.20 V had become depleted as indicated from the diminution of the charge under the oxide reduction peak in a subsequent cathodic sweep. The electrode then remained covered by a residual film of the compact (α) Au oxide which otherwise could have been directly formed at 1.90 V, as is confirmed by the similarity of EIS behaviour at 1.65 and 1.55 V. Thus, it is only the EIS recorded at 1.75 V (RHE) that is characteristic of the β-oxide surface.

Effects of Cl^- addition were also studied at concentrations of 10^{-4} M (Fig. 12). The impedance behaviour of thin oxide films in 10^{-4} M Cl^- solutions showed trends similar to those observed in 10^{-3} M Cl^- within the potential of range of 1.75 V to 1.45 V but, as expected, with different magnitudes of the responses. Thus, the R_f values were much higher for a thin film in contact with a solution of low Cl^- concentration and R_f values determined from EIS spectra of Au-oxide electrodes in H_2SO_4 are still higher than in $HClO_4$ solution.

Comparison of the EIS response at 1.35 V measured at both thin and thick oxide films in 10^{-3} M and 10^{-4} M Cl^- solutions is of interest. In solutions containing 10^{-3} M Cl^- at 1.35 V, the EI spectra are characteristic of a diffusion-controlled process while for solutions of 10^{-4} M Cl^-, under the same potential conditions, the response is that of a Faradaic reaction with diffusion effects being no longer observed. This may seem anomalous but arises because it is

only in the more concentrated Cl^- solution (10^{-3} M) that attack of Au as *metal surface* arises, as noted below.

Evaluation of the oxide-reduction charges following all EIS experiments shows that for thin oxide films in the presence of 10^{-3} M Cl^-, ca. 10 % of the oxide is dissolved during the course of the experiments, whereas in 10^{-4} M Cl^- only ca. 5 %, or less, of the oxide is dissolved. In solutions of 10^{-3} M Cl^-, areas of metallic Au are becoming exposed and it is these that become dissolved as $AuCl_4^-$ as recognized in ref. 54. Qualitatively similar results are observed at thick Au-oxide films where ca. 90 % of the oxide disappears during the EIS part of the experiment and again $AuCl_4^-$ is formed in a Faradaic process. The identity of the dissolved species was proven by means of spectrophotometry in the UV (see section 4.2.4 in Part II). However, further discussion of dissolution mechanisms is outside the scope of this part of the work.

Importantly, while there is evidence for a Faradaic reaction occurring at potentials positive to 1.35 V (RHE), the total charge passed over the potential range 1.75 to 1.45 V (RHE) was insufficient to account for the reduction of the thick oxide film; this suggests that dissolution of that oxide occurs through a *chemical* mechanism e.g. $AuO + Cl^- \rightarrow Au + OCl^-$ involving Cl^- ion in solution, analogous to that observed in the well known cases of oxidative reactivity of PbO_2 and MnO_2 in the presence of chloride [55].

Complementary EQCN studies of Au β-oxide films in contact with halide solutions are described in Part II of chapter 3. Preliminary results confirm that oxide dissolution occurs in the presence of halides since the electrode specific surface mass is found to decrease. The EIS response for thick Au-oxide films over the potential range 1.75 to 1.55 V in the presence of 10^{-4} M Cl^- differs, however, from that in a solution containing 10^{-3} M Cl^-.

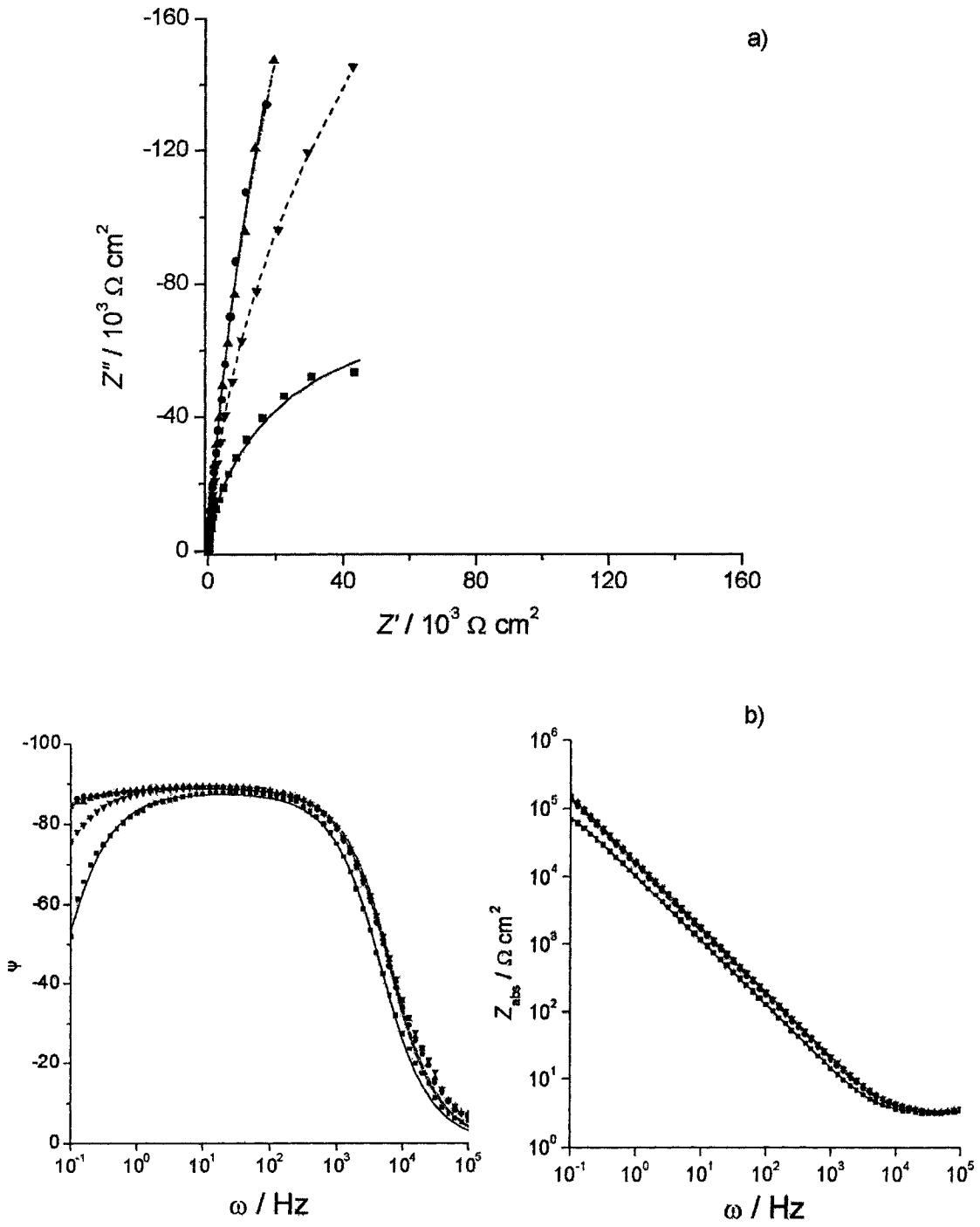

Figure 12. Nyquist (a) and Bode (b) diagrams for the impedance behaviour of the oxidized gold electrode in the presence of 10^{-4} M Cl^-. Oxide films were formed at 2.20 V during 30 seconds in 0.5 M $HClO_4$. Measurements were made at 1.75 V (▼), 1.65 V (▲), 1.55 V (●) and 1.35 V (■); experimental data symbols; fitted data lines, as for Figs. 10 and 11.

The response in 10^{-4} M Cl^- is more purely capacitative (as for oxide films in the absence of added halide anions) than that in 10^{-3} M [cf. the near vertical (Fig. 12) rather than semi-circular (Fig. 11) Nyquist plots, indicating onset of a Faradaic process]. The Faradaic process indicated by the EI spectra at oxide surfaces in the presence of Cl^-, at potentials positive to 1.40 V (RHE), may be tentatively assigned to residual anodic corrosion processes.

3.4 Double-layer capacitance values of the Au oxide interface

3.4.1 Behaviour in 0.5 M H_2SO_4 and 0.5 $HClO_4$

Figure 13 shows the derived double-layer capacitance values for a series of thin and thick Au oxide films formed anodically under potentiostatic conditions as described in section 3.1 for 0.5 M $HClO_4$ and also for 0.5 M H_2SO_4 acid solutions. The formed films were from near one to several hundreds of equivalent monolayers of O-species in nominal thickness. The results in Fig. 13 are for oxide films thus formed by polarizing the electrode at various potentials for a duration of 1 minute. For a thin oxide film formed at a potential of 1.80 V (RHE) in $HClO_4$ solution, in the absence of Cl^- or Br^-, capacitance values are represented by the square symbols in that figure. The nominal thickness of such a film is approximately 1.5 equivalent O-monolayers based on an observed reduction charge of 620 $\mu C\ cm^{-2}$. Capacitance values in the range 21 to 22 (± 1) $\mu F\ cm^{-2}$ were obtained. Values somewhat smaller, 18 to 19 (± 1) $\mu F\ cm^{-2}$, were derived for the H_2SO_4 solution for films formed at 1.80 V (RHE) and 1.45 V (RHE).

For an oxide film grown at 2.20 V for 1 minute in $HClO_4$ solution (◆, Fig. 13), lower capacitance values of 12 (± 1) $\mu F\ cm^{-2}$ at 1.75 V (RHE), up to 16 (± 1) $\mu F\ cm^{-2}$ at 1.45 V (RHE), were derived, with quite similar values for H_2SO_4 solution, viz 11 (± 1) $\mu F\ cm^{-2}$ at 1.75

V (RHE) compared with 14 (±1) μF cm^{-2} at 1.45 V (RHE). The thickness of such a film is approximately 40 nominal O monolayers, greater than that of the film formed at 1.80 V (ca. 1 ~ 2 O monolayers).

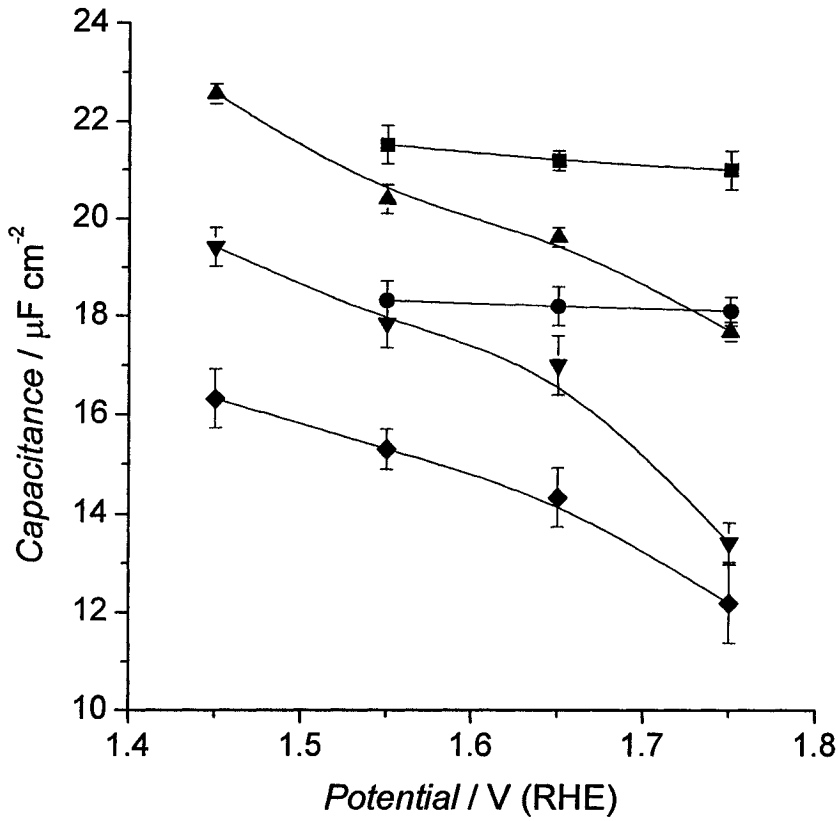

Figure 13. Capacitance values derived from EIS experiments at stable oxide films formed by anodic polarization at 1.80 V(■), 1.90 V(●), 2.00 V(▲) 2.10 V(▼), 2.20 V(◆) for 1 minute in 0.5 M $HClO_4$ corresponding, respectively to 1.48, 1.86, 2.19, 5.8 and 44.5 equivalent O monolayers.

Capacitance values were also determined for films formed at various potentials but for an oxide-formation time of 5 minutes. The films thus generated (ranging from 5 to 200 nominal O monolayers) are then, of course, thicker than those giving the results of Fig. 13. However, capacitance behaviour, qualitatively similar to that shown in Fig. 9 for thin (ca. 1 monolayer) films, was found, even for a film thickness of the order of few hundred nominal O-monolayers. For a film generated at 2.20 V (RHE) for 5 minutes in $HClO_4$ solution, the

values are again around 12 (±1) μF cm^{-2}. The reduction charge of this oxide film was 83 (±2) mC cm^{-2}, corresponding to an equivalent thickness of approximately 200 nominal O-monolayers on the Au electrode which may correspond to a structure having some porosity.

In Fig. 9, the results of the impedance measurements over the oxide region were presented in the form of Nyquist and Bode plots. Qualitatively similar Nyquist plots were obtained for oxide films formed in $HClO_4$ and H_2SO_4 solutions. Results were fitted according to the circuit model shown in Fig. 6a, as described earlier. A general result, based on these measurements at Au electrodes covered by a thin (1~2 ML) or thick (~200 ML) oxide films in the absence of halide ions, is that there is no major dependence of the interfacial capacitance on oxide film thickness. This means that the observed capacitance is *not* that of the oxide film dielectric itself, as in the case with the valve-metals bearing insulating films. Thus, at Au, the oxide-film is conducting (as indicated by the more or less normal-valued Tafel slopes observed for anodic O_2 evolution at Au) and hence exhibits an effectively infinite dielectric constant. Then, in series combination with the double-layer capacitance at the solution interface with the film, the dielectric capacitance of the oxide film does not influence the interphasial capacitance that is measured. It is for this reason that double-layer capacitance values for thick and thin oxide films are little dependent on film thickness and are determined only by the capacitance of the oxide / solution interface arising at the external surface of the films. That the oxide surface is conductive is indicated not only by the observed normal behaviour of Tafel polarization for O_2 evolution but also by ellipsometric studies at metallic and oxide surfaces. Thus, Ohtsuka found [56] that the complex refractive index of the oxide layer, simultaneously calculated, depends on its thickness, and concluded that the oxide layer is metallic or semiconductive. Furthermore, Tremiliosi-Filho et al. [57] determined that the ellipsometric parameters, Δ and Ψ, are shifted only 1 to 3° towards lower values upon

formation of the α-oxide and that the determined values for the complex refractive index for both metallic and oxide-covered gold electrodes differed by less than a third of an order of magnitude, thus confirming that the oxide film is conductive.

It is of interest that the double-layer capacitance at *oxidized* Au surfaces is within 15 % of the values at Hg in NaF [34] at potentials negative to the p.z.c., viz ca. 16 μF cm^{-2} which supports the view that, at the oxide film, anions of the electrolyte are not specifically adsorbed as is also indicated by radiotracer studies [23]. This is not surprising since the electronic bonding capacity of the atoms of the metal surface are already satisfied by their interaction with the inner O atoms of the film.

3.4.2 Behaviour in 0.5 M H_2SO_4 and 0.5 M $HClO_4$ in the presence of Cl^- or Br^- anions

Figure 14 shows capacitance data derived from impedance measurements conducted at several potentials for films having various thicknesses, in the presence of Cl^- anions. Here the oxide film was first formed at constant potential in the absence of Cl^-, after which the potential was stepped back to 1.75 V (RHE) and held for 15 minutes to allow degassing of O_2 from the solution and (as for the other experiments on oxide-free Au), termination of film formation, and also to inject a stock solution aliquot of Cl^- or Br^- (as the K^+ or Na^+ salts) over a range of concentrations, e.g. $10^{-4} \sim 10^{-3}$ M. Figure 14 shows results for films grown at 1.90 V for 1 minute. Data for 10^{-3} M of Cl^- are represented by the circular symbols and are similar to those obtained in the absence of Cl^-. The same trend in capacitance arose at oxidized Au electrode surfaces in 0.5 M H_2SO_4 solution in the presence of Cl^-. Qualitatively and quantitatively similar results were obtained in the presence of Br^-, with capacitance at the oxide film electrode ranging from 20 to 25 (±1) μF cm^{-2}.

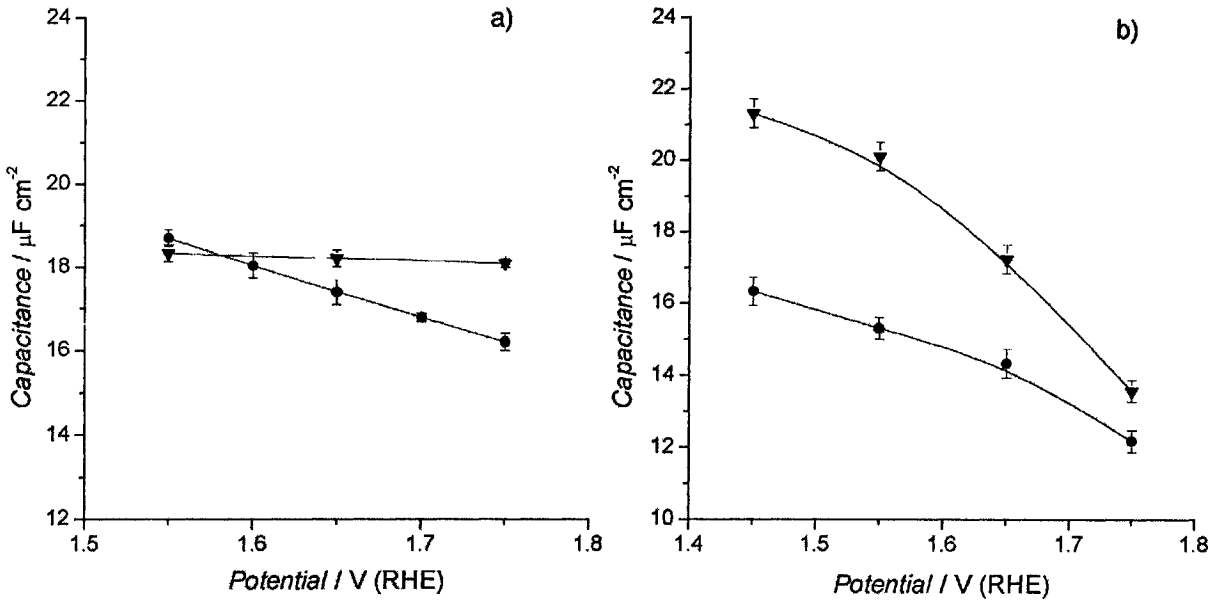

Figure 14. (a) Capacitance values derived for various potentials with (●) and without (▼) Cl^- anions present at 10^{-3} M concentration for an oxide film formed at a potential of 1.90 V for 1 minute in 0.5 M $HClO_4$ electrolytes (1.86 equivalent O monolayers); (b) capacitance values derived for various potentials with (●) and without (▼) Cl^- anions (10^{-3} M) for an oxide film formed at a potential of 2.20 V for 1 minute in 0.5 M $HClO_4$ electrolytes (44.5 equivalent O monolayers).

Figure 14b shows impedance measurements for thicker films grown at 2.20 V (RHE) for 1 minute. The resulting thickness of such films, prior to anion addition, was ca. 40 equivalent O-monolayers and were thus mostly composed of the hydrous, β-form, of gold oxide [53]. Again, capacitance values for Cl^- solutions were a little higher than those obtained in Cl^--free solutions, differences being on the order of 10 % for $HClO_4$ and 20 % for H_2SO_4 solution. The variation in capacitance becomes more significant as the potential becomes less positive in the case of H_2SO_4 solution. In the presence of Br^-, similar values were derived from the impedance experiments: 15 (±1) μF cm^{-2} at 1.75 V up to 22 (±1) μF cm^{-2} at 1.45 V in $HClO_4$.

Figure 15 shows a conveniently plotted recapitulation of the capacitance behaviour, comparing results at the metallic Au electrode surface with those for the oxidized Au electrode, with or without the presence of Cl^- ions in a 0.5 M $HClO_4$ solution. A strong influence of Cl^- or Br^- anions on the capacitance is observed at the non-oxidized Au electrode but only small differences arise when an oxide film covers the electrode, thus saturating the coordination capability of Au surface atoms for potential chemisorption of Cl^- or Br^-.

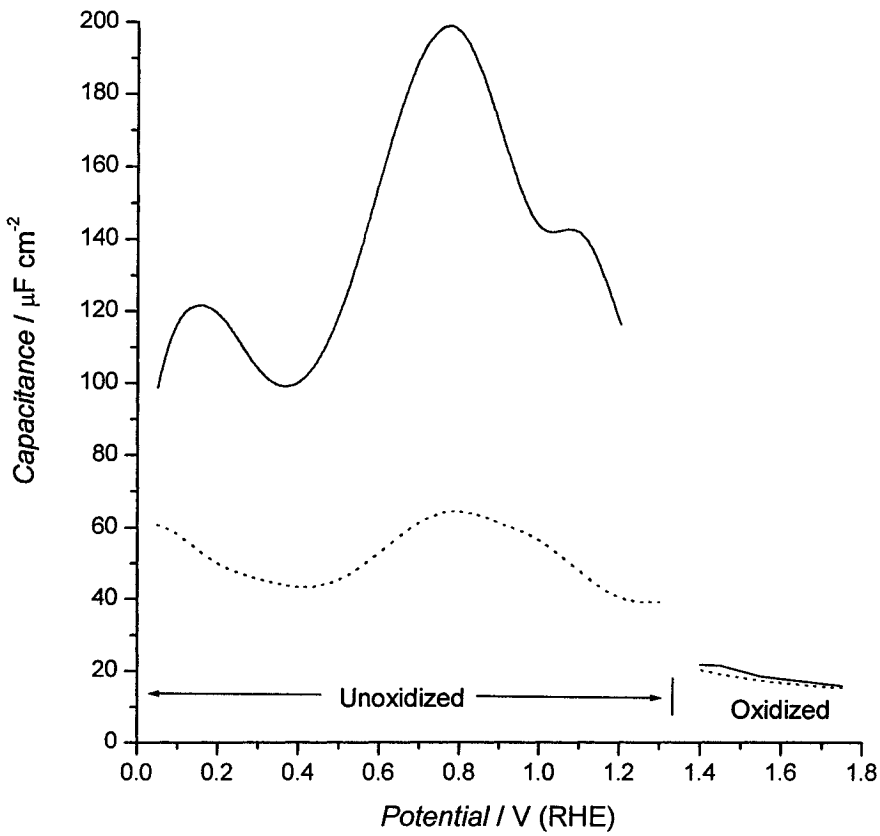

Figure 15. Combined diagram of the double-layer capacitance results as a function of electrode potential at Au metal and oxidized Au surfaces, with (—) or without (·····) Cl^- ions in a 0.5 M $HClO_4$ solution.

This figure illustrates the major transition of interfacial capacitance behaviour from that for the non-oxidized surface to that for Au bearing an oxide film. It is to be noted that the

substantial maxima in capacitance that arise both with and without Cl^- ion present, between 0.50 and 1.10 V in Fig. 14, is not due to a diffusional pseudocapacitance arising from Au dissolution since we have shown elsewhere [21, 22] that onset of such a process in the presence of Cl^- does not arise until a potential of at least 1.30 V is reached.

3.5 Comparison of impedance results for Au vs. Pt

EIS studies were recently performed in our group in regard to the study of the effect of halide anions at unoxidized and oxidized Pt electrodes [1, 3]. In the absence of halide anions, derived capacitance values for metallic Pt and Au electrodes are quite different from those at their respective oxides. Capacitance at the oxide films of both Pt and Au are relatively independent of the presence or concentration of Cl^- or Br^- anions, and were generally lower than those determined for the oxide-free metallic surfaces. The capacitance values at Pt oxide films were, however, higher by a factor of as much as 3 than those for oxidized Au electrodes, a result that could be due to pseudocapacitance, arising from a residual Pt^{2+}/Pt^{4+} redox reaction coupled with double-layer capacitance. However, the capacitance values at oxidized Pt surfaces decrease appreciably with increasing positive potential (70 down to 45 $\mu F\ cm^{-2}$ in 0.5 M H_2SO_4 [1]), more so than at the α-Au oxide, see Fig. 14.

The EIS response at metallic Au electrodes is complicated by the dissolution of Au at potentials negative to that for oxide formation and includes a diffusion-controlled Warburg component. Furthermore, in more concentrated halide solutions, Au oxide was also found to dissolve prior to the EIS experiments. The capacitance measured at metallic Au electrodes showed a dependence on the concentration of the two-halide ions in solution, as might be expected, on account of chemisorption. Thus at both the metal interfaces of Au and Pt, EIS results show evidence of specific anion adsorption not found at the oxidized metal surfaces for the reasons adduced earlier in this chapter. The results for both Au and Pt electrodes indicate,

significantly, that the capacitance determined over potentials corresponding to the metal "double-layer" region cannot with any justification be simply extended by extrapolation into the potential range of oxide formation when corrections for double-layer charging are made in transient experiments involving potential ranges for which Au electrodes bear an oxide film.

Part II. Stability of Anodically Formed Oxide Films as a Function of Potential and in the Presence of Halide (Cl^- or Br^-) Anions

Chapter 4

4.1 Characterization of the α-type and β-type oxide films by cyclic voltammetry

Interest in the stability of oxide films has arisen from the importance of passivity of metals bearing oxide films formed either anodically or as a result of corrosion in aqueous media. Especially the role of effects of strongly adsorbing anions such as Cl^-, Br^- or I^- in leading to breakdown of such oxide films has attracted attention in the areas of corrosion and metal-finishing.

In this second part of the present thesis, techniques developed and employed in the first part for evaluation of differences of double-layer capacitance behaviour at Au electrodes in the presence and absence of oxide films at Au have been complemented by use of *in situ* nanogravimetry using an Electrochemical Quartz Crystal Nano-balance (EQCN) employed in a "cyclic-voltammetric" mode and also in some studies of time-dependent changes of Au electrode surfaces in the presence of Cl^- and Br^- anions.

This part of the work first requires procedures for characterization of the states of oxide films that can be controllably generated at various potentials at Au other metal surfaces, as will be described in the following and other sections.

In the previous section, the results of impedance measurements were described under potentiostatic conditions at the potential of zero current where no passage of charge was observed. If this condition applies, the thickness of the oxide film on the electrode should be equivalent before and after an EIS measurement because zero cathodic current was read. A negative-going voltamogram was recorded after each impedance measurement and charges for

each cathodic peak were derived in order to compare them with the cathodic charges derived from a "blank" experiment. The blank experiments consisted in the growth of an oxide film at a certain potential (1.8, 1.9, 2.0, 2.1, 2.2 and 2.3 V (RHE)) for a controlled period of time (30s, 1 min, 2 min and 5 min) with the potential then being stepped back to 1.80 V (RHE) for 10 minutes in order to degas the solution from any O_2 evolved during the oxide formation. After this period of 10 min, the potential was stepped back to 1.75 V, held for 7 minutes, and then stepped back every 50 mV for the same period until a potential of 1.45 V was reached. These holding periods, *without* EI measurements, were used to simulate the EIS acquisition time which usually is approximately 7 min. Voltammograms were then recorded over the range 1.45 V down to 0.050 V (RHE), and reduction charges were derived in the usual way.

Figure 16 shows typical voltammograms recorded during such "blank" experiments for a wire gold electrode in 0.5 M HClO4 solutions. On the anodic scan (not shown in Fig. 16), oxide formation starts above 1.30 V (RHE) and shortly afterwards reaches a maximum. The current then goes through a minimum at ca. 1.70 V (RHE) which is believed to indicate the completion of a monolayer coverage of oxygen. The further increase of anodic current beyond this minimum is due to oxygen evolution as well as continuing oxide formation. With increase of the oxide growth potential, E_g, several types of oxides appear, as the cathodic scan reveals. The first oxide generated, the α-type oxide film [5], forms a compact anhydrous film of AuO on the gold. The second oxide, named the β-oxide, is a porous and hydrated oxide film. The α-oxide grows only to a limiting value of a few molecular layers (1~3) while the β-oxide can grow to a thick film (up to several hundreds of O-layers), depending on time and anode potential. The cathodic charges, Q, of the peaks of such oxide films are represented in the insets of Fig. 16.

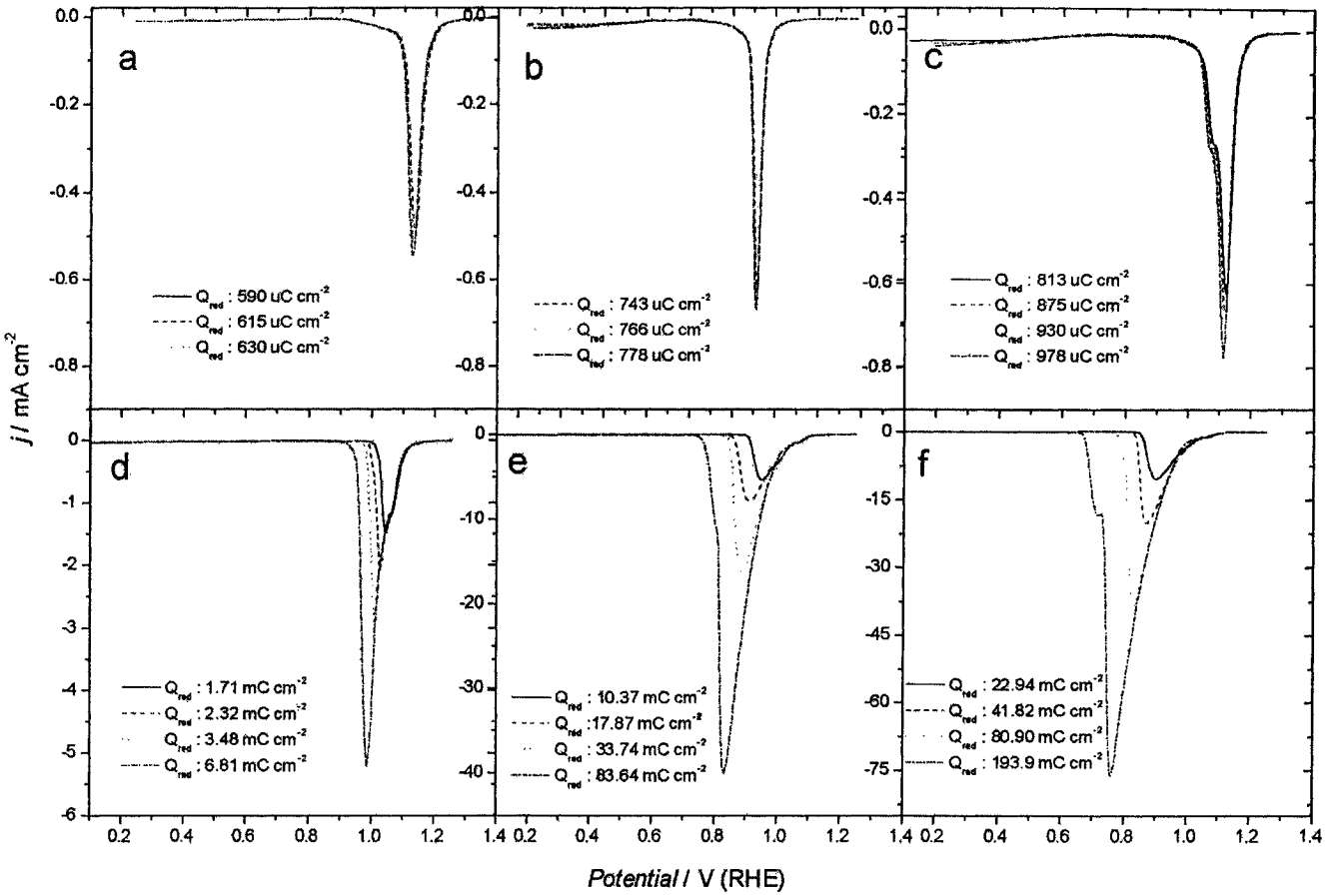

Figure 16. Reduction profiles of a Au electrode at 50 mVs^{-1} in 0.5 M $HClO_4$ after oxide growth at a) 1.80 V, b) 1.90 V, c) 2.0 V, d) 2.1 V, e) 2.2 V and f) 2.3 V. Oxide films were grown during (—) 30 sec, (--) 1 minute, (····) 2 minutes and (-··-) 5 minutes. Insets show charges for the reduction peaks.

Oxide films grown at potentials below 2.0 V (RHE) show clearly the presence of the α-oxide film. Cathodic charges from 590 (±10) to 778 (±10) μC cm^{-2} were derived from the voltammograms indicating the presence of 1~2 monolayers of oxide. For oxide films formed at 2.0 V and above, the appearance of a second cathodic peak is observed, corresponding to reduction of the β-oxide at a more negative potential indicating its greater stability. Cathodic charges ranging from 1.71 to 193 mC cm^{-2} were derived indicating the appreciable thickness to which this hydrous oxide film can be grown.

Voltammograms were then recorded after each impedance experiment. In the absence of halide ion, the cathodic charges were within 5% of the charges derived in the "blank" experiments, proving the stability of these oxide films throughout the impedance measurements. The second series of experiments consisted in measurement of the capacitance of the double-layer in the presence of halide ions such as Cl^- or Br^-. Voltammograms were recorded after each EI measurement and, this time, the cathodic charges derived were considerably smaller than before the addition of halide ions, indicating destabilization of the oxide film in the presence of such ions.

Figure 17 shows the voltammograms recorded after an EI measurement for oxide films at a gold electrode formed at four different potentials. The cathodic peak at 1.15 V corresponds to the oxide reduction and that located at 1.0 V is believed to correspond to the cathodic redeposition of dissolved gold back on to the electrode. Cathodic charges for the reduction of the oxide *remaining* on the electrode in the presence of Cl^- (Fig. 17) after EI measurements were of 214, 280, 365 and 420 $\mu C\ cm^{-2}$ for oxide films formed during 1 minute at 1.80, 1.90, 2.0 and 2.1 V (RHE), respectively.

In all the cases, reduction charges for the oxide films formed *before* the addition of Cl^- and EI measurements were of 615, 743, 875 and 2320 $\mu C\ cm^{-2}$, respectively. It was noticed that the β-oxide film formed previously was completely depleted and the oxide film left was composed of the α-type film.

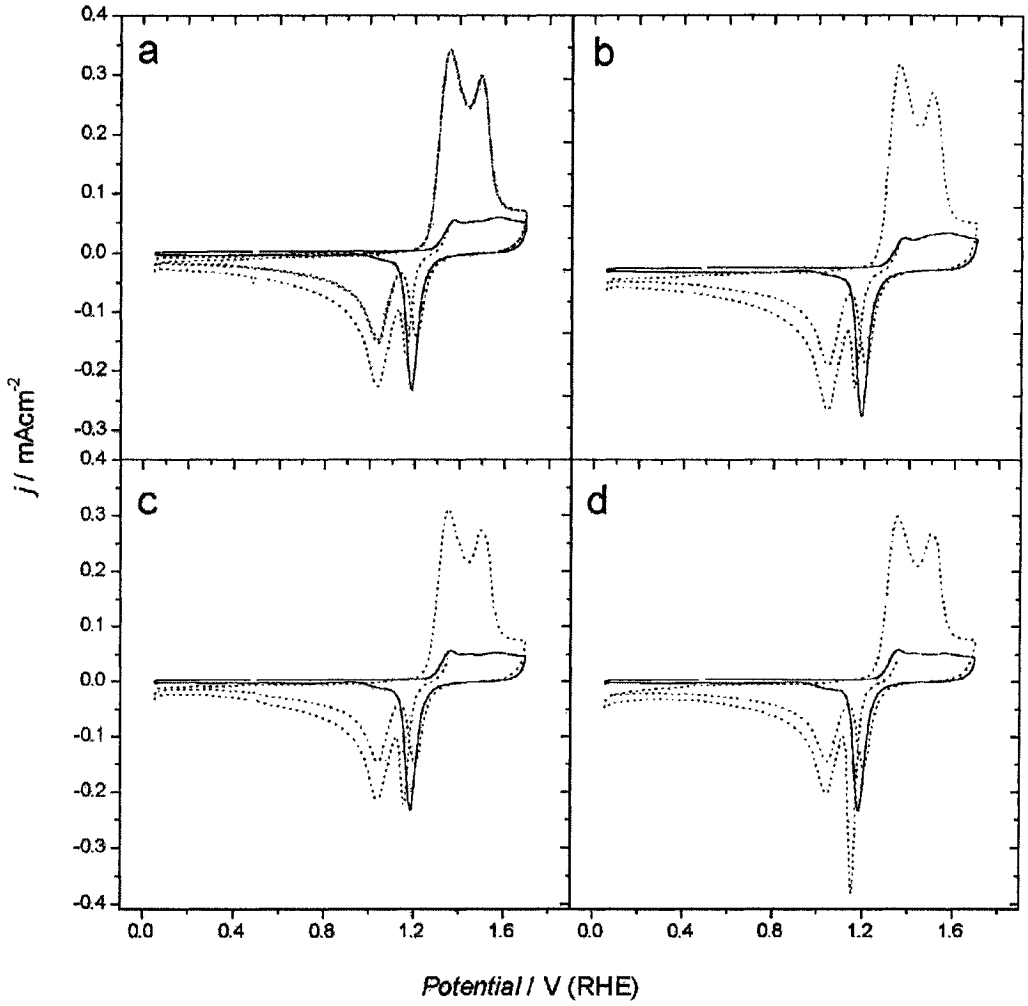

Figure 17. Reduction profiles (·····) of a Au electrode at 50 mVs^{-1} in 0.5 M $HClO_4$ + Cl^- 10^{-3} M after oxide growth at a) 1.80, b) 1.90, c) 2.0, d) 2.1 V (RHE). Oxide films were grown during 1 minute. CV's recorded before each experiments, without halide in solution, are also shown (—).

Similar results were observed when Br^- ions were added to the electrolyte. Again, the remaining quantity (equivalent reduction charge) of oxide film after each EI measurement was considerably smaller than that formed prior to the addition of the halide ion, followed by the impedance measurements.

Figure 18 shows the voltammograms, recorded after the impedance measurements, for a gold electrode in 0.5 M $HClO_4$ where 10^{-3} M Br^- had been added to the electrolyte after the

oxide formation but before the EI measurements. Oxide films were formed, during 1 minute, at potentials of 1.8 V, 1.9, 2.0 and 2.1 V (RHE), respectively.

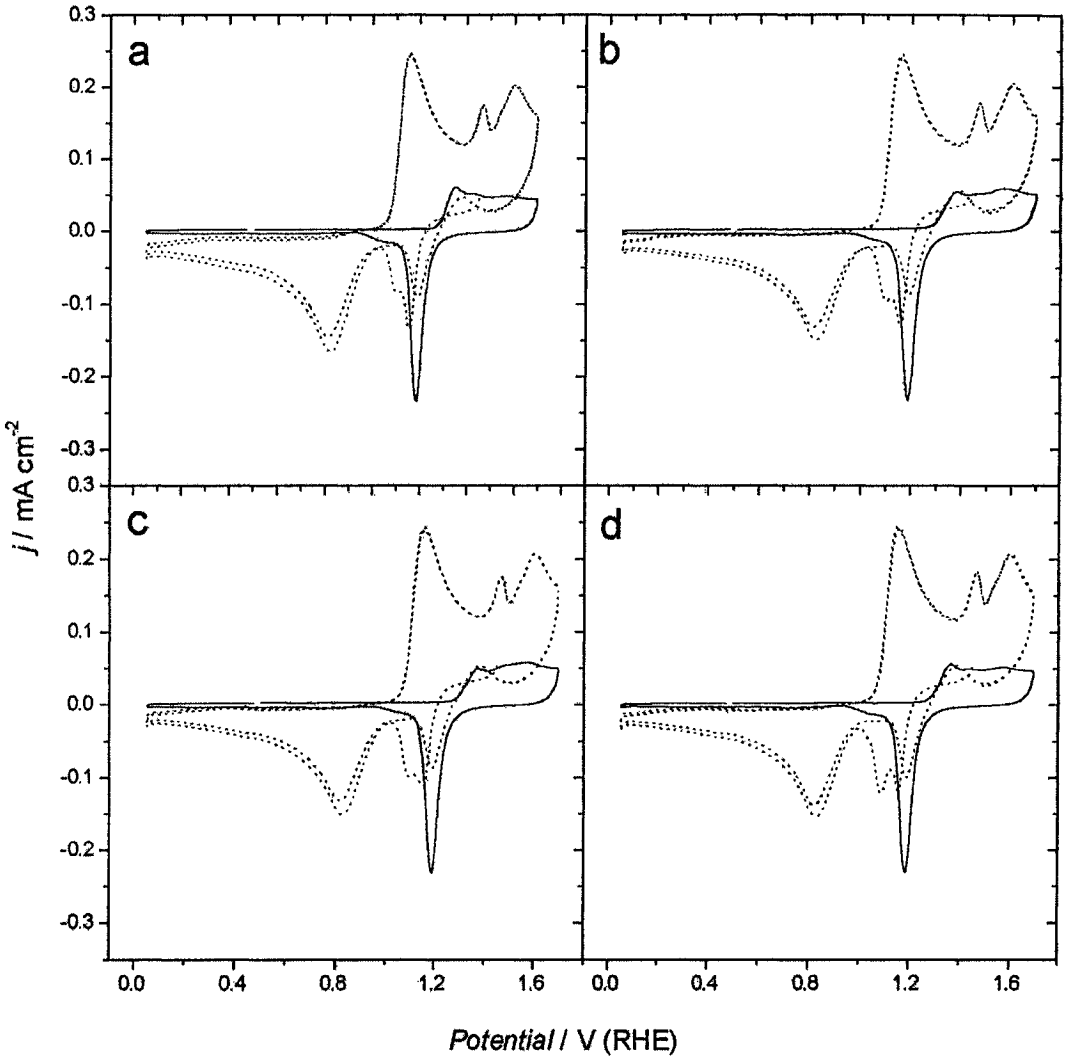

Figure 18. Reduction profiles (·····) of a Au electrode at 50 mVs^{-1} in 0.5 M $HClO_4$ + Br^- 10^{-3} M after oxide growth at a) 1.80 V, b) 1.90 V, c) 2.0 V, d) 2.1 V. Oxide films were grown during 1 minute. CV's recorded before each experiments, without halide in solution, are also shown (—).

The cathodic regions of the voltammograms are rather similar to those of the voltammograms recorded in the presence of Cl^- with few differences. The presence of 3 cathodic peaks located at potentials of 1.15, 1.10 and 0.80 V (RHE) can be observed. The first two peaks are overlapping and could be attributed to the reduction of the α-oxide film and the

third peak at 0.80 V can be attributed to the cathodic redeposition of previously dissolved gold on the electrode as confirmed by the effect of stirring.

The charge from the first two peaks can be derived from the four voltammograms in Fig. 19 giving; 254, 291, 261 and 285 $\mu C\ cm^{-2}$ respectively. Again, the extent of oxide film remaining after each EI measurement was considerably smaller than that of the oxide film formed before the addition of the halide ion, followed by the impedance measurements.

In order to find out what had happened to the oxide film "missing" after each EI experiment in the presence of halide, UV-Vis spectrophotometry was coupled with the impedance spectroscopy technique. Two oxide films of various thicknesses were formed. Firstly, a thick film mostly composed of β-oxide was potentiostatically generated at 2.20 V (RHE) for 1 minute. After the formation of the oxide, Cl^- was added to the electrolyte and a sample of the latter was collected every 7 minutes and scanned from 200 nm to 500 nm on the UV-Vis spectrophotometer. Based on prior calibration experiments, even after 7 minutes, $AuCl_4^-$ was found in solution in a measurable concentration. With time, the concentration of $AuCl_4^-$ became increased observably as the oxide film was becoming decreased because most of it was gone after the experiment (see Fig. 17).

Figure 19a shows the UV-Vis spectra for samples of the electrolyte collected after the formation of a thick oxide film followed by the addition of Cl^-. Increases of the absorbance at 225 and 320 nm, are observed corresponding to peaks due to formation of the gold complex $AuCl_4^-$.

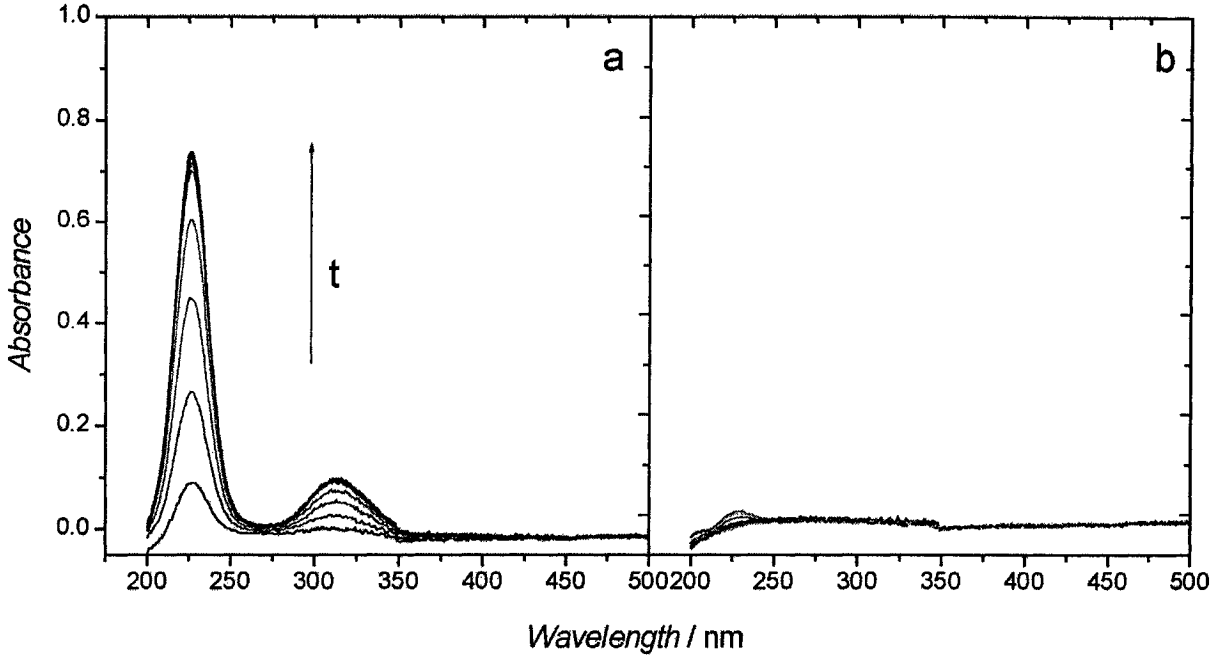

Figure 19. UV-Vis spectra of the electrolyte sampled in the electrochemical cell during impedance measurements for an oxide film formed at a) 2.20 V and b) 1.90 V. Halide ion, 10^{-3} M of Cl^-, was added to the cell after the oxide formation.

The same conditions were repeated with a thinner oxide film formed at 1.90 V (RHE) during 1 minute but in this case, only a trace of $AuCl_4^-$ was detected by UV-Vis (Fig. 19b). In order to understand the effect of halides on these oxide films, the Electrochemical Quartz Nano-balance was employed to provide mass-change results; the latter are analyzed in the following section, complementary to the information from linear-sweep voltammetry described above.

4.2 Results on oxide-film behaviour at Au derived from EQCN measurements

4.2.1 Formation of α-oxide films on Au

As was explained in section 2.2, anodic oxide film formation and growth at noble metals, including Au, has been studied by various groups, including our own, over some years [5, 6, 7, 58, 59] and at least two different types of oxide films are now known to be formed: one, the α-oxide, is a compact, non-hydrated oxide film distinguished from the other, β-oxide type, which is hydrous and porous [5, 32]. According to Birss et al. [5], the α-type oxide film is formed between 1.40 and 1.80 V during anodic polarization applied for 1 to 7 minutes, while β-oxide films are formed after polarization at more positive potentials for similar or longer periods [32].

Figure 20 shows a typical voltammogram and corresponding changes in quartz-crystal frequency, Δf, recorded at the Au EQCN electrode cycled in 0.5 M $HClO_4$ solution at 50 mV s^{-1}. The observed CV and corresponding EQCN responses, plotted comparatively in Fig. 20, can usefully be divided into three distinguishable regions corresponding to: *i*) double-layer charging between 0.40 and 1.25 V (RHE), at the oxide-free metal [60]; *ii*) the initial, including a pre-oxidation (ref. 32), stage of oxide formation, between 1.25 and 1.40 V (RHE) to nominal half-coverage by O species (cf. refs. 5, 30), and *iii*) a continuing oxide formation and growth region between 1.40 and 1.70 V (RHE), or greater [5], eventually leading to co-evolution of O_2.

A large decrease in Δf (increase in mass) is observed from 0.40 to 1.25 V (RHE) which is associated with changes in the structure and composition of the double-layer, accompanied by ion (ClO_4^-) adsorption (EQCN Δf negative) and changes of coverage and orientation [5] by

H_2O dipoles at the unoxidized Au electrode [61, 62], together with effects of a non-Faradaic kind as envisaged by Hepel [63] and Tsionsky et al. [64].

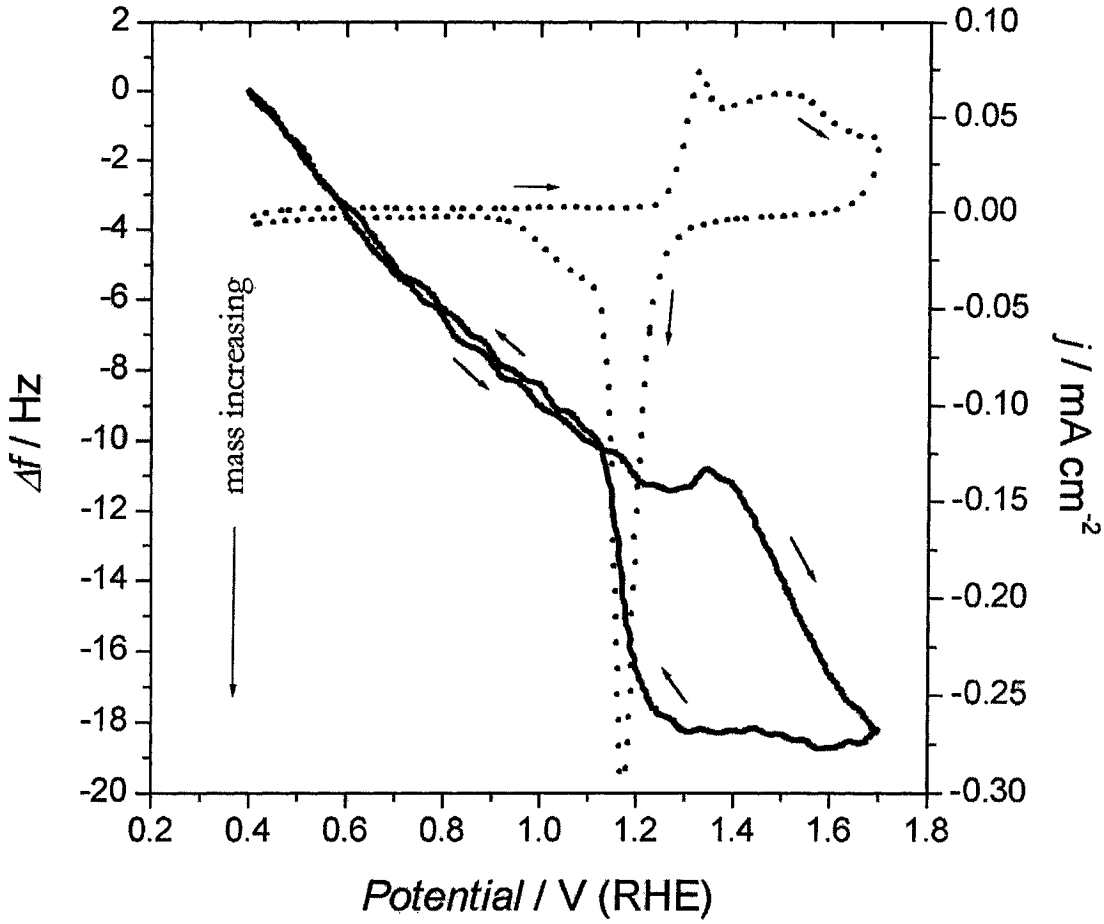

Figure 20. Cyclic voltammogram (·····) and EQCN profile (—) of a Au electrode in 0.5 M $HClO_4$ at 50 mV s^{-1}.

Following the double-layer effects noted above, further detectable mass increase in 0.5 M $HClO_4$ begins only at 1.40 V, some 150 mV more positive than the observable onset of initial increase in Faradaic oxidation charge. This suggests that two or more processes are concurrently occurring in the very early stage of surface oxide formation. The deposition of O species (cf. refs. 5, 48) takes place competitively versus previous adsorption of anions (ClO_4^-), as in the case of Cl^- ion effects on surface oxidation of Pt [5].

Then, no net mass change would tend to occur if the mass of the species (here ClO_4^-) displaced from the electrode surface, normalized to the same specific surface area requirement as that for O species, was close to the mass of the latter species. Adsorbed ClO_4^- trigonally occupies 3 sites, e.g. on a (111) surface, and also has a co-circle of influence on H_2O-molecule adsorption, so the O adsorption at 3 ~ 4 sites could be influenced, corresponding to a mass gain of ca. 48 ~ 64 g mol^{-1} electrons compared with a mass loss of ca. 100 g mol^{-1} electrons for ClO_4^- desorption; that is, there is still a substantial mass deficiency which could conceivably be due to trace dissolution of Au [65].

Following reversal of the potential scan at 1.70 V, both charge and Δf remain at first almost constant down to ca. 1.30 V (Fig. 20 and previous literature [63]), indicating that the oxide formed during anodic polarization remains unchanged during the period of time involved in traversal of this potential change. However, below ca. 1.30 down to 1.10 V (RHE), Δf increases by ca. 11 Hz, due to oxide reduction in the usual way with passage (Fig.16) of ca. 480 (±10) μC cm^{-2}, corresponding to a mass-to-charge ratio of ca. 8 g per mole of electrons as found in previous works [5, 30], equivalent to electrosorption of O species rather than OH, on the anodic sweep, as concluded in ref. [18].

4.2.2 Restructuring of the α-oxide film in relation to its stability in halide free solution

First it is necessary to establish the conditions for stability, or otherwise, of Au metal and its oxidized surface in the absence of halide (Cl^- or Br^-) ions. Figure 21a shows the EQCN responses plotted against time, during potentiostatic formation of an α-oxide [5, 6] film at 1.80 V (RHE) for 30s in 0.5 M $HClO_4$ solution and subsequent polarization for a period of 15 minutes at various controlled values in the potential range 1.75 to 1.45 V (RHE), selected as

that within which only very small or zero residual currents pass (cf. ref. 1) prior to onset of film reduction in a subsequent negative-going sweep at potentials below ca. 1.28 V (RHE), as described in section 2.1 of this thesis.

The EQCN and charge vs time profiles (the latter derived from voltammetry) were recorded simultaneously. The observed apparent EQCN mass-change responses, recorded as Δf (Fig. 21a), depended, of course, on both the holding potential and polarization time, t, which determined the extent of prior formation of the Au-oxide film at 1.80 V (Fig. 21). From Fig. 21a it is seen that Δf becomes *less negative* with time of holding at the three potentials, i.e. (apparent) mass is decreasing but there is not a correspondence with change of charge passed (see below). Also (Fig. 21a), small but significant increases in slope of the Δf vs t relations are observed as the holding potentials were increased in the order 1.45 < 1.60 < 1.75 V (RHE).

If cathodic reduction of the α-oxide film were occurring at some small, residual rate during the holding period, it would tend to be more pronounced at potentials closer to the usual reduction peak potential 1.18 V (Fig. 20), so that the rate of increase of Δf (mass decrease) would tend to be greatest at the *less positive* potentials. Surprisingly, the opposite effect is observed: thus, after 15 minutes of holding at 1.75 V, a Δf of 11.4 (±0.5) Hz was observed compared to 9.2 (±0.5) and 7.5 (±0.5) Hz for the lower holding potentials of 1.60 and 1.45 V (RHE), respectively. Hence, since Δf increases with holding potential (Fig. 21a), it cannot be attributed to residual cathodic currents.

Figure 21b shows three voltammetric oxide-reduction profiles from which the reduction charges calculated over the potential range 1.30 to 0.95 V, RHE, are 900 (±10), 836 (±10) and 820 (±10) μC cm^{-2}, corresponding to previous potential holding at 1.75, 1.60 and 1.45 V, respectively. These values are within 3.8 % of the charge of 849 (±10) μC cm^{-2} found

for reduction after the initial oxide formation at 1.80 V (RHE) for 30s, without subsequent holding at the three potentials in the negative-going sweep (+51 μC cm^{-2}, -15 μC cm^{-2}, -30 μC cm^{-2}, following holding at 1.75, 1.60 and 1.45 V (RHE), respectively). In summary, Fig. 21a indicates that mass loss increases with holding potential, while Fig. 21b indicates just the opposite, that the mass of oxide formed (remaining after the holding period) increases with holding potential. Clearly, the above Δf results cannot be interpreted in terms of reduction of Au oxide occurring during the holding period.

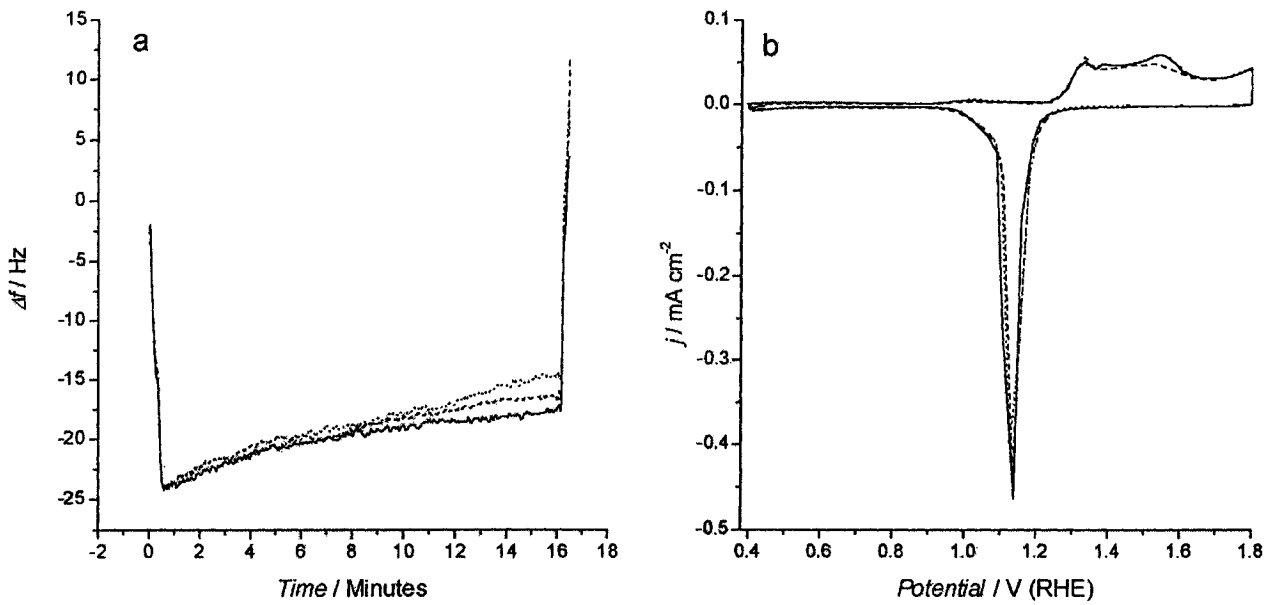

Figure 21. (a) EQCN response of an Au electrode having a thin oxide film (ca. 1 ML) in 0.5 M $HClO_4$ during potential polarization at 1.45 V (—), 1.60 V (--) and 1.75 V (·····) for 15 minutes immediately following oxide formation at 1.80 V (RHE); (b) cyclic voltammograms recorded at 50 mV s^{-1} subsequent to the potentiostatic polarization experiments.

Cadle and Bruckenstein [65] observed dissolution of Au as Au(III) from a rotating ring-disk Au electrode (RDE) in the absence of halide ions but only at potentials greater than ca. 1.40 V (RHE) and also during oxide reduction.

Dissolution of Au, as Au(III), during formation of the oxide film and possibly also during the holding period would certainly contribute to a mass loss and a corresponding increase in Δf. The actually observable, residual, formation of Au oxide (51 (±10) μC cm^{-2}) at 1.75 V, during the holding period, should give a small *decrease* in Δf (of ~ 1 Hz) due to a gain in mass instead of the 11.4 Hz *rise* that is observed. A fraction of this Δf has therefore to come from dissolution of Au to Au^{3+} during the holding period, (but not reduction of AuO) resulting in a mass decrease of the Au electrode. These results indicate that small but significant anodic dissolution currents do actually pass, given a succession of holding times in a continuing, negative-going direction.

In order to estimate the mass of Au atoms lost by this dissolution, results obtained during the experiment at 1.45 V (RHE) are useful. Thus, it may be supposed that this missing charge of some 30 (±10) μC cm^{-2} arises from small but significant dissolution. If the latter were a 3e process, a 30 μC cm^{-2} charge would correspond to the oxidation of 21 ng of Au, leading to an increase in Δf of 3.6 Hz. Cadle and Bruckenstein's papers [65, 66] demonstrated that anodic dissolution of Au at the RDE increased at more positive potentials, but no such experiments have been realized yet on EQCN electrodes. Hence, we shall assume the above Δf increase of 3.6 Hz applies at least as a minimum at the other two holding potentials. Then, if a 3.6 Hz contribution due to Au dissolution during the holding period were to be subtracted, the changes in frequency after 15 minutes holding at 1.75 V, 1.60 V and 1.45 V would be 7.8, 5.6 and 3.9 Hz, respectively but could not then, it seems, be due to actual mass changes (see Table 1).

In work relevant to interpretation of the above results, Tsionski et al. [64] have proposed that EQCN frequency changes can arise not only on account directly of mass changes but also due to other factors, as follows:

$$\Delta f = \Delta f_m + \Delta f_p + \Delta f_\eta + \Delta f_r \qquad (36)$$

where Δf_m is related to the desired actual mass change, but with added non-Faradaic contributions Δf_p due to interphasial compression, Δf_η to a solution-viscosity effect and finally Δf_r to a microscopic roughness factor which causes hydrodynamic lowering of frequency. (cf. ref. 46). For the behaviours shown in Fig. 21a, the principal factor that could explain the difference in the observed slopes of the plots of Δf in time is Δf_r. Thus, if restructuring of the oxide occurs during the holding periods, micro-roughness of the electrode could also be simultaneously changing.

Table 1. Δq's and Δf's measured on a gold oxide film (formed at 1.80 V for 30 s) during a 15 minute holding period at various potentials in the absence of Cl^-.

	1	2	3	4	5
	Holding Potential / V	Cl^- Absent			
		Δq / μC cm^{-2}	Δf_{obs} / Hz	Δm / ng cm^{-2} (based on Δq)	Δf *net* / Hz (restructuring)
A	1.45	-30	7.5	33 (5.5 Hz)	2
B	1.60	-15	9.2	33 (5.5 Hz)	3.7
C	1.75	51	11.4	33 (5.5 Hz)	5.9

By maintaining the potential of a freshly-formed oxide constant, restructuring of the oxide can, in fact, arise as observed morphologically by Vitus et al. [67], and independently by Nichols et al. [68] at Au (111) by means of scanning-tunneling microscopy. In earlier works [31, 69] it has been proposed that an Au electrode surface is oxidized through an island-growth mechanism but, with time, such surfaces become restructured to a more stable configuration.

Thus, initially formed islands tend to coalesce, through surface diffusion, to form flatter terraces, resulting in a smoother surface (on a micro-, or nano-scale) illustrated schematically in Figs. 22a and 22b. This would lead (through Eq. 36) to an increase of frequency with time, as is found (Fig. 21a) corresponding to an apparent-mass decrease.

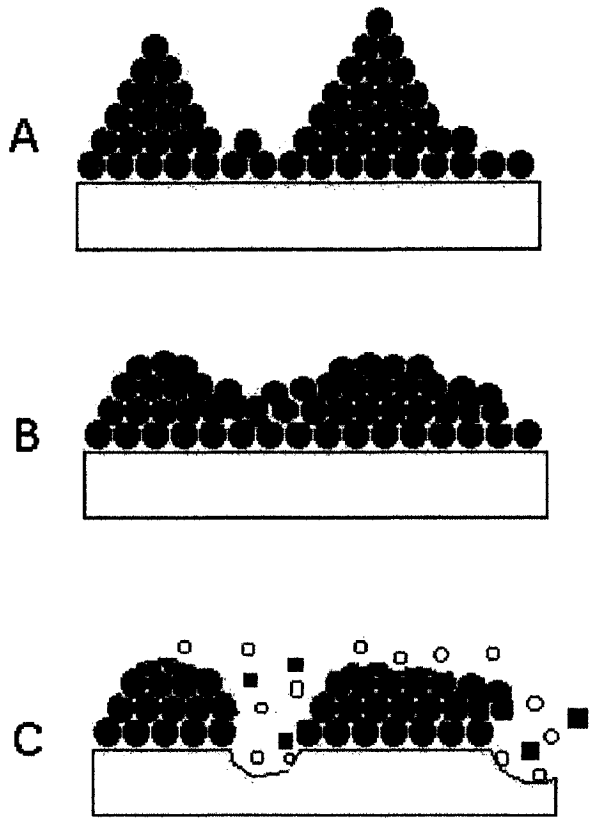

Figure 22. Schematic representation of a gold oxide film before (a) and after (b) the reconstruction of the surface. In (c) is shown a schematic representation of a reconstructed oxide film in presence of Cl^- (o) presumably forming a gold chloride complex (■).

Figure 23 shows a nanogravimetric response during holding of the potential at 1.60 V (RHE) (at B on Fig. 23) for 15 min, following formation of oxide at 1.80 V for 30s (A on Fig. 23). The increase in frequency (decrease in mass) during its subsequent reduction (C on Fig. 23) is ca. 13.5 (±0.5) Hz while for holding at potentials of 1.75 and 1.45 V (RHE) the increases were, respectively, 16.0 (±0.5) and 13.2 (±0.5) Hz.

The increase in Δf of 13.5 Hz (at C in Fig. 23) following holding at 1.60 V, is due to reduction of Au-oxide since it occurs simultaneously with the appearance of the reduction peak in the CV, and corresponds to an apparent decrease in mass of 75 (±2) ng cm^{-2}, based on Sauerbrey's equation, ref. [37]. Assuming (cf. refs. 5 and 30) a mass-to-charge ratio of 8 g per

mole of electrons for reduction of O species, this mass would correspond to a cathodic charge of 878 (±24) μC cm^{-2}. Integration of the respective CV peak (Fig. 21b), gives a cathodic charge of 820 (±10) μC cm^{-2}, i.e. within 6.8 % of that derived from the EQCN results.

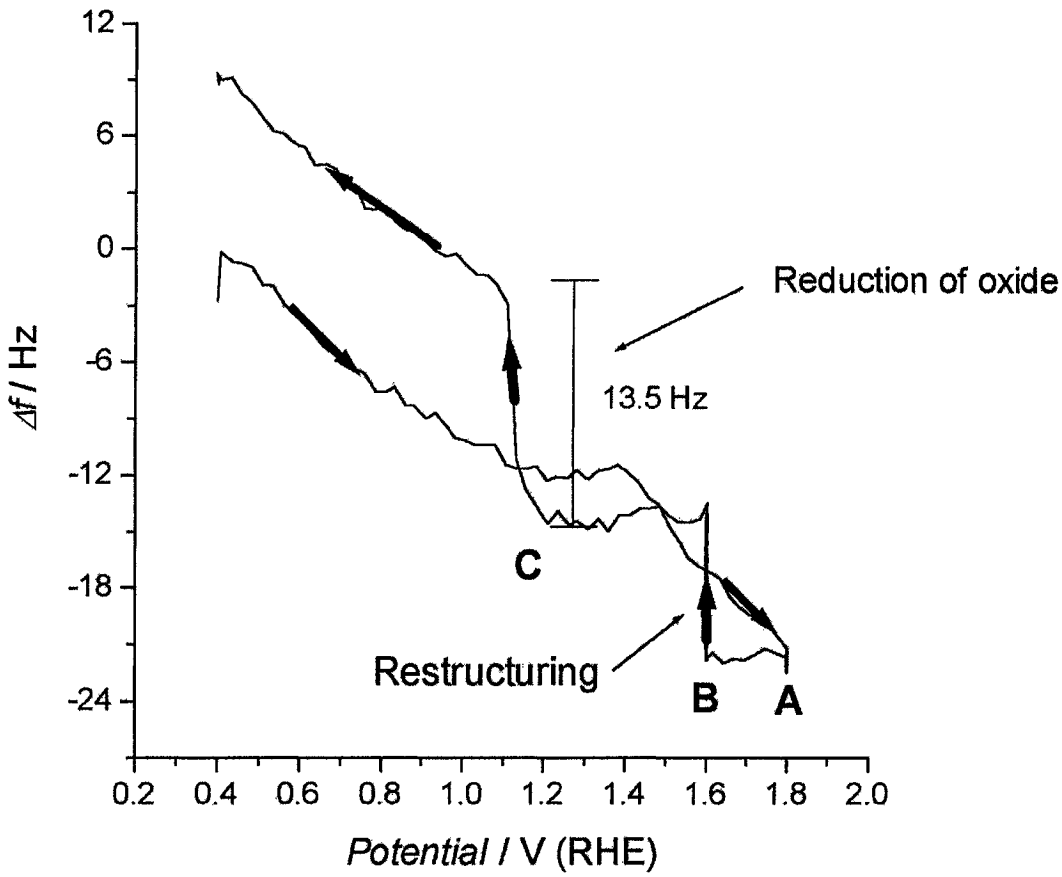

Figure 23. EQCN profile of a Au electrode in 0.5 M $HClO_4$ showing a decrease in Δf of 13.5 Hz due to the reduction of the oxide film, after a period of holding at 1.60 V.

For holding at 1.75 V, the Δf of 16.0 Hz corresponds to a decrease in mass of 90 (±2) ng cm^{-2}, and to a corresponding cathodic charge of 1080 (±24) μC cm^{-2}, compared with 904 (±10) μC cm^{-2} found from the CV. These reasonable consistencies provide proof that quite similar α-oxide films are being formed and then reduced, on the Au electrode under these conditions. The values and durations of the holding potential (at B in Fig. 23), however, evidently determine in a detectable way the amounts of oxide remaining.

4.2.3 Reactivity and instability of the Au α-oxide in the presence of halide ions

Of special and additional interest in the present work is the stability of Au metal and its oxide film to the presence of halide ions, Cl^- and Br^-, in solution. This has obvious general relevance to stability of passive films at baser metals in corrosive halide-ion solutions. Figures 24a and 24b, respectively show the oxidation-reduction CV current-density profiles and EQCN responses determined under the experimental conditions described in section 4.1 of Part II, with potential-holding at 1.75 (—) and 1.45 (·····) V (RHE), but with Cl^- present.

Table 2. Δq's and Δf's measured on a gold oxide film (formed at 1.80 V for 30 s) during a 10 minute holding period at various potentials in the presence of Cl^-

1	2	3	4	5
	Holding Potential / V	Cl^- Present			
		Δq / μC cm^{-2}	Δf_{obs} / Hz	Δm / ng cm^{-2} (based on Δq)	Δf *net* / Hz
D	1.75	-14	25	9.8	19.1 (25-5.9) (Viscosity)
E	1.45	-66	490	46.2	469.9* (Dissolution)

*469.9 Hz = 490 Hz – 19.1 Hz – 5.9 Hz – 1 Hz + 5.9 Hz (see Eq. 36)

In the *first part* of this section we shall present the results obtained for potential-holding at 1.75 V (solid lines in Figs. 24a and 24b). However, in contrast to Fig. 21a, at the start of the 15 minutes holding period, Cl^- was injected quantitatively into the cell to give a concentration of 10^{-3} M.

The reduction charge was 886 (±10) μC cm^{-2} (cf. 900 (±10) μC cm^{-2} in the absence of Cl^-), indicating that the oxide, once anodically formed, is neither reduced nor significantly

affected by the presence of Cl^- (Fig. 24b) so that almost unchanged EQCN responses would be expected but this was *not* the case. Thus, Fig 24a(—) shows how *Δf decreases appreciably* by ca. 25 (±1) Hz (see line D, column 3, in Table 2) with time at an α-Au oxide film in the 10^{-3} M in Cl^--solution at a potential maintained for 15 minutes at 1.75 V (RHE) (cf. 11.4 (±1) Hz in the absence of Cl^-).

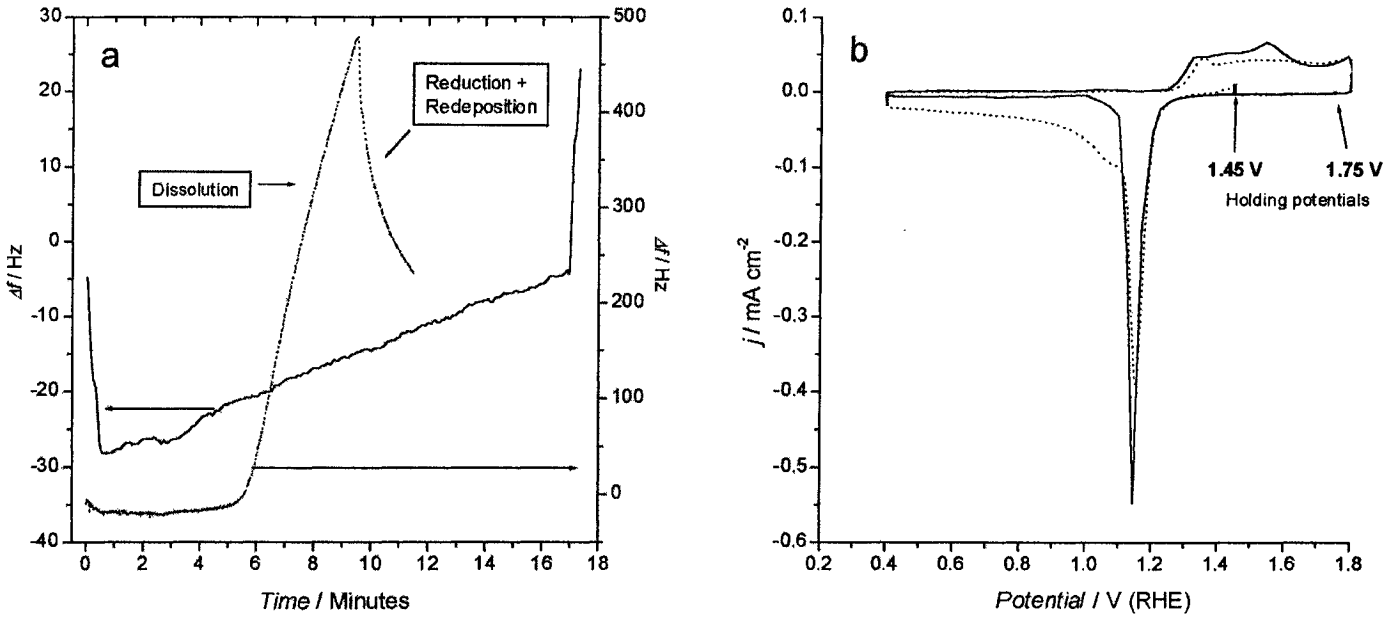

Figure 24. EQCN profiles (a) of oxides films in contact with Cl^- 10^{-3} M at 1.45 V (·····) and at 1.75 V (—) during 10 and 15 min, respectively. In (b), Cyclic voltammograms of oxide films in contact with Cl^- 10^{-3} M after an holding period of 10 min at 1.45 V (·····) and 15 min at 1.75 V (—).

This cannot be attributed either to any decrease in oxide-film mass due to reaction with Cl^- ion (since the reduction charge remains unchanged) or to any change of hydrostatic pressure (Eq. 36), and the Δf_η, in Eq. 36, would be negligible since the added Cl^- concentration is 500 times smaller than that of the $HClO_4$ already present.

Keeping in mind the results shown in Fig. 21, a contribution of the order of 8 Hz could, however, arise from the change in microscopic roughness of the oxidized surface due to its

restructuring (Fig. 22) but this is very small as shown by the Burshtein [45] O-accommodation experiments. Note, however, that chemisorbed anions could also lead to non-uniformity of an otherwise smooth metal surface on a sub-nano-scale by their very presence [70, 71]. Thus, substitution of ClO_4^- ions by Cl^- in the compact region of the double-layer could result in a change of slip between the Helmholtz plane and the contiguous interphase since the hydrophilicity of a ClO_4^- film would be greater than that of a Cl^- layer, and the former ion is 5 times larger.

Tests were made to confirm (or otherwise) that a change in Δf could result from addition of Cl^- anions. In a first experiment, the potential was held at 1.0 V (RHE) for 10 min in the absence of Cl^- ion (conditions for which no oxide film is formed) and EQCN (Fig. 25a(1)) and CV (Fig. 25b (—)) profiles were recorded simultaneously.

No recordable current arose during this holding period and no frequency changes were observable (Figs. 25a and 25b). Hence, in the absence of an oxide film (potential = 1.0 V), no effect that could be due to restructuring at the Au metal surface itself is detectable by either procedure. During a second experiment, the potential was held again at 1.0 V (RHE) but now in the presence of Cl^- at 10^{-3} M in the cell (Fig. 25a (2), Fig. 25b (·····)).

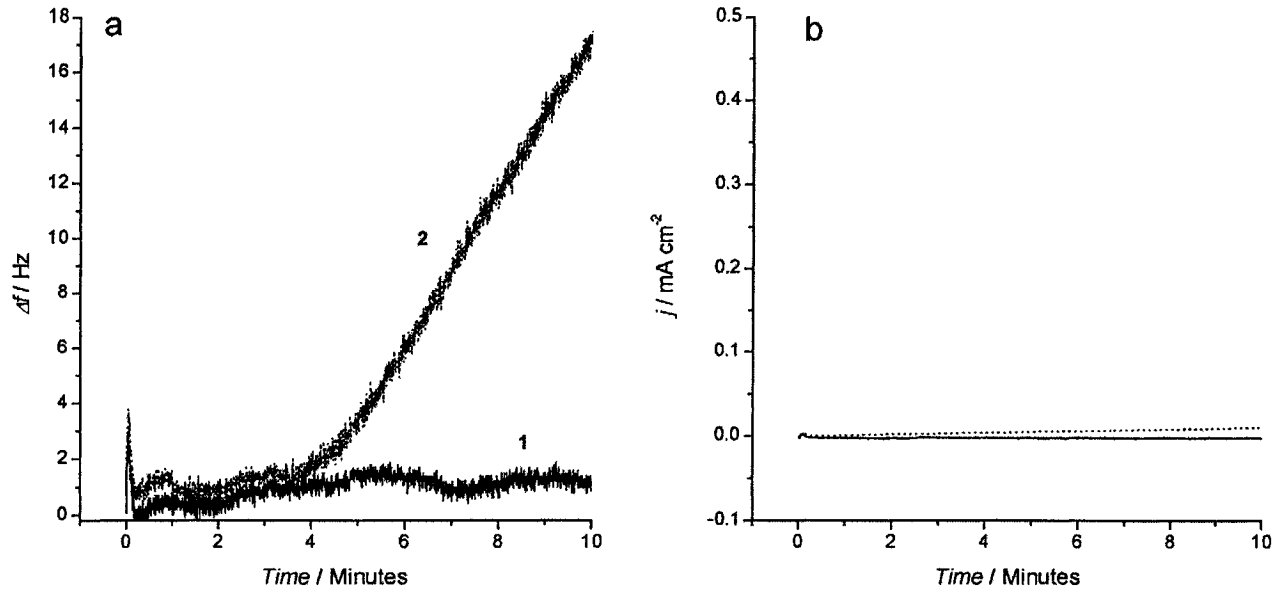

Figure 25. (a) EQCN response of an Au electrode during potentiostatic polarization at 1.00 V (RHE) for a period of 10 minutes in absence (1) of Cl^- and in presence (2) of Cl^-; (b) current profile of the electrode in the absence (—) of Cl^- and in the presence (·····) of Cl^- during the holding period.

Our previous studies [72] have shown that dissolution of Au as $[AuCl_4]^-$ in Cl^- solutions begins at only 1.30 V (RHE). During the above holding experiment at 1.0 V in the presence of 10^{-3} M Cl^-, no anodic current for Au dissolution was detectable (Fig. 25b) so no Δf would be expected. However, under the same conditions, 4 min. after addition of the Cl^-, a pronounced increase in Δf in fact arises (Fig. 25a), not observed in the absence of Cl^- ion. The delay is due to the time required for Cl^- to reach the EQCN Au electrode down the channel in the Sherbrooke design of the cell [48] used in the present work. Hence, the observed Δf increase must be due to another of the effects represented in Eq. 29.

In the *second half* of this section 4.2.3 we shall present the results obtained at the oxidized Au surface under the experimental conditions described in section 2.2, with potential holding at 1.45 V (RHE) for 10 minutes and addition of Cl^- (to 10^{-3}M). After this holding

period, the oxide reduction profile (Fig. 5a) gave a cathodic charge of 754 (±20) μC cm^{-2}, i.e. 66 μC cm^{-2} less than the reduction charge in the absence of Cl^- (compare with the minimal loss of 14 μC cm^{-2} for holding at 1.75 V (RHE) under the latter condition). The missing 66 μC cm^{-2} would correspond to an increase in Δf of 8 Hz if it were due to dissolution or of 1 Hz for oxide reduction. In the latter case, a small surface exposure of Au^0 sites to the Cl^--containing solution would arise, which, between 1.10 and 1.50 V, could lead to corrosive dissolution of Au as represented in Fig. 22c.

Figure 24b(·····) demonstrates that a significant decrease in Δf arises after *ca.* 5 min of holding at 1.45 V (RHE) in the presence of 10^{-3} M Cl^-, a period probably needed for small extents of oxide reduction (the missing 66 μC cm^{-2}, referred to in the above paragraph) to take place and also for Cl^- anions to reach and react with exposed metallic sites on the oxidized Au electrode, giving $[AuCl_4]^-$ (Eq. 37) in solution with consequent loss of mass of the Au oxide-film electrode. The Δf between the 6th and the 10th minutes of holding at 1.45 V is large, ca. 490 Hz. (Fig. 24b). By plotting the current response versus time, as in Fig. 26, an anodic current appears at the 6th minute after Cl^- addition corresponding to

$$Au + 4\ Cl^- \rightarrow [AuCl_4]^- + 3e^- \qquad (37)$$

and passage of 3660 (±30) μC cm^{-2}. From Eq. 37 (cf. ref. 73), it is possible to estimate the charge that would correspond to the Δf of 490 (±5) Hz observed in Fig. 24b during the 10 min. holding period allowing, through Eq. 38, for the possible effect of other factors on Δf_{obs} :

$$\Delta f_{obs} = \Delta f_{\text{dissolution}} + \Delta f_{\text{reconstruction}} + \Delta f_{\text{viscosity}} + \Delta f_{\text{oxide reduction}} - \Delta f_{\text{roughness}} \qquad (38)$$

where:

$$\Delta f_{\text{dissolution}} = \Delta f_{obs} - \Delta f_{\text{reconstruction}} - \Delta f_{\text{viscosity}} - \Delta f_{\text{oxide reduction}} + \Delta f_{\text{roughness}} \qquad (39)$$

Thus, the following frequency accounting was applied;

17.2 Hz for $\Delta f_{viscosity}$ (as was done for the 1.75 V (RHE) potential)

7.8 Hz for $\Delta f_{reconstruction}$ (see Table 1)

1 Hz for $\Delta f_{oxide\ reduction}$ (from the 66 μC cm^{-2} charge missing due to reduction during holding)

7.8 Hz for $\Delta f_{roughness}$ (dissolution probably increase the roughness of the electrode. Therefore, the Δf value should be on the same order as for restructuring)

These estimates are needed in order to isolate the net Δf contribution that would be due to Au dissolution which is then 464 (±10) Hz.

The mass loss of 2598 ng cm^{-2}, calculated from the Sauerbrey equation [37], for formation of the $[AuCl_4]^-$ complex is equivalent to passage of anodic charge of 3817 μC cm^{-2}, a value satisfactorily close to 3660 (±30) μC cm^{-2} evaluated by integration of the current vs time transient (Fig. 26) from 6 min to commencement of cathodic reduction at 9.5 min. As was observed in Fig. 24a, the voltammogram of the experiment conducted at 1.45 V (dashed line) provides further proof that Au dissolution is occurring. However, on account of formation of $[AuCl_4]^-$, a gold-redeposition charge component can arise as a shoulder in the oxide-reduction peak (Fig. 24a (·····)).

The total cathodic charge for the latter is 3000 (±40) μC cm^{-2} where 754 (±10) μC cm^{-2} (evaluated above) is due to the reduction of the α-oxide film so that 2246 (±40) μC cm^{-2} would arise, in this case, from redeposition of Au from $AuCl_4^-$ (Eq. 32).

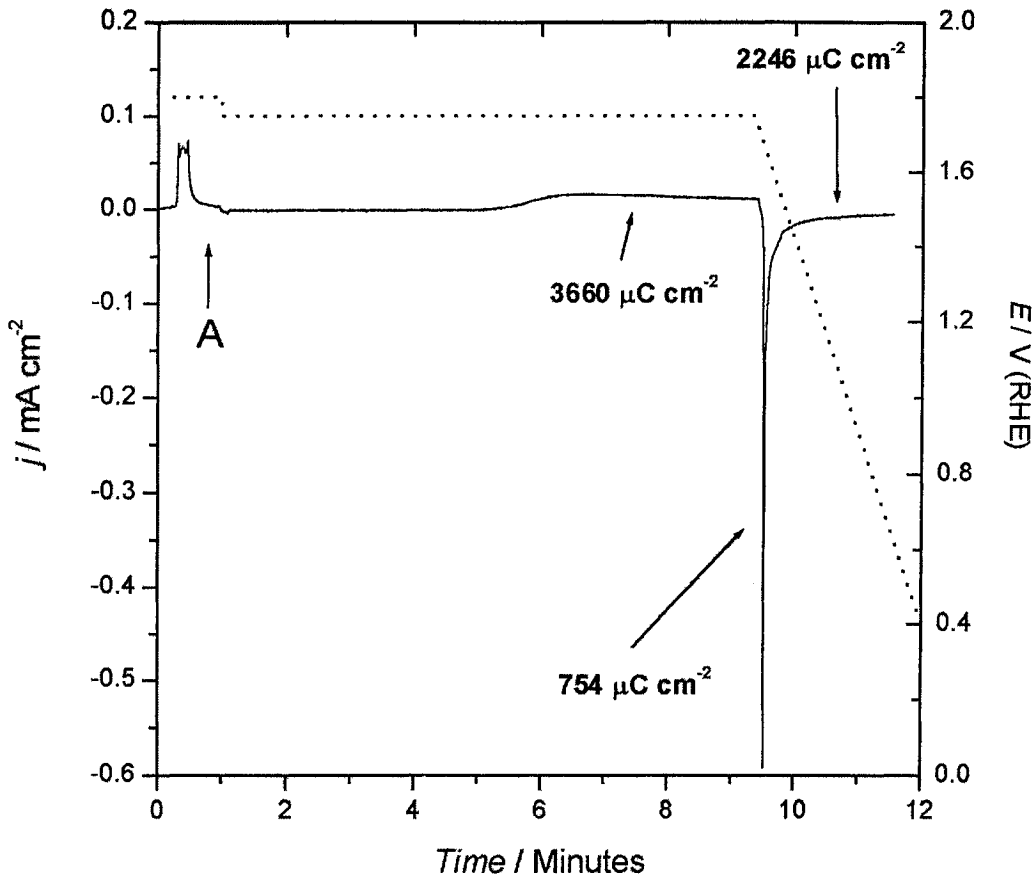

Figure 26. Current (—) and potential (·····) profiles for a Au electrode; Cl^- (10^{-3} M) is added at A.

From examination of the EQCN results shown in Fig. 24a, it is useful to calculate the net change in mass that would correspond to these above two processes for the overall Δf of 245 (±5) Hz (reduction + redeposition, (·····) Fig. 24b for ≥ ca. 9 min). Reduction of the α-oxide should increase the frequency while redeposition of Au should decrease it, i.e. $\Delta f = \Delta f_{redeposition} - \Delta f_{reduction}$. From the known Δf due to α-oxide film reduction, ca. 10 Hz, the Δf due to redeposition would be 255 (±5) Hz, which corresponds to a mass gain of 1428 ng per geometric cm^{-2} due to Au redeposition. The calculated charge for this 3e redeposition would be 2098 (±40) μC cm^{-2} which is in impressive agreement with the charge of 2246 (±40) μC

per geometric cm^{-2}, given by analysis of the voltammogram. In studies by Bruckenstein et al. [66], using a ring-disc system, reduction of dissolved "Au species" took place in the range of the peak for reduction of Au oxide at the Au surface in linear sweep voltammetry, suggesting involvement of a partial process of reduction by dissolution.

However, the oxide film that is formed above ca. 1.34 V, (depending on the anion of the electrolyte) could also becomes partially dissolved in Cl^- solution by a chemical redox reaction:

$$Au/O + Cl^- \rightarrow Au + {}^-OCl \quad (33)$$

coupled with

$$2H^+ + {}^-OCl + Cl^- \Leftrightarrow Cl_2 + H_2O \quad (34)$$

Such processes would be similar to the well known reactions of higher oxides such as MnO_2 or PbO_2, with Cl^-, producing Cl_2 or OCl^-. The freed Au sites in process (33) would then be avalaible for the corrosion process referred to earlier, leading to $[AuCl_4]^-$ in solution.

4.2.4 UV-Vis identification of the dissolved gold chloride complex

In order to identify the type of Au complex produced in solution, as a result of dissolution of Au in Cl^- solution, multiple voltammetric cycling was applied at an Au electrode at 50 mV s^{-1} between potentials of 0.60 V and 1.35 V (RHE) in an electrolyte of 0.5 M $HClO_4$, 10^{-3} M in Cl^-. Figure 27 shows two voltammograms in the presence of Cl^- anions. The CV response in the absence of bubbling or agitation is plotted as a dashed line. A broad anodic current peak for Au dissolution at ca. 1.05 V (RHE) is clearly observed on the subsequent, negative-going sweep.

Our previous work [29, 30, 59] showed that electrosorptive formation of O species at Pt or Au still arises, respectively, at potentials positive to 0.95 or 1.30 V (RHE) in the presence of Cl^- or Br^-, but in competition with the halide-ion adsorption while reduction of the α-type of oxide film is indicated by a sharp cathodic-current peak (at oxidized Au) centered at ca. 1.15 V, as in Figs. 21 and 24. The cathodic peak at 1.05 V (RHE) in Fig. 27 (dashed line), is hence attributable to the diffusion-controlled reduction of the unknown Au complex, arising from anodic dissolution, probably back to Au^0 in the reverse of Eq. 38. The solid line in Fig. 27 represents a cycle during which Ar was bubbled to assist transfer of Cl^- ions and dissolved Au-complex away from the EQCN electrode surface and thus minimizes its subsequent reduction and consequent redeposition as Au.

The purpose of such conditions is to achieve a spectrophotometrically detectable concentration of the Au complex in the bulk solution. The absence of a cathodic peak in the voltammogram (solid line) of Fig. 27 indicates, as expected under these conditions, that Au was not significantly redeposited so that the desired conditions for removal of the dissolved complex into the bulk solution were achieved.

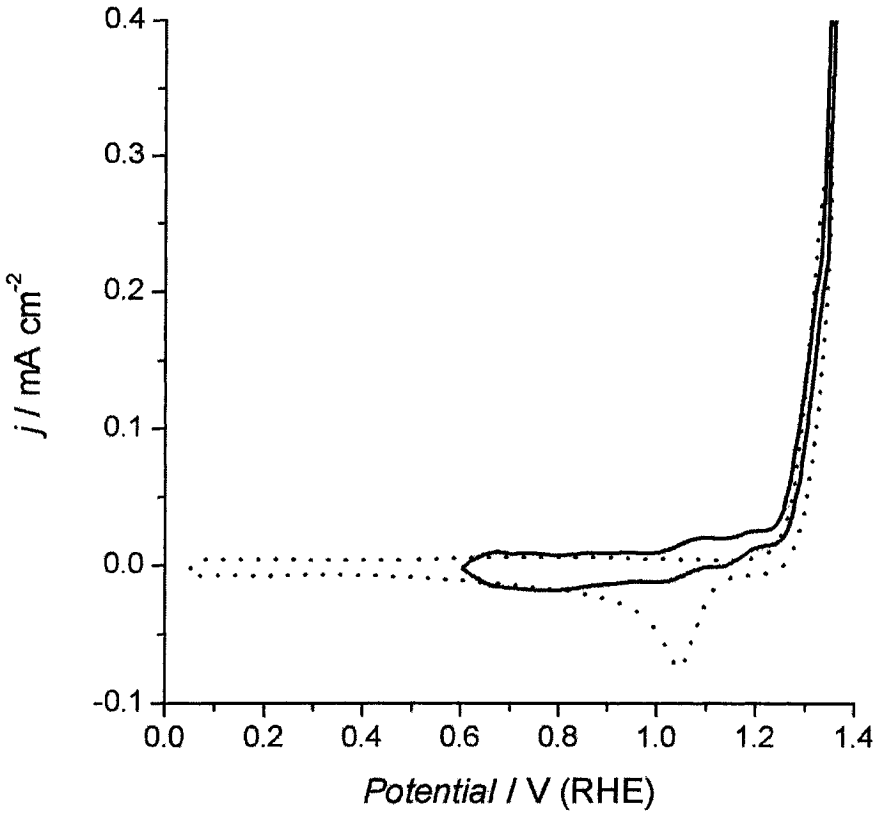

Figure 27. Sensitive scale voltammograms of a Au electrode in 0.5 M $HClO_4$, 10^{-3} M Cl^- with stirred (—) between 0.60 V and 1.35 V (RHE) and without stirring (·····) between 0.05 V and 1.35 V (RHE).

Figure 28 shows UV-spectra obtained using the above procedure. The solid line (A) corresponds to the spectrum of a standard solution of $AuCl_4^-$ at a concentration of 8.0 x 10^{-5} M. The band at 312 nm is assigned to the $AuCl_4^-$ species and that at higher energy, 227 nm, to $[AuCl_3(OH)]^-$ as based on the literature [74]. The spectra obtained following 2500 voltammetric cycles (between 0.60 and 1.35 V, RHE) at an Au electrode in 10^{-3} M Cl^- in 0.5 M $HClO_4$ are shown in Fig. 28 as (△). Two bands (line B) similar to those of the standard $AuCl_4^-$ solution, are clearly observed, proving that the dissolution of *non-oxidized* Au in the presence of Cl^-, at potentials more positive than 1.00 V (RHE), takes place giving the aurichloride (III) complex (Eq. 31). Figure 28 (·····, line C) shows the spectrum of the

electrolyte from a cell in which an α-oxide covered Au electrode had been left for 1 h at 1.75 V (RHE) in the presence of 10^{-3} M Cl^-. Then, the absorbance peak at 312 nm is very small, corresponding to only a trace amount of Au-oxide having been dissolved by Cl^- anions, a result demonstrating the high chemical stability of the α-Au oxide in the presence of Cl^- anions in the range of potentials for virtually zero Faradaic currents.

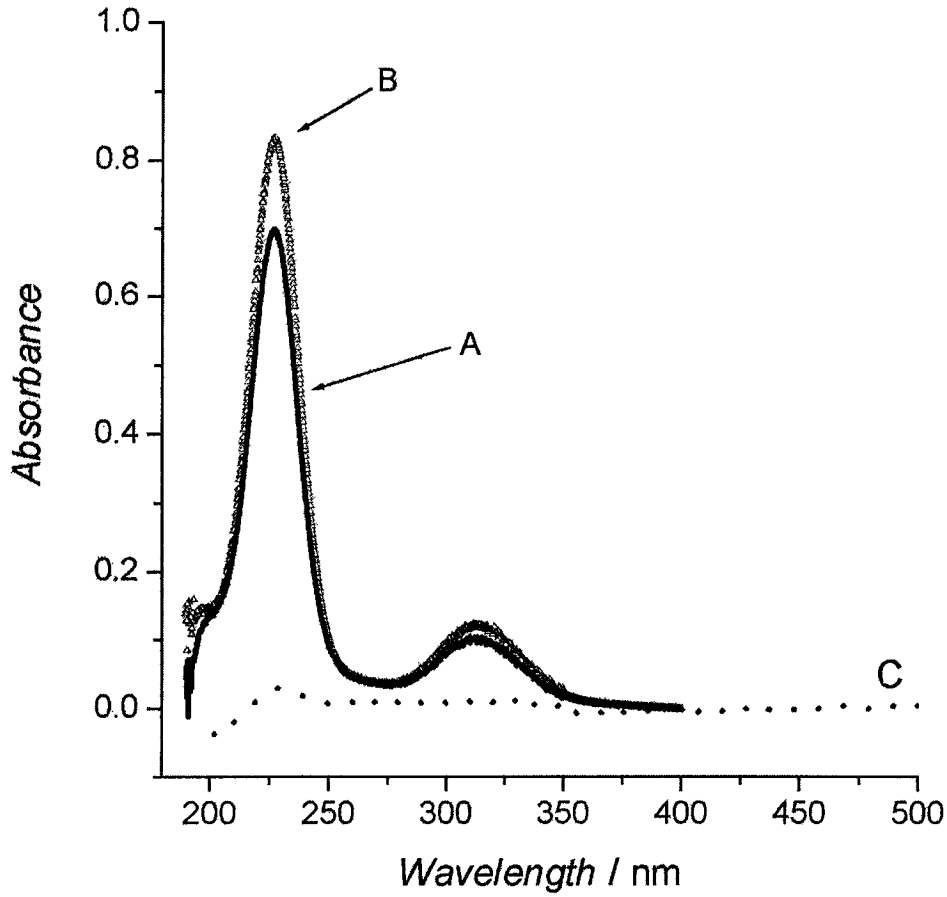

Figure 28. UV-Vis spectra of a standard 8.0 E^{-5} M $AuCl_4^-$ solution in 0.5 M $HClO_4$ (a); of 0.5 M $HClO_4$, 10^{-3} M Cl^- electrolyte following 1500 CV cycles of a metallic Au electrode between the potential limits 0.80 and 1.50 V (RHE) (b); and of 0.5 M $HClO_4$, 10^{-3} M Cl^- electrolyte in contact with an oxidized Au electrode (c).

4.2.5 Gold dissolution in the presence of bromide ions

Comparisons between effects of Br^- ion, relative to those of Cl^- are always of interest [30], Br^- is a larger and more electron-donative anion than Cl^- and, coupled with its consequent weaker hydration [75], is more strongly chemisorbed at electrodes than is Cl^-, e.g. ref. 34. Also, Br^- is a stronger reducing agent than Cl^-. Comparative experiments on the stability of the Au α-type oxide in contact with Br^- ions were therefore carried out using procedures similar to those described above for Cl^-.

Figure 29 shows the EQCN and current-density profiles recorded during a linear sweep and a holding period at 1.45 (dashed) and at 1.75 V (solid) at an oxidized Au electrode in the presence of 10^{-3} M Br^-. The results are similar to those in Cl^- solutions. Dissolution of the Au electrode seems to occur approximately 5 minutes after the addition of the Br^- ions when the potential is held at 1.45 V, as was found for Cl^-. However, the Δf observed with Br^- is ca. 560 (±5) Hz (compare 490 (±5) Hz for Cl^-), which, assuming Au dissolution is again the primary process occurring, would correspond to a mass loss of 3136 (±30) ng cm^{-2}. A corresponding charge of 4623 (±40) μC cm^{-2} was calculated assuming dissolution of Au occurs by a 3 e^- process, as in Eq. 31 for Cl^- solution. This charge is considerably smaller than the 9560 μC cm^{-2} of anodic charge determined from integration of the current-density (j) transient (dashed line) in Fig. 24b. A much lower change in frequency was observed (ca. 50 Hz) for an electrode polarized at 1.75 V (Fig. 29a, solid line) compared with that at 1.45 V (RHE). A Δf of 50 Hz corresponds to a mass loss of 280 ng cm^{-2} which, for a 3-electron dissolution process, is equivalent to a charge of 420 μC cm^{-2}. The net anodic charge, determined by integration of the current-density transient was 12.8 (±0.3) mC cm^{-2}. The correlation between Δf and the calculated passage of charge cannot, therefore, be so well established for this case, as it was (sections 4.2.2 and 4.2.3) for Cl^-.

The presence of the shoulder at ca. 0.90 V, RHE (a potential more negative than the peak potential for reduction of the α-oxide) indicates, however, (inset Fig, 24b), as for Cl^-, that reductive redeposition arises at the Au electrode, giving a Δf of -110 Hz (dotted line, Fig. 24a). Assuming this Δf results from the reduction of $[AuBr_4]^-$ back to Au^0, the charge associated with the above Δf of -110 Hz, would be 868 (±10) μC cm^{-2} which is in good agreement with that, viz is 840 (±10) μC cm^{-2}, calculated by integration of the voltammogram over the appropriate potential limits, indicating that the Δf can be attributed to redeposition, as was the case for Cl^-. Thus, in the presence of Br^-, charges calculated from the EQCN profiles for the *anodic process* do not correlate well with results obtained by integrating the corresponding voltammogram, while the EQCN profiles for the *cathodic process* do correlate well with data from integration of the voltammograms.

4.2.6 UV/Vis identification of the dissolved gold bromide complex

Spectrophotometric experiments similar to those in Cl^- solution on dissolution of Au in Br^- solutions confirmed the generation of a $[AuBr_4]^-$ complex which is formed significantly during 2000 voltammetric cycles at 50 mVs^{-1} at a non-oxidized Au electrode in 10^{-3} M Br^- solution. Traces of anodically formed Br_2 can also be detected.

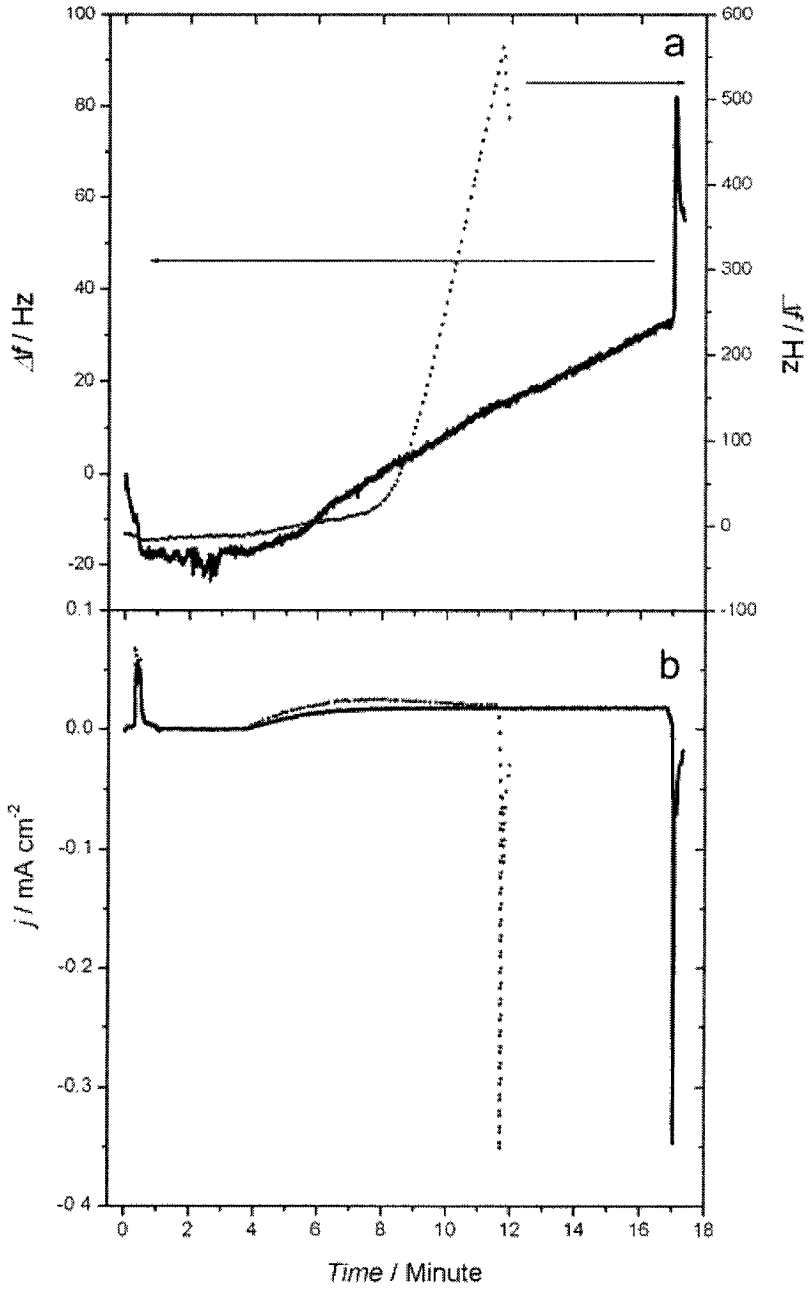

Figure 29. EQCN profiles (a) of oxides films in contact with Br^- 10^{-3} M at 1.45 V (- - -) and at 1.75 V (—) during 10 and 15 min, respectively. In (b), current profile of the electrode in the presence of Br^- during the holding period at 1.45 V (- - -) and at 1.75 V (—).

Conclusions

Anodic development of surface oxide films at noble metals leads to major changes of the properties of the metal surface and its chemical affinities, e.g. in electrosorption processes. Voltammetry and impedance spectroscopy measurements made at polycrystalline Au enable these effects to be clearly demonstrated; thus substantial differences of double-layer capacitance of the oxidized, compared with the non-oxidized, surfaces in aqueous $HClO_4$ and H_2SO_4 are observed at Au, as at Pt. The capacitance values are also appreciably potential-dependent but in different ways at the oxidized, compared with the non-oxidized, surface.

Addition of Cl^- or Br^- anions at low concentrations leads to their chemisorption at the non-oxidized metal surface and subsequent dissolution of Au as a Cl^- or Br^--complex, as indicated by EIS measurements which require fitting by inclusion of a distributed element of the Warburg type, *W*, (Fig.6c) arising from faradaic dissolution of Au. Thus between 0.05 and 1.30 V, a low concentration of Cl^- such as 10^{-4} M, already gives a large increase of the capacitance by a factor of ca. 2 and a factor of almost 4 for a concentration of 10^{-3} M. However, the presence of the halide ions causes little change of capacitance at a Au surface on which either a thin (1 nominal ML) or a thick (ca. 200 nominal MLs) oxide film has been generated anodically. This is because the affinity of the free metal (non-oxidized) surface, exhibited in halide adsorption, is already satisfied when O-ligands of an electrochemically generated oxide film become present at the surface.

A main conclusion from the capacitance results, as at Pt [1], is that "double-layer charging corrections" made in transient experiments at oxidized Au (or other noble metals) electrodes cannot be based just on extrapolation of double-layer capacitance behaviour of the unoxidized surface into the potential range where oxide films become formed. The present results show that corrections made by such a procedure would be highly erroneous.

Complementary use of electrochemical nanogravimetry employing an EQCN and linear-sweep voltammetry provides quantitative information on the stability of the so-called compact α-surface oxide that can be anodically formed at Au electrodes in aqueous $HClO_4$. Following anodic generation of an α-oxide film at Au at 1.80 V (RHE), its stability with respect to corrosion at three constant potentials, 1.75, 1.65 and 1.45 V, was evaluated in the presence of Cl^- or Br^- anions at 10^{-3} M concentration. During arrested negative-going, linear potential-sweeps, following surface oxide formation at 1.80 V, the above three potentials are in the range where almost zero Faradaic currents arise, either for continuing surface oxide formation or onset of oxide-film reduction. These conditions are those required for subsequent examination of the stability of the formed oxide film to corrosion in the Cl^- or Br^- anion solutions.

Combination of EQCN mass and voltammetric charge evaluation enables the extents of dissolution of the oxide film to be quantitatively determined in relation also to behaviour on open-circuit (initially at the above three potentials). Comparative experiments in the potential range where only a non-oxidized Au surface exists, i.e. below 1.30 V (prior to surface oxide generation in a positive-going sweep), or < 1.00 V (RHE), following oxide-film reduction, show that free Au-metal surfaces are not corroding in the Cl^- or Br^- solutions at potentials ranging from 0.1 to 1.20 V (RHE). UV/Vis spectrophotometry shows that when dissolution occurs, even in the presence of the oxide film, it is by a 3e process forming aurichloride or auribromide complexes of Au (III).

Critical examination of the significance of the EQCN results obtained under certain conditions leads to the conclusion that Δf changes at Au oxide can arise not only from surface mass changes but indirectly from a sub-nano-roughness effect connected with anion chemisorption and restructuring of the oxide film.

Claims to original research

- In earlier literature it has been assumed that the capacitance of the double-layer at oxide-free metallic Au surfaces, as a function of potential, can be smoothly extrapolated to and through, the potential range for oxide-film formation at Au, even though such an assumption seems chemically naïve. A main part of the present work establishes experimentally and very clearly that the above is an unacceptable assumption, so that "double-layer charging corrections" to transient charge or current data over the oxide film range of potentials at Au cannot simply be based on extrapolation from otherwise evaluated data for the non-oxidized free metallic surface.

- The above problem is dealt with by experimentally determining the values and potential dependence of the capacitance of the electrical double-layer in the metallic surface region at Au, results for which are shown to be quantitatively different from those for the interface of Au bearing an oxide film. Therefore, the capacitance evaluated over the metallic Au region cannot be extrapolated, to or through, the oxide region. The thickness of the oxide film, once formed, has only a small effect on the capacitance values thus, as the film is thicker, the value of the capacitance becomes only a little diminished.

- It is shown that the concentration of halide, Cl^- or Br^-, in solution determines the rate at which the oxide film will dissolve. The more concentrated is the solution, the faster does the oxide film become corroded as aurichloride complex ion.

- The α-oxide film was shown to be more stable to halide solutions than the β-oxide, even if both were dissolving, at different rates, in halide solution to form soluble gold complex anions characterized, as aurihalides, by UV-Vis spectrophotometry.

- It is argued that the chemical basis of this difference arises from residual affinity of the non-oxidized Au surface for electron-donative anions (here Cl^- and Br^-) whereas this affinity is already satisfied when Au bears an oxide film even of monolayer thickness due to strong interaction of Au metal sites for O species of oxide films. However, at low potentials of oxidation of Au, competition between Cl^- or Br^- adsorption arises vs electrosorption of O species forming the oxide films.

- The observable double-layer capacitance behaviour of Au in H_2SO_4 and $HClO_4$, in the presence and absence of Cl^- or Br^- ions is compared and contrasted with previously derived results for the Pt electrode under comparable conditions.

References

[1] W. G. Pell, A. Zolfaghari, B. E Conway, J. Electroanal. Chem., 532 (2002) 13.

[2] B. Piela, P. K Wrona, J. Electroanal. Chem., 388 (1995) 69.

[3] D. M. Novak, B. E. Conway, J. Chem. Soc., London, Faraday Trans., I, 77 (1981) 2341.

[4] A. Wieckowski, P. Zelenay, K. Varga, J. Chim. Phys., 88 (1991) 1247.

[5] S. J. Xia, V. I. Birss, J. Electroanal. Chem., 500 (2001) 562.

[6] B. E. Conway, Prog. in Surface Sci., 49 (1995) 331.

[7] L. D. Burke, Chapter 4 in Modern Aspects of Electrochemistry, Eds. J. O'M. Bockris, R. E. White, B. E. Conway, 18 (1986), Plenum Publ. Co. New York.

[8] H. A. Kozlowska, B. E Conway, J. Electroanal. Chem., 277 (1990) 233.

[9] P. Zelenay, L.M. Rice-Jackson, A. Wieckowski, J. Electroanal. Chem., 283 (1990) 389.

[10] Figure 6 in ref. 6, p. 359.

[11] B. Lobrg de Bruyn, Rec. Trav. Chim. Pays Bas, 40 (1921) 53.

[12] B. E Conway, D. M. Novak, J. Electroanal. Chem., 99 (1979) 133.

[13] M. Rao, A. Damjanovic, J. O'M. Bockris, J. Phys. Chem., 67 (1963) 2508.

[14] J. Richer; J. Lipkowski, J. Electrochem. Soc. 133 (1986) 121.

[15] L. Stolberg, J. Lipkowski, D.E. Irish, J. Electroanal. Chem. 207 (1986) 213.

[16] A. Iannelli, J. Richer, J. Lipkowski, Langmuir 5 (1989) 466.

[17] H. A. Kozlowska, B.E. Conway, K. Tellefsen, B. Barnett, Electrochim. Acta, 34 (1989) 1045.

[18] B. E Conway, H. A. Kozlowska, W. B. Sharp, J. Electroanal.Chem., 43 (1973) 9.

[19] H. A. Kozlowska, B. E Conway, B. Barnett, J. Mozota, J. Electroanal.Chem., 100 (1979) 417.

[20] B. E. Conway, E. Gileadi, Trans. Faraday Soc., 58 (1962) 2493.

[21] M. Tian, W. G. Pell, B. E. Conway, J. Electroanal. Chem., in press (2003).

[22] P. Batic, B. Pesk, R. H. Sergent, Metall. Trans. B24 (1993) 419.

[23] G. Horanyi, Chapter 27 in Interfacial Electrochemistry, Ed. A. Wieckowski, Marcel Dekker Inc., New York (1999).

[24] W. K. Paik, J. O'M. Bockris, J. Phys. Chem., 74 (1970) 4266.

[25] B. D. Cahan, J. Horkans, E. B. Yeager, Symposia of the Faraday Society, No. 4 (1979) 36.

[26] D. M. Novak, B. V. Tilak and B. E. Conway, chapter 4 in Modern Aspects of Electrochemistry, Eds, B. E. Conway and J. O'M. Bockris, 14 (1978), Plenum Publ. Co., New York.

[27] S. Trasatti, J. Electroanal. Chem., 66 (1975) 815.

[28] S. Trasatti, J. Electroanal. Chem., 329 (1992) 237.

[29] B. E Conway, Y. Phillips, S. Y. Qian, J. Chem. Soc., Faraday Trans., 91 (1995) 283.

[30] A. Zolfaghari, G. Jerkiewicz, B. E Conway, Electrochim. Acta, 47 (2002) 1173.

[31] D.A. Harrington, J. Electroanal., Chem. 420 (1997) 101.

[32] L. D. Burke, P. F. Nugent, J. Electroanal. Chem., 400, (1998) 19

[33] B. E. Conway, G. Jerkiewicz, J. Electroanal. Chem., 297 (1991) 435

[34] D. C. Grahame, Chem. Rev. 41 (1947) 441.

[35] Watts-Tobin, R. J., Mott, N. F. Electrochim. Acta, 4 (1961) 79

[36] R. S. Nicholson, I. Shain, Anal. Chem., 36 (1964) 706.

[37] G. Sauerbrey, Zeit. Phys. 155 (1959) 206.

[38] T. Nomura, M. Iijima, Anal. Chim. Acta, 131 (1981) 97.

[39] R. K. Burshtein, M. R. Tarasevich, V. S. Vilinskaya, Elektrokhim., 3 (1967) 349.

[40] H. A. Kozlowska, in J. O'M. Bockris, E. Yeager, B. E. Conway (Eds.), Comprehensive Treatise of Electrochemistry, vol. 9, 1984, Ch. 2, Plenum Publ. Co. New York.

[41] J.R. Macdonald, W.B. Johnson in Impedance Spectroscopy, Emphasizing solid materials and systems, Ed. J. R. Macdonald, John Wiley and Sons, New York, 1987, p17.

[42] G. J. Brug, A. L. G. Van den Eedem, M. Sluyters-Rehbach, J. H. Sluyters, J. Electroanal. Chem., 176 (1984) 275.

[43] A. Lasia, in: B. E. Conway, J. O'M. Bockris, R. E. White (Eds.), Modern Aspects of Electrochemistry, vol. 32, 1999, p. 204, Plenum Publ. Co., New York.

[44] T. Pajkossy, J. Electroanal. Chem., 364 (1994) 111.

[45] R. K. Burshtein, M. R. Tarasevich, V. S. Tilinskaya, Elektrokhim 3 (1967) 349.

[46] R. Schmacher, G. Borges, K. Kanazawa, Surface Science 163 (1985) 1621.

[47] G. Vatankhah, J. Lessard, G. Jerkiewicz, A. Zolfaghari, B. E. Conway, Electrochimi. Acta, 48 (2003) 1613.

[48] G. Jerkiewicz, G. Vatankhah, A. Zolfaghari, J. Lessard, Electrochem. Commun. 1 (1999) 419.

[49] T. Pajkossy, T. Wandlowski, D.M. Kolb, J. Electroanal. Chem. 414 (1996) 209.

[50] Z. Kerner, T. Pajkossy, Electrochim. Acta 47 (2002) 2055.

[51] P. Delahay, J. Phys. Chem. 70 (1966) 2373.

[52] Figure 4b in ref 7, p. 423.

[53] L. D. Burke, J. F. O'Sullivan, J. Electroanal. Chem., 285 (1990) 195.

[54] S. Ye, C. Ishibashi, K. Shimazu, K. Uosaki, J. Electrochem. Soc., 145 (1998) 1614.

[55] F.A. Cotton, G. Wilkinson, Basic Inorganic Chemistry, p.398, John Wiley and Sons, (1976).

[56] T. Ohtsuka, Denki Kagaku oyobi Kogyo Butsuri Kagaku, 60 (1992) 1123.

[57] G. Tremiliosi-Filho, L.H. Dall'Antonia, G. Jerkiewicz, J. Electroanal. Chem., 422 (1997) 149.

[58] B. E. Conway, G. Jerkiewicz, J. Electroanal. Chem. 297 (1991) 435.

[59] B. E. Conway, D. M. Novak, J. Chem. Soc., Faraday Trans. I 77 (1981) 2341.

[60] P. S. Germain, W. G. Pell, B. E. Conway, Electrochim. Acta, In Press (2004).

[61] Z. Jusys, S. Bruckenstein, Electrochemical and solid-state letters 1 (1998) 12.

[62] W. Stockel, R. Schumacher, Ber. Bunsenges. Phys. Chem. 91 (1987) 345.

[63] M. Hepel in A. Wieckowski (E.d.) Interfacial Electrochemistry, Marcel Dekker Inc, New York, 1999, Ch.24.

[64] V. Tsionsky, L. Daikhin, E. Gileadi, J. Electrochem. Soc. Vol. 143, No 7 (1996) 2240.

[65] S. H. Cadle, S. Bruckenstein, J. Electroanal. Chem. 48 (1973) 325.

[66] S. H. Cadle, S. Bruckenstein, Anal. Chem. 46 (1974) 16.

[67] C. M. Vitus, A. J. Davenport, J. Electrochem. Soc. Vol.141, No 5 (1994) 1291.

[68] R. J. Nichols, O.M. Magnussen, J. Hotlos, T. Twomey, R. J. Behm, D. M. Kolb, J. Electroanal. Chem. 290 (1990) 21.

[69] L. Han-Wei, U. Hiroyuki, W. Masahiro, Langmuir 1997, 13, 3523-3528

[70] G. Zilberman, V. Tsionsky, E. Gileadi, Can. J. Chem. 75. (1997) 1674.

[71] J. Wiecher, T. Twomey, D. M. Kolb and R. J. Behm, J. Electroanal. Chem., 248 (1988) 451.

[72] M. Tian, W. G. Pell, B.E. Conway, J. Electroanal. Chem. 552 (2003) 279.

[73] B. Lovrecek, K. Moslavac, D. Matic, Electrochim. Acta 26 (1981) 1087.

[74] J. A. Peck, C. D. Tait, B. I. Swanson, G. E. Brown, Geochim. et Cosmochim. Acta, 55 (1991) 671.

[75] B. E. Conway, Ionic Hydration in Chemistry and Biophysics, Elsevier Publ. Co., Amsterdam (1982).